CHARACTERISATION AND NUCLEATION KINETICS OF CARBAMAZEPINE-SACCHARIN CO-CRYSTAL
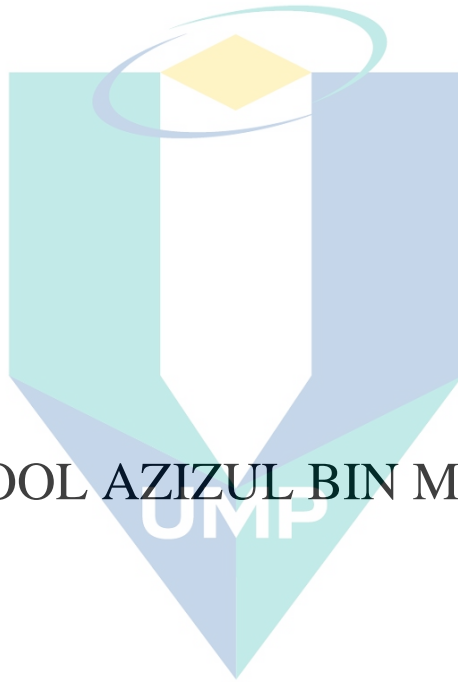
KHAIROOL AZIZUL BIN MOHAMMAD

DOCTOR OF PHILOSOPHY

UNIVERSITI MALAYSIA PAHANG

UNIVERSITI MALAYSIA PAHANG

DECLARATION OF THESIS AND COPYRIGHT	

Author's Full Name : <u>KHAIROOL AZIZUL BIN MOHAMMAD</u>

Date of Birth : <u>13 OCTOBER 1983</u>

Title : <u>CHARACTERISATION AND NUCLEATION KINETICS OF</u>
<u>CARBAMAZEPINE-SACCHARIN CO-CRYSTAL</u>

Academic Session : <u>SEMESTER 2 2019/2020</u>

I declare that this thesis is classified as:

☐ CONFIDENTIAL (Contains confidential information under the Official Secret Act 1997)*

☐ RESTRICTED (Contains restricted information as specified by the organization where research was done)*

☒ OPEN ACCESS I agree that my thesis to be published as online open access (Full Text)

I acknowledge that Universiti Malaysia Pahang reserves the following rights:

1. The Thesis is the Property of Universiti Malaysia Pahang
2. The Library of Universiti Malaysia Pahang has the right to make copies of the thesis for the purpose of research only.
3. The Library has the right to make copies of the thesis for academic exchange.

Certified by:

_____
(Student's Signature)

831013-11-5235
_____
New IC/Passport Number
Date:

_____
(Supervisor's Signature)

DR. SYARIFAH ABD RAHIM
_____
Name of Supervisor
Date:

NOTE : * If the thesis is CONFIDENTIAL or RESTRICTED, please attach a thesis declaration letter.

SUPERVISOR'S DECLARATION

I hereby declare that I have checked this thesis and, in my opinion, this thesis is adequate in terms of scope and quality for the award of the degree of Doctor of Philosophy.

_____

(Supervisor's Signature)

Full Name   : DR. SYARIFAH ABD RAHIM
Position   : ASSOCIATE PROFESSOR
Date   : 11 AUGUST 2020

STUDENT'S DECLARATION

I hereby declare that the work in this thesis is based on my original work except for quotations and citations which have been duly acknowledged. I also declare that it has not been previously or concurrently submitted for any other degree at Universiti Malaysia Pahang or any other institutions.
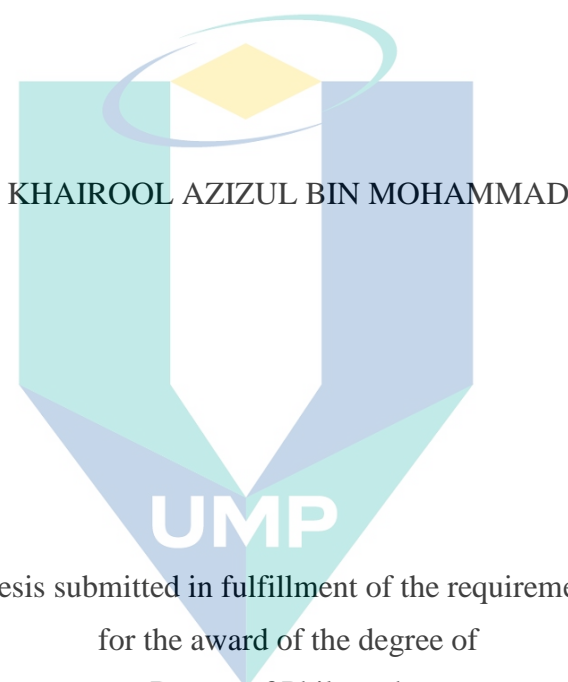
_____
(Student's Signature)
Full Name   : KHAIROOL AZIZUL BIN MOHAMMAD
ID Number   : PKC13013
Date   : 11 August 2020

CHARACTERISATION AND NUCLEATION KINETICS OF
CARBAMAZEPINE-SACCHARIN CO-CRYSTAL

KHAIROOL AZIZUL BIN MOHAMMAD

Thesis submitted in fulfillment of the requirements

for the award of the degree of

Doctor of Philosophy

Faculty of Chemical & Process Engineering Technology

UNIVERSITI MALAYSIA PAHANG

AUGUST 2020

ACKNOWLEDGEMENTS

ABSTRAK

Carbamarzepine (CBZ) mempunyai lima jenis morfologi dan merupakan sejenis dadah yang digunakan untuk merawat penyakit sawan (epilepsy). Masalah utama CBZ adalah daya serapannya yang rendah dan lambat larut di dalam cecair. Ini menyebabkan dos yang banyak diperlukan untuk memberikan kesan kepada pesakit yang mengambil ubat ini melalui saluran mulut. Ko-kristal daripada CBZ dan Saccharin (SAC) diperkenalkan bagi tujuan meningkatkan sifat fisiko-kimia sesuatu ubat. Buat masa ini, begitu sedikit kajian yang dijalankan terhadap kinetik bagi CBZ-SAC ko-kristal. Uniknya kajian ini adalah kerana penyelidikan terhadap kinetik bagi CBZ-SAC ko-kristal dijalankan dengan mengaplikasikan pelbagai nisbah molar SAC/CBZ iaitu 1.0, 2.0, 2.5, 3.0 dan 3.5. Kajian dijalankan dengan pelbagai kepekatan CBZ melalui cara politermal pada kadar penyejukan yang pelbagai. Daripada kajian dapat disimpulkan bahawa kondisi yang terbaik untuk penghasilan ko-kristal adalah dengan kepekatan CBZ sebanyak 17.96 mg/ml pada nisbah SAC/CBZ sebanyak 2.0. Nilai tertib nukleasi (nucleation order), m yang diperolehi daripada proses pengkristalan secara perlahan adalah pada julat diantara 1.65 dan 4.9. Nilai ini adalah bertepatan dengan julat bagi nukleasi untuk sebatian organik. Eksperimen pengkristalan secara laju dijalankan setelah kondisi pengkristalan yang optima diketahui daripada proses pengkristalan secara perlahan. Daripada kajian pengkristalan secara laju, maklumat penting seperti tempoh induksi (pembentukan kristal melalui pengekalan suhu dalam Metastable Zone Width, MSZW), radius kritikal kristal dan tenaga antara permukaan kristal (interfacial energy) dapat diperolehi. Nilai yang diperolehi daripada kaedah Kashchiev–Borissova–Hammond–Roberts (KBHR) dalam menentukan nilai kinetik ko-kristal CBZ-SAC adalah menyamai dengan nilai yang diperolehi daripada kaedah isoterma. Kesan penambahan benih pada CBZ-SAC ko-kristal dikaji dengan mempelbagaikan jumlah benih yang dicampurkan, saiz benih dan suhu larutan semasa proses campuran benih dalam larutan. Proses nukleasi berlaku lebih cepat apabila pembenihan dilakukan hampir dengan garisan keterlarutan super (27.84^{o}C). Analisis pengedaran saiz kristal (CSD) menunjukkan saiz kristal yang lebih halus dibentuk pada suhu yang rendah. Di sisi lain, nukleasi berlaku lebih perlahan apabila penambahan benih hampir kepada garisan keterlarutan (47.55^{o}C) dan menghasilkan kristal yang besaiz lebih besar. Saiz ko-kristal CBZ-SAC yang didapati daripada analisis CSD adalah antara 100 hingga 200 µm. Melalui penggunaan Kalorimeter Pengimbas Kebedaan (DSC) dan Sistem Pembelauan sinar X (XRD), dapat dibuktikan bahawa CBZ-SAC ko-kristal yang stabil (Bentuk I) telah terbentuk.

ABSTRACT

Carbamazepine (CBZ) has five different polymorphs and is a drug used to treat epilepsy. Major issue with CBZ is its low absorption and dissolution rate, thus high dosage is required for the effectiveness of the drug via oral route. Aiming to enhance the physicochemical properties of the drug, co-crystals of CBZ with relevant co-former, saccharin (SAC) is introduced. To date, the kinetics of CBZ-SAC co-crystals has been poorly characterised. The novelty of this research presents the application of different SAC/CBZ molar ratios (1.0, 2.0, 2.5, 3.0 and 3.5) at different CBZ concentrations to deduce the kinetic parameters via polythermal method at different cooling rates. The optimum condition of the production of CBZ-SAC co-crystals were found to be as SAC/CBZ mole ratio of 2.0 at a CBZ concentration of 17.96 mg/ml. The nucleation orders obtained from slow cooling method were in between 1.65 and 4.9, which were within the range for nucleation of organic compounds. Based on the results of kinetic study from the slow cooling method, a fast cooling experiment was conducted to evaluate the induction time, the radius of the critical nucleus and interfacial energy of the co-crystal. The results from Kashchiev–Borissova–Hammond–Roberts (KBHR) method in determining the kinetic values of CBZ–SAC co-crystals were similar to those of the isothermal method. The effect of seed loading, seed size and the temperature of supersaturated solution at the time of seeding on the CBZ-SAC co-crystals were investigated. It was found that nucleation occurred faster when seeding is close to the super solubility curve (27.84 ºC) which is at the highest supersaturation. The analysis of crystal size distribution (CSD) showed more fine particles were formed at a lower seeding temperature. On the other hand, nucleation occurred slower when seeding is close to the solubility curve (47.55 ºC), which is at low supersaturation and therefore resulted in a smaller number of fine particles formed. The size of CBZ-SAC co-crystals formed from CSD analysis was in a range of 100 to 200 µm. Characterisation using Differential Scanning Calorimetry (DSC) and X-Ray Diffraction (XRD) of all CBZ-SAC co-crystal has proven that, the stable CBZ-SAC co-crystals of Form I were formed.

TABLE OF CONTENT

LIST OF TABLES

LIST OF FIGURES

LIST OF SYMBOLS

S	supersaturation / supersaturation ratio
σ	relative supersaturation
ΔT	supercooling
ΔG_{nucl}	free energies during nucleus formation
ΔG_s	free energy between the surface of a particle and the bulk
ΔG_v	free energy between a very large particle and solution's solute
r	radius of cluster
γ	interfacial tension
$\Delta \mu$	chemical potential
ν_c	molecular volume of the cluster
r_c	critical radius cluster
ΔG_{crit}	maximum free energy
κ	Boltzmann constant
C	actual solution concentration
C*	equilibrium concentration of the saturation at the given temperature
T_{diss0}	equilibrium dissolution temperature
T_{crys0}	equilibrium crystallization temperature
k	mass nucleation rate constant / nucleation kinetic constant
m	nucleation order
ΔC_{max}	absolute supersaturation
R	cooling / heating rate
ν_m	molar volume
A	pre-exponential factor / crystal surface area
T	temperature
θ	wetting angle
$\Delta G_{nucl,het}$	total free energy of heterogeneous nucleation
$\Delta G_{nucl,hom}$	total free energy of homogeneous nucleation
B_{sec}	secondary nucleation rate
k_{b2}	coefficient or order of magnitude of the secondary nucleation
C_S	concentration of solid in the solution
α	exponent for (S-1)

β	exponent for C_S
k_m	mass transfer coefficient
D	diffusion coefficient
δ	film thickness
k_d	diffusion mass transfer coefficient
k_r	reaction rate coefficient
K_G	overall crystal growth coefficient
ΔT_c	critical undercooling
T_e	equilibrium solubility temperature
T_{crys}	crystallisation temperature
T_{diss}	dissolution temperature
u_c	relative critical undercooling
γ	interfacial energy
T_n	nucleation temperature
t_{ind}	induction time
J	nucleation rate
ρ_{CBZ}	CBZ concentration
γ_{eff}	interfacial energy
r^*	critical size nucleus
i^*	molecular number of critical nucleus
k_n	nucleus shape factor
v_0	molecular volume in the crystal

LIST OF ABBREVIATIONS

API	Active Pharmaceutical Ingredients
BCS	Biopharmaceutical Classification System
MSZ	Metastable Zone
MSZW	Metastable Zone Width
CBZ	Carbamazepine
SAC	Saccharin
DSC	Differential Scanning Calorimetry
XRD	X-Ray Diffraction
RC	Reaction Co-Crystallisation
CCS	Co-Crystallization with Supercritical Solvent
SAS	Supercritical Anti-Solvent
SEA	Supercritical Fluid Enhanced Atomization
CBZ(D)	Carbamazepine (Dihydrate)
CSD	Crystal Size Distribution
TEOS	Tetraethylorthosilicate
AA	Adipic Acid
PCM	Paracetamol
CNT	Classical Nucleation Theory
KBHR	Kashchiev-Borissova-Hammond-Roberts
PN	Progressive Nucleation
wt%	Weight percent

LIST OF APPENDICES

CHAPTER 1

INTRODUCTION

1.1   Introduction

Broad spectrum of research and efforts have been done to find, select and control of the solid forms of active pharmaceutical ingredients (APIs) over the past decades. APIs can exist in a wide range of solid forms, such as polymorphs, pseudopolymorphs, salts, solvates, and amorphous phases (Jie Lu, 2012).

According to the U. S. Food and Drug Administration (2013) guidelines, co-crystals are defined as "solids that are crystalline materials composed of two or more molecules in the same crystal lattice." Co-crystals consist of a single crystalline phase of multiple components in a given stoichiometric ratio, where the different molecular species interact by hydrogen bonding or by other non-covalent bond. Co-crystals are able to alter the physicochemical properties of active pharmaceutical ingredient (API) through combining API and additional components (i.e. co-formers) in the same crystal structure thereby altering solid-state properties and solution behaviour without modifying chemical structure (Childs & Zaworotko, 2009). As a consequence, co-crystals increase the diversity of solid-state forms of an API and enhance pharmaceutical properties by modification of chemical stability, moisture uptake, mechanical behaviour, solubility, dissolution rate, and bioavailability (Ghadi et al., 2014).

Carbamazepine (CBZ) was chosen as the drug model in this study. It is frequently a prescribed as a drug used to treat epilepsy and trigeminal neuralgia (Novartis Pharmaceuticals Corporation, 2018). Since CBZ has five different anhydrous polymorphs, it has served as a model to study crystal polymorphism (Grzesiak et al., 2003). The issue with CBZ is its low absorption and dissolution rate, thus high dosage is required for the effectiveness of the drug (Cuadra et al., 2018). According to

Biopharmaceutical Classification System (BCS) that classifies drugs into four categories according to their permeability and solubility properties, CBZ which has low solubility and high permeability is classified as a class II drug (Lee et al., 2015). Co-crystals of carbamazepine are identified with relevant co-former, saccharin (SAC) using the crystal engineering principles. SAC is widely used as co-former in the preparation of co-crystals. SAC has good water solubility and one known polymorph (Cuadra et al., 2018). Crystallisation from solution has been studied intensively and is widely used in many industries and applications. The main purpose of crystallisation is to separate and purify solids in a suitable solvent which lead to the control of the shape and size of final crystalline products. This technique provides an end compound with a high degree of purity that has many desirable properties such as good solubility, dissolution rate, and chemical and physical stability (Mullin, 2001).

There are two steps in forming a crystal/solid from a solution: (i) nucleation, which is the creation of minute nuclei in a supersaturated solution (ii) crystal growth, that transforms the stable nuclei into solid crystals (Mullin 2001). The crystallisation occurs in a metastable region, which exists in a supersaturated solution. Metastable zone width (MSZW) is located between supersaturation and saturation limit of a system. The optimisation of a crystallisation process and the quality of the forming crystal can be simply controlled when the crystallisation runs within the MSZW (Kannan & Brahadeeswaran, 2013; Mota et al., 2014). The factors that can affect the MSZW are cooling/heating rates, solution temperature, impurities or seeds, stirring rate and solvent (Camacho Corzo et al., 2014; Mota et al., 2014; Qian et al., 2014). Therefore, it is particularly important to identify these parameters precisely for accessing the MSZW. An analysis of the change in physical quantities such as particle count number, turbidity, intensity (absorbance or transmittance), and electrical conductivity were used in the research works as an indicator of the nucleation event (Kubota, 2008). Among these, the turbidity measurement is an inexpensive method which several chemical processes are using it (Bernardo & Giulietti, 2010).

1.2 Problem Statement

Co-crystal was introduced to enhance the pharmaceutical properties of drug. Pure CBZ, used in treatment of epilepsy, has low solubility, low dissolution and low absorption rate as taken in oral route. The pharmaceutical properties of CBZ can be improved by converting the conversional drug to co-crystal drug. Recently, various research in drug discovery and development have mostly focused on formation, solubility and dissolution of CBZ co-crystals. However, to the best of authors knowledge, far too little attention has been paid to the kinetics and particle size of CBZ cocrystals. In the present work, nucleation kinetics for different molar ratio and concentration of CBZ co-crystals with SAC as a co-former were studied.

Deep understanding of crystallisation kinetics is important to design and control of the shape and size of final crystalline products. The kinetics of Carbamazepine (CBZ)-Saccharin (SAC) co-crystals with enhanced pharmaceutical properties has been poorly characterised. This kinetic study can be conducted by determining the MSZW. This region is vital for crystallisation process because the supersaturation can be controlled within this region to get the desired crystal properties. Furthermore, nucleation order of the co-crystals can be obtained via slow cooling and induction time, radius of the critical nucleus and interfacial energy of the stated co-crystal are obtained via fast cooling.

Nucleation kinetics is important for controlling crystal particle size. Crystallisation is only occurred if solubility limit is exceeded or by introduction of seed in metastable solution. Therefore, to know the metastable zone is an integral part for crystallisation process, so that the desired crystal particles can be achieved when the supersaturation is controlled within the metastable region. By understanding the nucleation kinetics of CBZ-SAC cocrystals, a suitable crystalliser and a good crystallisation process can be designed and operated. Finally, the characterisation process of CBZ-SAC co-crystals are vital, so that desired form I (stable form) of CBZ-SAC co-crystals are obtained. The novelty of this research presents the application of different SAC/CBZ molar ratios (1.0, 2.0, 2.5, 3.0 and 3.5) at different CBZ concentrations to deduce the kinetic parameters via polythermal method at different cooling rates. In addition, an application of newly Kashchiev–Borissova–Hammond–Roberts (KBHR)

method in defining nucleation kinetics of CBZ-SAC cocrystals optimises the experiment process.

1.3   Objectives of Research

This work focuses on the formation, analysing and characterisation of poorly characterised CBZ-SAC co-crystals. Experiments with different ratios of SAC to CBZ and different concentration of CBZ were performed to address specific objectives as follows:

1.   to determine the effect of cooling rate, heating rate and SAC/CBZ molar ratio on MSZW of CBZ-SAC co-crystals.

2.   to analyse the nucleation kinetics of CBZ-SAC co-crystals for different SAC to CBZ molar ratios at different CBZ concentration.

3.   to investigate the effect of seeding temperature, seed loading and seed size to the crystal size distribution of CBZ-SAC co-crystals.

4.   to characterise the CBZ-SAC co-crystals.

1.4   Scope of Work

For nucleation kinetics, the slow and fast cooling crystallisation experiments were conducted. In slow cooling experiment, crystallisation and dissolution temperatures of CBZ-SAC co-crystals for different CBZ concentrations and different SAC to CBZ mole ratios were obtained. In addition, a new technique in determining the dissolution temperature of the co-crystals was applied, in which uniformed temperature profiles before heating were applied for the comparison of dissolution temperatures. For the slow cooling experiment, four CBZ concentrations (19.14, 17.96, 17.01 and 15.83 mg/ml), five mol ratios of SAC to CBZ (3.5, 3.0, 2.5, 2.0 and 1.0) and eight cooling rates (1.0, 0.8, 0.75, 0.6, 0.5, 0.4, 0.25 and 0.2 ℃/min) were used in these experiments. The nucleation kinetics parameter such as MSZW, nucleation orders and nucleation kinetic were calculated.

Once the preferred metastable zone from slow cooling experiments was selected, the research followed by fast cooling test, where the induction time, the radius of the

critical nucleus and interfacial energy of the co-crystal was determined. The variable parameters in these experiments were four temperatures within a mestastable region (32, 36, 40, and 44 ºC), and two fast cooling rates (1.2 and 1.0 ºC/min). In addition, the kinetics of CBZ-SAC co-crystals were evaluated by applying polythermal methodology modelled by Kashchiev–Borissova–Hammond–Roberts (KBHR).

The addition of seeds to the metastable zone induces the nucleation process, therefore seeds with different size and weight were prepared and added to the supersaturation region at different temperature to have control over particle size distribution, flow properties, yields of the co-crystals. The seeds were added at a seeding temperature of (44, 40, 36, and 32 °C) and with a different seed mass of (0.5, 1.0 and 1.5 %) of the total product mass.

Lastly, the co-crystal physical properties produced from all experiments were identified using Differential Scanning Calorimetry (DSC) and X-ray Diffraction (XRD). The crystal size distribution (CSD) of the CBZ-SAC co-crystals was determined using sieve shaker and Malvern Mastersizer.

1.5   Significance of Study

The findings of this study will redound to the benefit of society considering that pharmaceutical plays an important role in medical science and technology today. The greater demand for enhanced drug properties justifies the need for introducing co-crystals. Thus, researchers that apply a newly improved method in determining dissolution temperature of the co-crystals derived from this study will be able to make the right comparison of the effect of heating rate on metastable zone width of the co-crystals. This technique can be easily applied to other organic compounds. By knowing the metastable zone of CBZ-SAC co-crystals for a different CBZ concentration and various mol ratio of SAC to CBZ, more research can be proceeded such as effect of seeding on that region and modelling of supersaturation control. The KBHR method applied in determining nucleation kinetics of co-crystals will help researchers to optimise the cost and duration of experiments. The details approach on different parameters in this current study will surely contribute to the pharmaceutical industry since CBZ–SAC co-

crystals showed advantages, such as a favourable dissolution profile and suspension stability, compared to commercial immediate-release products.
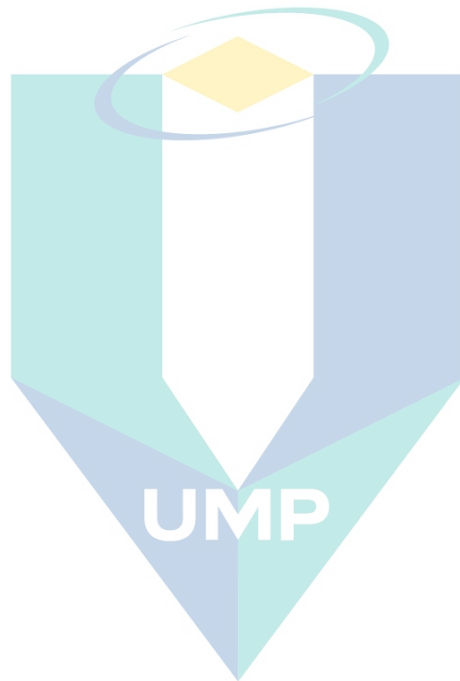
CHAPTER 2

LITERATURE REVIEW

2.1   Solubility and Supersaturation

The knowledge of solubility of a substance in a solvent is important in order to understand the crystallisation process. The solubility of solute in a solvent can be defined as the maximum concentration of the solute, which can be retained in the solvent in equilibrium at a given set of temperatures and pressures (Jones, 2002). The point where the maximum of solute can be dissolved in the solvent is named as saturation point (Gillespie, 2018; Myerson, 2001). Miers and Isaac in 1906 constructed solubility and supersolubility diagram and explained the supersaturation and spontaneous crystallisation correlation (Miers & Isaac, 1906). The diagram (Figure 2.1) shows the zones where the crystallisation can occur.

Figure 2.1 provides an overview of three zones relating to crystallisation process; (i) the stable zone, which is located on the right side of solubility curve and is unsaturated. The crystallisation is not possible to occur in this zone; (ii) the metastable zone, which is located in between solubility and supersolubility curves and is in supersaturated. In this region, spontaneous crystallisation is unlikely to occur, but crystallisation is possible by existence of foreign particle such as an addition of seed; (iii) the labile zone, which is a non-stable zone and spontaneous crystallisation occurs mostly to in this zone (Mullin, 2001). In case of co-crystals, the solubility of co-crystal is higher than solubility of single crystal, thus the co-crystal dissolves faster in the solution as the temperature increases. Thus, the metastable zone width (zone (ii) of Figure 2.1) for cocrystal is narrower than single crystal (Surov et al., 2017).

7
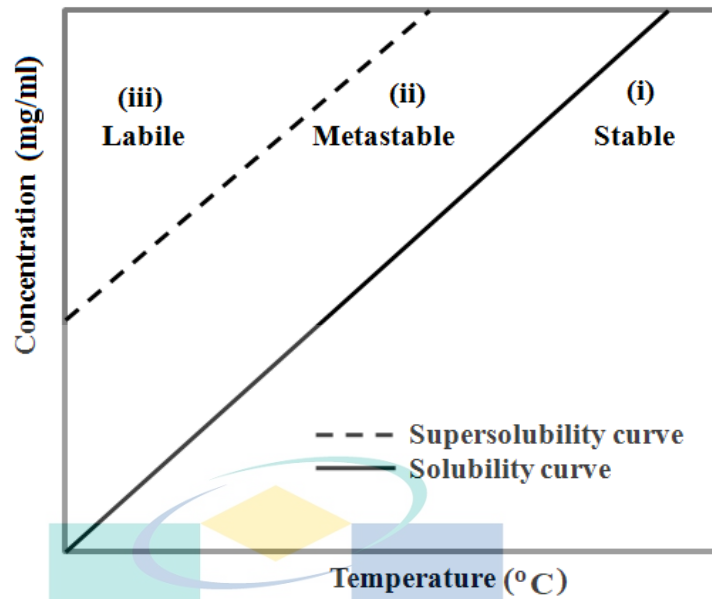
Figure 2.1   Solubility and supersolubility curves of stable, metastable and labile zones.

Source: Mullin (2001).

Crystallisation in solution can achieve nucleation condition when the temperature of solution in stable zone is cooled down across the solubility curve to become a supersaturated solution (Randolph & Larson, 1988). In crystallization process, supersaturation acts as a driving force, which mostly affects the nucleation rate and the forming of the crystals. Supersaturation can be defined as:

$$\Delta C = C - C^* \hspace{4cm} 2.1$$

Where,

ΔC = the concentration driving force (mg/ml),

C   = the actual solution concentration at the same temperature (mg/ml)

C* = the equilibrium saturation of the saturation at the given temperature(mg/ml).

Besides, supersaturation ratio, S is:

8

$$S = \frac{C}{C^*} \qquad\qquad 2.2$$

The supersaturated solution is achieved when value of S is greater than 1. Furthermore, the relative supersaturation, σ is:

$$\sigma = \frac{\Delta C}{C^*} = S - 1 \qquad\qquad 2.3$$

The state of supersaturation can also be described by supercooling, ΔT as shown in equation 2.4.

$$\Delta T = T^* - T \qquad\qquad 2.4$$

Where,

T* = the saturation temperature

T = the actual temperature.

2.2   Metastable Zone

Metastable zone is an area between solubility and supersolubility curve, where the solution is supersaturated, and spontaneous crystallisation is unlikely to occur. This region is vital for crystallisation process because the supersaturation condition can be controlled within this region to get desired crystal properties. Metastable zone width (MSZW) depends on several factors, such as cooling and heating rate, initial solution concentration, stirring speed, volume of vessel or reactor, impurities or seeds addition, temperature controls and solvent used (Wang, Feng, Dong, Peng, & Li, 2016). The crystal forming in supersaturated solution with specific characteristics of nucleation leads to the

9

changes of MSZW values. Therefore, MSZW acts as a characteristic property for crystallisation process (Shiau, 2016).

Determination of MSZW can be done via polythermal or isothermal methods. Until now, the polythermal method is commonly used to determine the MSZW (Zhou et al., 2016). In polythermal technique, the supersaturation changing with time, in which the solution is cooled from stable zone with a constant and slow cooling rate. Whereas in isothermal method, the solution temperature was brought down to the constant temperature within metastable zone with a fast cooling rate and the supersaturation is kept constant, due to the isothermal temperature of the solution. Both methods are accomplished after a 'first nuclei' is detected via various determination technique, for example turbidity, intensity measurement via absorbance or transmittance, particle count number, electrical conductivity and many more. The isothermal method requires longer time in particularly when the isothermal temperature is high, which means a low supersaturation value (Randall et al., 2012).

2.3   Nucleation

Nucleation is a first step in crystallisation process, where a new solid phase is formed in a supersaturated solution (Jones, 2002). If the supersaturation level surpasses the supersolubility curve, i.e goes to the labile zone, then the formation of nuclei takes place spontaneously (see Figure 2.1). The nuclei formation is due to the system attempts to reach the equilibrium i.e stable state. Nucleation mechanisms are classified into two categories; primary and secondary nucleation (Jones, 2002; Mullin, 2001). The primary and secondary nucleation is differentiated by absence and presence of solute crystals, respectively. Primary nucleation is mainly takes place at high level of supersaturation and is often prevalent in unseeded crystallisation (Nemdili et al., 2016). Homogeneous nucleation happens spontaneously in/from a pure solution, whereas heterogeneous nucleation is induced by foreign particles. Secondary nucleation occurs when the supersaturated solution is induced by crystals such as seeds or impurities. The nucleation process begins possibly even at a very low supersaturation levels, which is impossible for primary nucleation. In pharmaceutical industry, the secondary nucleation can be easily controlled (Veesler & Puel, 2014).

Primary and secondary nucleations can also be presumed from Figure 2.2, which shows that metastable zone width is smallest for secondary nucleation and largest for primary homogeneous nucleation. MSZW for primary heterogeneous nucleation is in between these two (Ulrich & Strege, 2002). In relation to co-crystal, MSZW is expected to be narrower for all primary and secondary nucleation, since co-crystal has higher solubility than single crystal (Surov et al., 2017).
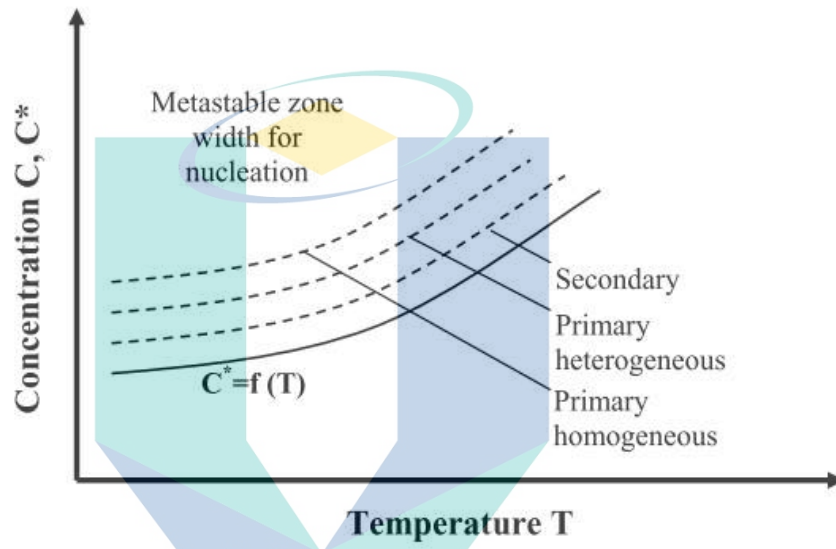
Figure 2.2   Metastable zone width for all types of nucleation process.
Source: Ulrich & Strege (2002).

2.3.1   Primary Nucleation

2.3.1.1   Homogeneous Nucleation

Primary nucleation, which takes place mostly at high supersaturation level is homogeneous when there are no foreign particles in the supersaturated solution. It occurs spontaneously or in random manner from a clear solution. At high supersaturation level, a cluster which later can become a larger crystal, is formed by coagulation of the small solute molecules. If the size of cluster is larger than a critical size r_c, it can resist the tendency to re-dissolve back to the solvent. Furthermore, the molecules will transformed into fixed lattice, which later it can multiply to a several thousands of crystals (Mullin, 2001). Forming of stable nucleus is extremely very rare from simultaneous collisions of

certain number of molecules, rather the forming of critical size nucleus is mostly from the collision of monomers, dimers, trimers and larger aggregates, which act as a growth unit.

Theory for homogeneous nucleation namely classical nucleation theory (CNT) developed by Volmer (1939) stated that, cluster will be stable if its size is bigger than the critical value. The change of the free energies during nucleus formation (ΔG_{nucl}) associated homogeneous nucleation can be derived by following equation:

$$\Delta G_{nucl} \; = \; \Delta G_s \; + \; \Delta G_v = 4\pi r^2 \gamma - \frac{4\pi r^3 \Delta\mu}{3v_c} \qquad 2.5$$

Where,

ΔG_s = free energy between surface of a particle and bulk

ΔG_v = free energy between a very large particle and solution's solute.

r = radius of cluster, m

γ = interfacial tension, N/m

$\Delta\mu$ = chemical potential

v_c = molecular volume of the cluster.

Figure 2.3 illustrates that, ΔG_s is proportional to r^2 and will give a positive quantity, whereas ΔG_v is proportional to r^3, will give a negative quantity. Summation of ΔG_s and ΔG_v result in ΔG_{nucl} which has the maximum free energy (ΔG_{crit}), which is corresponding to the critical radius cluster, r_c.
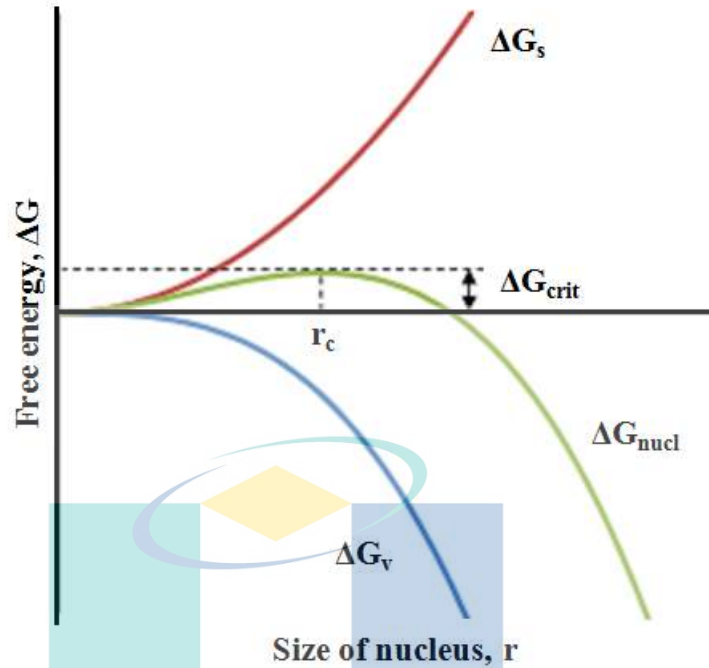
Figure 2.3   Changes in Gibbs free energy in nucleation process.
Source: Myerson (2015).

By differentiating Equation 2.5, with respect to r, the critical size nucleus for a spherical nucleus can be obtained as follow:

$$\frac{d\Delta G}{dr} = 8\pi r\gamma - \frac{4\pi r^2 \Delta\mu}{v_c} = 0 \qquad 2.6$$

or,

$$r_c = \frac{2\gamma v}{\Delta\mu} \qquad 2.7$$

And,

$$\Delta G_{crit} = \frac{4\pi\gamma r_c^2}{3} = \frac{16\pi\gamma^3 v_c^2}{3\Delta\mu^2} \qquad 2.8$$

Equation 2.7 shows that critical radius, r_c is inversely proportional to chemical potential, $\Delta\mu$. Following equation shows the relation between chemical potential and supersaturation:

$$\Delta\mu = \kappa T \ln S = \kappa T \ln\left(\frac{C}{C^*}\right) \qquad 2.9$$

Where,

κ = Boltzmann constant (1.3805 x10^{-23} J/K),

C= actual solution concentration, and

C* = equilibrium concentration of the saturation at given temperature.

Equation 2.8 illustrates that, chemical potential is a function of supersaturation. From Mullin (2001), the rate of nucleation, J can be defined as:

$$J = Ae^{(-\Delta G/\kappa T)} \qquad 2.10$$

Where,

A= pre-exponential factor, and

T= temperature, K.

By combining ΔG_{crit} and $\Delta\mu$, the homogeneous nucleation can be defined as follows:

$$J = Aexp\left(-\frac{\Delta G_{crit}}{\kappa T}\right) = Aexp\left(-\frac{16\pi\gamma^3 v_c^2}{3\kappa T \Delta\mu^2}\right) \qquad 2.11$$

Or,

$$J = Aexp\left(-\frac{16\pi\gamma^3 v_c^2}{3\kappa^3 T^3 \ln S^2}\right) \qquad 2.12$$

From Equation 2.12, the rate of nucleation J is a function of free energy ΔG and is a function of supersaturation. This connection leads to the graph in Figure 2.4.
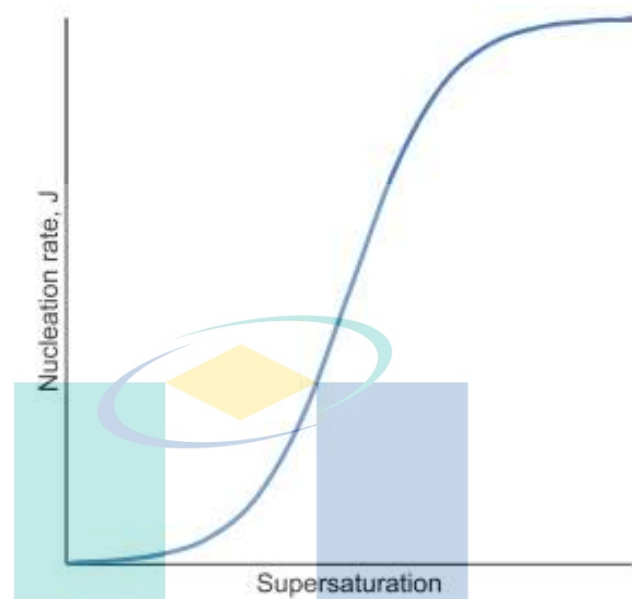
Figure 2.4   Nucleation rate vs. Supersaturation.
Source: Davey & Garside (2001).

The classical nucleation theory (CNT) works with some assumptions. These assumptions cause flaws in a prediction of nucleation rate of the process. Where:

i.   Nuclei are assumed to be a spherical drop, which means if it is not spherical, the CNT theory is no longer valid. Besides it is neglecting the size or curvature dependence of the surface tension.

ii.   In forming of a nuclei, only one monomer is added at a time. Therefore, the formation of pre-nucleation clusters and collision between them is ignored. As a result, final crystal has the same structure as the nuclei array.

iii. The determination of the stability of nuclei is only based on the size of nuclei.

Erdemir, Lee, and Myerson (2009) proposed a two-step nucleation model which addressing and overcome issues from CNT. In this model, nucleation of solids from solution followed a complex route rather than a classical one. After formation of an adequate cluster in supersaturated solution, the cluster is rearranged into a structured crystal. The rearrangement acts as rate determining step (Myerson, 2015). In this step, the nucleation rate is proportional to the complexity of the molecules. Then the model continues in CNT, where ordered crystalline nuclei was formed and finally producing a solid crystal. The steps of CNT and two-step nucleation model has been shown in Figure 2.5.
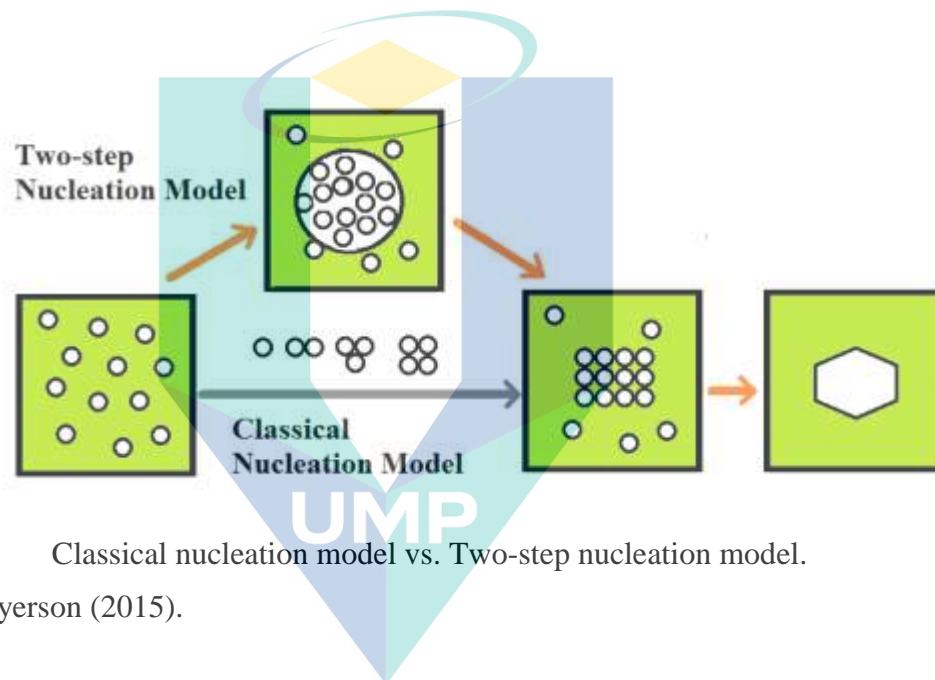
Figure 2.5   Classical nucleation model vs. Two-step nucleation model.
Source: Myerson (2015).

2.3.1.2   Heterogeneous Nucleation

Formation of nuclei via heterogeneous nucleation is more often than homogeneous nucleation. Heterogeneous nucleation occurs at phase boundaries, surfaces or induced by impurities like dust. Total free energy to be overcome for formatting nuclei in heterogeneous nucleation is much lower than that in homogeneous nucleation (see Figure 2.6).

16
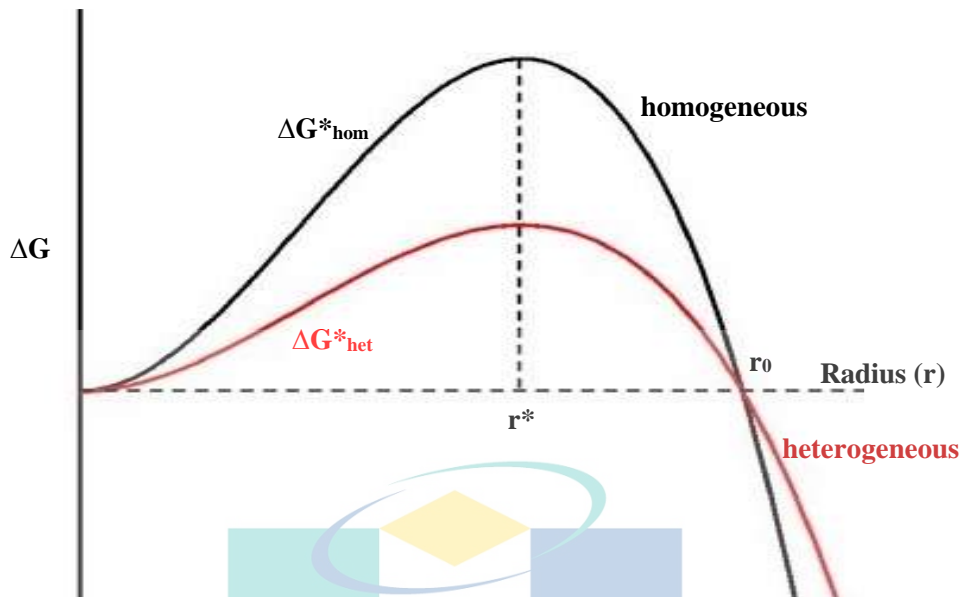
Figure 2.6   Total free energy of homogeneous and heterogeneous nucleation.
Source: (Çelikbilek et al., 2012).

Correlation between homogeneous and heterogeneous nucleation can be found as follow:

$$\Delta G_{crit,het} = f * \Delta G_{crit,homo} \qquad 2.13$$

Where,

Value of f is between 0 and 1and can be defined as:

$$f = \frac{2 - 3cos\theta + cos^3\theta}{4} \qquad 2.14$$

Wetting angle, θ, influences total free energy of heterogeneous nucleation, which can reduce the energy barrier in nucleation process. Followings are the result from the value of wetting angle;

If θ = 180°, f = 1, then the total free energy ΔG is equal to value of homogeneous nucleation, where there is no wetting on the surface.

17

If θ = 0°, f = 0, there will be no barrier for nucleation to occur, where there is a full wetting on the surface.

By substituting Equation 2.8 and Equation 2.14 into Equation 2.13, the value of total free energy of heterogeneous nucleation $\Delta G_{nucl,het}$ can be calculated as follows:

$$\Delta G_{crit,het} = \frac{4\pi\gamma^3 v_c^2 (2 - 3cos\theta + cos^3\theta)}{3\Delta\mu^2}$$

2.15

2.3.2 Secondary Nucleation

In pharmaceutical industry, secondary nucleation is the most prevalence process to form crystalline structure. It occurs due to an addition of foreign substance to a supersaturated solution. Secondary nucleation is more controllable compared to primary nucleation. The factors that inducing the nucleation are listed as follows:

Table 2.1   Factors inducing secondary nucleation.

Factors	Description
Initial breeding	known as dust breeding. Dust adhered to dry seed crystals is swept off and forms secondary nuclei.
Needle breeding	at high supersturation level, crystal breaks into fragile needles, which acts as nucleation sites.
Poly-crystalline breeding	at high supersaturation level, irregular poly-crystalline breaks into secondary nuclei.
Fluid shear	at high supersaturation, nuclei formed after the removal of adsorbed layer of crystal due to the shear between fluid and crystal.

Secondary nucleation rate, B_{sec} depends highly on supersaturation S and concentration of solids in solution. It can be calculated as follows:

18

$$B_{sec} = k_{b2}(S - 1)^{\alpha} C_s^{\beta} \qquad\qquad 2.16$$

Where,

k_{b2} = coefficient or order of magnitude of the secondary nucleation

C_S= concentration of solid in the solution

α = exponent for (S-1)

β= exponent for C_S

Values of α and β are normally in between 0 and 2.

2.4   Crystal Growth

In supersaturated solution, stable nuclei are formed and start to grow with time. Most popular theory to explain crystal growth is known as diffusion theory. The diffusion theories assume that solid is deposited on the crystal surface is due to the different concentration at the solution bulk and crystal surface (Jones, 2002; Mullin, 2001). Rate of deposition of solid follows below Equation 2.17 (Noyes & Whitney, 1897):

$$\frac{dm}{dt} = k_m A(c - c^*) \qquad\qquad 2.17$$

Where,

m= mass of solute deposited (kg)

t= time for deposition of solid (s)

k_m= mass transfer coefficient (kg/sm^2)

A= crystal surface area (m^2)

c= concentration of solute in supersaturated solution

c*= concentration at equilibrium

Nernst & von Lerch (1904) has found that, there is a layer which consists of stagnant film between crystal surface and solution. Diffusion will first happen within this film. The film thickness is inversely proportional to the agitation rate of the system. Thus, Equation 2.17 can be modified as follows:

$$\frac{dm}{dt} = \frac{D}{\delta} A(c - c^*)$$

2.18

Where,

D= diffusion coefficient

δ= film thickness

From 1912 onwards, Berthoud (1912) has found that, the mass deposition consists of two steps. First step is diffusion, where molecules from bulk of solution with concentration c were carried to the crystal surface with concentration c_i. Rate of deposition can be written as:

$$\frac{dm}{dt} = k_d A(c - c_i)$$

2.19

Where,

k_d = diffusion mass transfer coefficient

Second step is called reaction, where first order reaction or the arrangement process of the molecules from crystal surface with concentration c_i to the crystal lattice with concentration c^*. Rate of deposition can be written as:

$$\frac{dm}{dt} = k_r A(c_i - c^*)$$

2.20

Where,

k_r= reaction rate coefficient

Both steps can be illustrated in Figure 2.7. Since the interfacial concentration is difficult to be measured, it can be ignored and therefore the rate of deposition is calculated by following equation:

$$\frac{dm}{dt} = K_G A(c - c^*)$$

2.21

Where,

K_G= overall crystal growth coefficient.
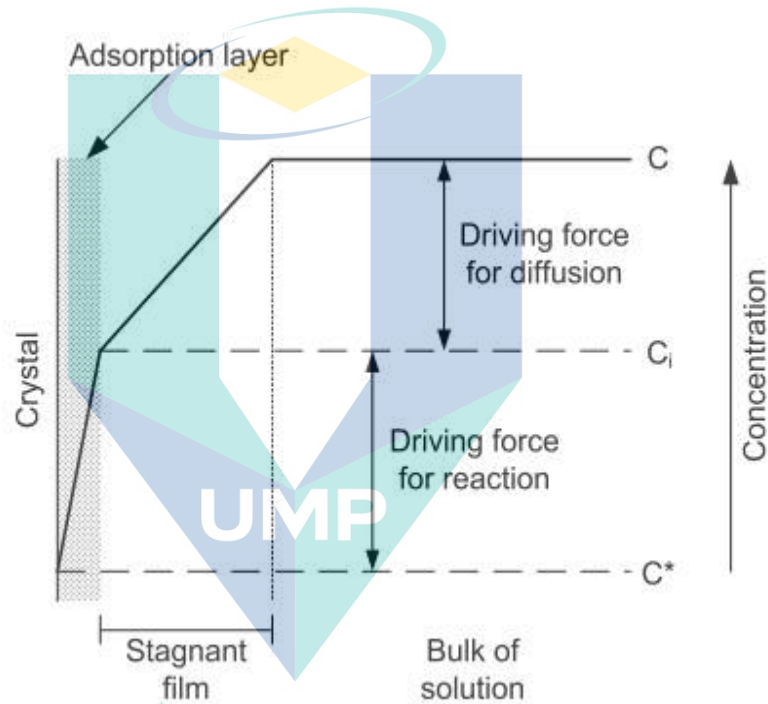
Figure 2.7   Steps in deposition process. Driving force for diffusion and reaction (concentration).

Source: Mullin (2001).

2.5   Determination of Nucleation Kinetics

2.5.1   Nyvlt's Approach

Nývlt (1968) has introduced a polythermal method to determine the kinetics of the nucleation. This is the common useful method until today. The nucleation rate J is expressed by;

$$J = k(\Delta C_{max})^m \qquad\qquad 2.22$$

where

k= nucleation rate constant,

m= nucleation order,

ΔC_{max} = the absolute supersaturation (kgm^{-3}).

ΔC_{max} is defined as a function of the maximum possible undercooling ΔT_{max} through the equation:

$$\Delta C_{max} = \frac{dC}{dT} \Delta T_{max} \qquad\qquad 2.23$$

ΔT_{max} is equal to MSZW which can be calculated by differencing the value of crystallisation temperature and saturation temperature. Figure 2.8 show that, when the solution approaches the critical supersaturation, ΔC_{max} the nucleation rate increases sharply (Nývlt, 1968).
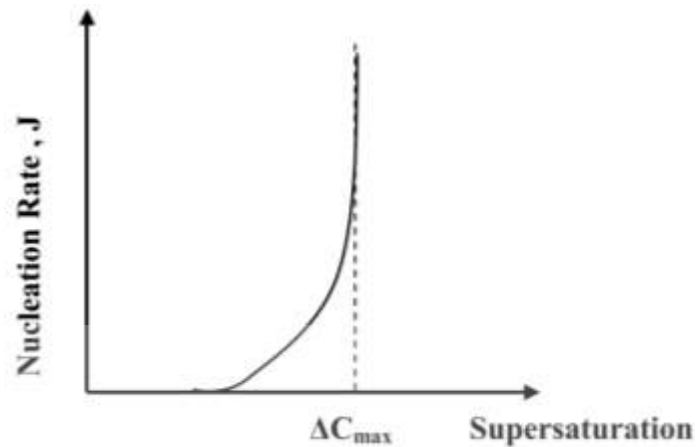
Figure 2.8   Schematic plot of nucleation rate versus degree of supersaturation.

Source: Nývlt (1968).

The nucleation rate may be expressed to be equal to the rate at which supersaturation is achieved at the time when first nuclei are detected. J also can be defined as

$$J = \frac{dC}{dT}R \qquad \text{2.24}$$

where, R is a cooling rate. By substitutes the Equation 2.22 and Equation 2.23 into Equation 2.24, the following expression is obtained:

$$ln(R) = (m-1)ln\frac{dC}{dT} + ln(k) + m\,ln(MSZW) \qquad \text{2.25}$$

By plotting ln(R) vs. ln(MSZW), the value of m and k can be calculated. Nucleation order, m is the slope of the graph and the interception of the graph, b is equal to:

$$b = (m-1)ln\frac{dC}{dT} + ln(k) \qquad \text{2.26}$$

By substituting the value of b and m, the nucleation kinetic constant, k can be calculated.

23

2.5.2 Kashchiev–Borissova–Hammond–Roberts (KBHR) Method

The method was in details explained by Camacho Corzo et al. (2014) and Turner et al. (2016). In brief, the critical undercooling, ΔT_c is calculated at a different between equilibrium solubility temperature, T_e and at crystallisation temperature, T_{crys}.

$$\Delta T_c = T_e - T_{crys} \qquad 2.27$$

Then, the dimensionless relative critical undercooling, u_c can be defined by

$$u_c = \frac{\Delta T_c}{T_e} \qquad 2.28$$

The graph of $\ln u_c$ vs $\ln (R)$ resulted in straight line. If the slope is higher than 3, then it is a progressive nucleation, otherwise the nucleation is instantaneous if the slope is less than 3 (RULE OF THREE). In progressive nucleation, the forming of nuclei occurs at various temperature which resulting in different crystallite sizes. To proceed further, the inequalities $u_c < 0.1$ and $a u_c < 1$ must be met. Value a is defined as

$$a = \frac{\lambda}{\kappa T_e} \qquad 2.29$$

where λ is the molecular latent heat of crystallisation and κ is the Boltzmann constant. Next, is to solve the values of $\ln (R0)$ and a_2 from the equation:

$$\ln R = \ln R0 + a_1 \ln u_c - \frac{a_2}{(1 - u_c) u_c{}^2} \qquad 2.30$$

where the value of $a_1 = 3$. This can be solved via least square method. Lastly, the interfacial energy γ_{eff}, the radius of critical nucleus r^*, and the molecular number of critical nucleus i^* can be calculated from the following equations:

$$a_2 = \frac{k_n v_0{}^2 \gamma_{eff}{}^3}{\kappa T_e \lambda^2} \qquad 2.31$$

$$r^* = \frac{2\gamma_{eff} v_0}{\lambda u} \qquad 2.32$$

$$i^* = \frac{2a_2 \kappa T_e}{\lambda u^3} \qquad \text{2.33}$$

where k_n is the nucleus shape factor, and v_0 is the molecular volume in the crystal.

2.5.3 Induction Time Measurements

Nucleation rate can be expressed as

$$J = A\, exp\left(-\frac{16\pi\gamma^3 v_m^2}{3\kappa^3 T_n^3 (ln\, S)^2}\right) \qquad \text{2.34}$$

where A is the pre-exponential factor, γ is the interfacial energy, v_m is molar volume, K is the Boltzmann constant, T_n is the nucleation temperature and S is supersaturation. The induction time is in general inversely proportional to nucleation rate.

$$t_{ind} \propto \frac{1}{J} \qquad \text{2.35}$$

Substituting Equation 2.35 into Equation 2.34 resulted in

$$t_{ind} = K + \frac{16\pi\gamma^3 v_m^2}{3\kappa^3 T_n^3 (ln\, S)^2} \qquad \text{2.36}$$

The graph $ln(t_{ind})$ against $1/(ln\, S)^2$ at constant temperature give a straight line with a gradient,

$$m = \frac{16\pi\gamma^3 v_m^2}{3\kappa^3 T_n^3} \qquad \text{2.37}$$

The interfacial energy is then calculated following the formula:

$$\gamma = \left(\frac{3m\kappa^3 T_n{}^3}{16\pi v_m{}^2}\right)^{\frac{1}{3}}$$

<div align="right">2.38</div>

the critical size nucleus is defined as:

$$r^* = \frac{2v_m\gamma}{\kappa T \ln S}$$

<div align="right">2.39</div>

and the molecular number of critical nucleus is defined as:

$$i^* = \frac{4\pi r^{*3}}{3v_m}$$

<div align="right">2.40</div>

2.6   Co-Crystal

Co-crystals were defined differently depending on view point (Braga et al., 2013; Childs & Zaworotko, 2009; Dunitz, 2003; Ghadi et al., 2014; Stahly, 2007). In general, co-crystals are crystalline materials that contain more than one component (i.e. multicomponent crystals) in definite stoichiometric amounts (Ghadi et al., 2014). According to the U. S. Food and Drug Administration (2013) guidelines, which is the standard definition of co-crystals are defined as "solids that are crystalline materials composed of two or more molecules in the same crystal lattice." The reason for the construction of co-crystals is to modify the physicochemical properties of active pharmaceutical ingredient (API) by combining API and additional components (i.e. co-formers) in the same crystal structure thereby altering solid-state properties and solution behaviour without modifying chemical structure (Childs & Zaworotko, 2009). The co-crystals are known as pharmaceutical co-crystals if one of the constituents is a pharmaceutically active ingredient (Dunitz, 2003).

2.6.1 CBZ-SAC Co-Crystal

2.6.1.1 Structure and polymorphs of carbamazepine (CBZ)

Carbamazepine is an active pharmaceutical ingredient used in the treatment of epilepsy and trigeminal neuralgia. CBZ has strong hydrogen bonding among its polymorphs and have a nearly identical molecular conformation. Figure 2.9 shows the chemical structure of carbamazepine. At least four polymorphs and a dehydrate of CBZ, have been described in the literature (O'Mahony et al., 2012). Among those, CBZ Form III with C-monoclinic form is the most stable known anhydrous form in room conditions. All four polymorphs have density range between 1.24 g/cm^3 and 1.34 g/cm^3. Based on rule of density, polymorph with high density is most stable, in which at 0 K, its compound lacking strongly directional intermolecular interactions (Gadamasetti, 2007). Thus, CBZ Form III, which has density of 1.34 g/cm^3 is the most stable form of CBZ polymorph at room temperature. The melting points of the four polymorphs have been reported to be in the range 175-190 °C (Pinto et al., 2014). Forms I and III of CBZ are an enantiotropic pair with transition temperature of 185 °C (Byrn et al., 2017). If Form III is heated above 185 °C, the form will be converted to Form I. Figure 2.10 shows the polymorph of CBZ.
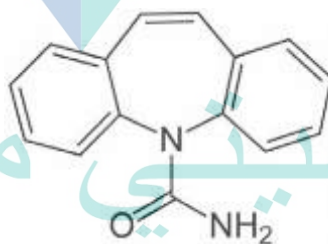
Figure 2.9   Structure of carbamazepine (CBZ).
Source: Pinto et al. (2014).
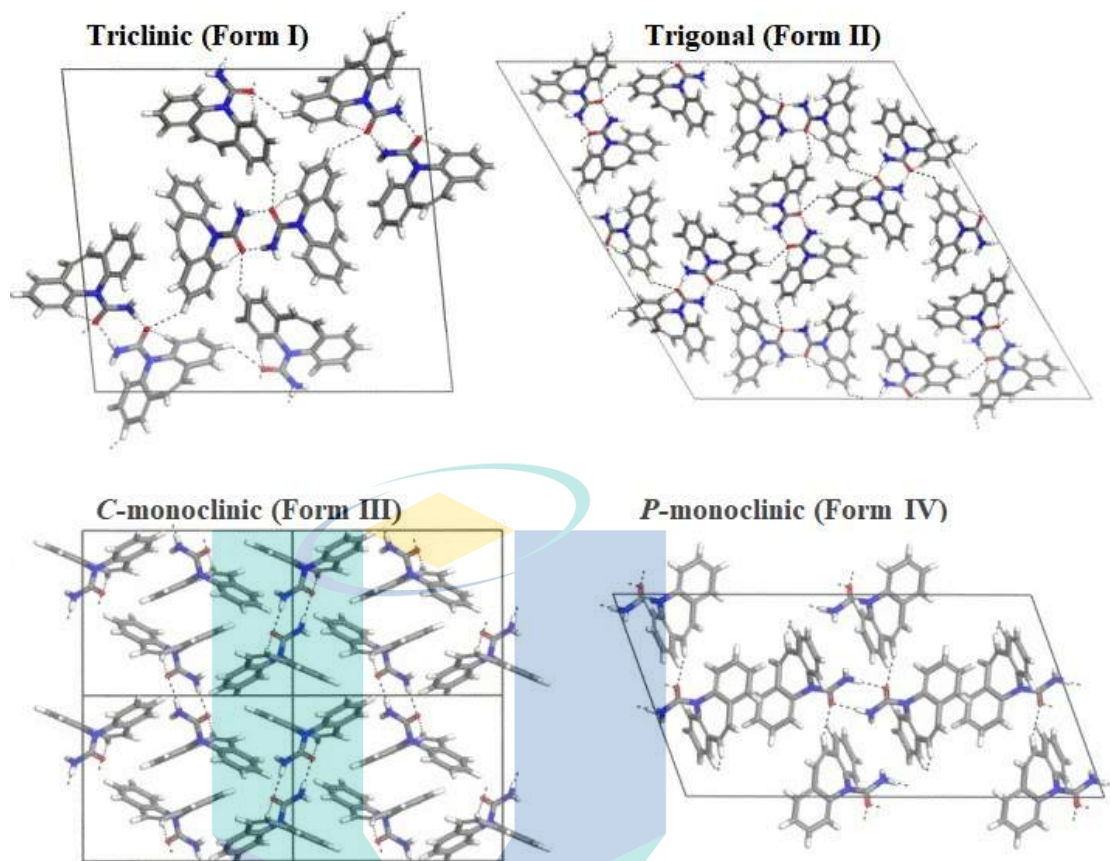
Figure 2.10   Polymorphs of carbamazepine (CBZ).
Source: Rodr guez-Spong et al. (2004).

2.6.1.2   Saccharin

Saccharin is a condensed heterocyclic o-sulfobenzimide, discovered in the late 1870s by chemists in the USA. It is commercially available in four forms: acid saccharin, sodium saccharin, potassium saccharin and calcium saccharin. Sodium saccharin is the most commonly used form because of its high solubility, stability, and low production costs (O'Mullane et al., 2014). Saccharin (molar mass=183.18 g mol−1) is widely used as co-former in the preparation of pharmaceutical salts (acting as a weak acid when combined with a sufficiently basic molecule), or co-crystals (remaining then a neutral molecule) (Cuadra et al., 2018). SAC has one known polymorph (Bart, 1968) and good water solubility (Pagire et al., 2013). Figure 2.11 shows molecular structure of saccharin.

28
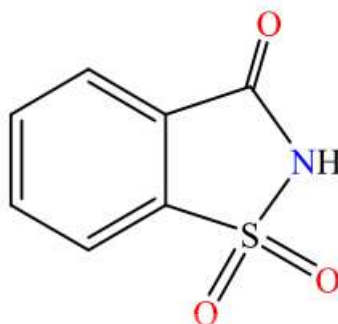
Figure 2.11   Molecular structure of saccharin (SAC).

Source: Cuadra et al. (2018).

2.7   Co-Crystal Formation Methods

Many protocols for the co-crystal formation have been established. Formation methods based on solution and grinding have been the most regular choice among the researchers (He et al., 2008). Solution methods include evaporation of a hetero metric solution method, reaction crystallisation method, and cooling crystallisation. Grinding methods comprise of neat grinding and solvent drop grinding. Other methods that have been established are co-crystallisation using supercritical fluid, hot-stage microscopy, and ultrasound assisted co-crystallisation.

2.7.1   Solution Methods

2.7.1.1   Evaporation Co-Crystallisation

In this method solvents are used to saturate the co-crystal consistently so that the compounds will have a common solubility. Two co-crystal components A and B have similar solubilities in a solvent S and the 1:1 pure co-crystal can be formed when equimolar components are dissolved in the solvent by evaporation (Abd Rahim, 2012).

2.7.1.2   Reaction Crystallisation (RC)

Reaction co-crystallisation (RC) is for components that have non-equivalent. By this method crystallising a single reactant can be avoided. RC experiments are performed

by adding reactant B to a saturated or close to saturated solution of reactant A and then the solution becomes supersaturated with respect to co-crystal AB (Tahti et al., 1999).

2.7.1.3   Cooling Crystallisation

In this method, co-crystal is formed by manipulating the temperature of the solution. By using a reactor or a jacketed vessel, the components and solvent are mixed and heated to a higher temperature to make sure all solutes are totally dissolved in the solvent and is followed by a cooling down step. Co-crystals will precipitate when solution becomes supersaturated with respect to co-crystal as the temperature drops. Through analysing the kinetic pathways and supersaturation levels of the components, it is possible to determine the optimal operating conditions for a cooling co-crystallisation process (Abd Rahim, 2012; Lewis & Olsen, 2007).

2.7.2   Grinding Method

There are two different techniques for co-crystal formation via grinding. The first method is neat grinding, which is also called dry grinding, consisting of mixing the stoichiometric co-crystal components together and grinding them either manually, using a mortar and pestle, or mechanically, using a ball mill or a vibratory mill. This method requires one or both reactants exhibiting significant vapour pressures in the solid state (Friščić & Jones, 2010). The second technique for co-crystal synthesis via grinding is that of liquid-assisted grinding (also referred to as kneading, solvent drop, wet co-grinding). Significant improvements in kinetics of co-crystal formation by grinding can be achieved by the addition of minor amounts of an appropriate solvent (Shan et al., 2002). The improvements in kinetics might be rationalised by the additional degrees of orientational and conformational freedom open to molecules at the various interfaces as well as the enhancement of opportunities for molecular collisions (Trask et al., 2004). In addition, tiny co-crystal seeds may be envisaged to form within the solvent during the grinding process so that the rate of co-crystallisation can be increased.

2.7.3   Supercritical Fluid Atomization Process

Supercritical fluids use offers additional advantages compared to the classical co-crystal production methods. Co-crystallization with supercritical solvent (CSS) is a method where an API and a co-crystal former are mixed together by magnetic stirring after being pressurized by supercritical CO_2 in a high-pressure vessel. Supercritical Anti-Solvent (SAS) technique explores the anti-solvent effect of supercritical CO_2 to precipitate particles (co-crystals) from solutions; the supercritical fluid enhanced atomization SEA technique explores essentially the CO_2 atomization enhancement in a spray drying process (Pando et al., 2016).

2.8   Co-Crystal Properties

There are many advantages of co-crystals. Major one is good change in physico-chemical properties such as solubility, dissolution, chemical stability, hygroscopicity, bioavailability, hydrate/solvate formation, crystal morphology and mechanical properties. Possible changes in physico-chemical properties of the cocrystal are due to design and formation of the cocrystals which lead to the alteration in the molecular interactions. Some properties of the co-crystals are listed in the next section.

2.8.1   Solubility

Solubility of the co-crystal is largely dependent on concentration and amount of the individual components (drug and co-former) (Ghadi et al., 2014). The solubility of the co-crystal is much lower than the combination of the individual components, when the co-crystal formed is more stable (high stability) than the individual constituents. Besides, the solubility of the co-crystals will be pH dependent, if one of both of drug and co-former are ionisable (Lipert & Rodríguez-Hornedo, 2015).

2.8.2 Dissolution

Like solubility, dissolution rate of co-crystals largely depends on co-former selection. By adding varieties of co-formers to the API drug to produce co-crystals, the dissolution rates are also increased. For instance, the curcumin cocrystals with the co-formers of Resorcinol and Pyrogallol have the dissolution rates five and twelve times higher than pure Curcumin respectively (Cysewski & Przybyłek, 2017). Another example is that, according to Ghadi et al. (2014) dissolution rate of indomethacin-saccharin co-crystal in 200mM phosphate buffer (pH 7.4) is fifty times higher than the corresponding drug, γ- indomethacin, the most stable polymorph.

2.8.3 Chemical Stability

Alteration of chemical stability of the co-crystals is due to changing of the molecular arrangement in crystalline lattice (Gadade & Pekamwar, 2016). For example, photodegradation occurs to pure API such as carbamazepine, in which the degradation is based on distance between azepine rings in chemical structure. By adding co-former such as saccharin, the azepine rings between CBZ molecules become long enough (more than 4.1 Å) to prevent the photodegradation to occur (Ghadi et al., 2014).

2.8.4 Hygroscopicity

Hygroscopy is the reaction when crystals interact with water possibly via adsorption on the surface, absorption and hydrate formation. Pharmaceutical co-crystals can prevent hydrate and solvate formation in APIs. For instance, anhydrous carbamazepine can easily transform to dihydrate form, CBZ(D) in presence of high relative humidity. Whereas drug carbamazepine with co-formers saccharin and nicotinamide show greater stability against CBZ(D) transformation by showing no hydrate formation after 3 weeks storage at 98% and 100% relative humidity respectively (Ghadi et al., 2014). Thus, it alters the hygroscopicity of API. Other co-crystals such as caffeine and theophylline cocrystals with dicarboxylic acids have also shown similar behaviour.

2.8.5 Mechanical Properties

Mechanical properties such as tensile strength, breaking force and other elastic properties of the co-crystals were influenced by molecular interactions and crystal structure. Co-crystals have the layered structure, which can improve the ability to make a tablet of adequate mechanical strength by powder compaction (tabletability) and the elasticity of the co-crystals. For example, CBZ-SAC co-crystals have better tabletability when compared to pure form of CBZ, in which CBZ(D) and CBZ(III) required the least compaction pressure of 5000 psi for 30 minutes to form the tablet, whereas tablet from CBZ-SAC co-crystals can be formed with lower pressure and in shorter than 30 minutes time (Spong, 2005). Similar results found for caffeine - methyl gallate co-crystals, in which the caffeine cocrystal formed higher tensile strength than pure caffeine and pure methyl gallate at compaction pressures between 40 and 400 MPa (Sun & Hou, 2008).

2.9   Seeding in Crystallisation Process

2.9.1   Seeding

Seeding has been studied over the latest few decades because it can alter the properties of desired final crystal. In seeding process, the supersaturated solution was enhanced by addition of crystalline (seed) to allow the growth of the seed crystals prior to the occurrence of nucleation (Hattori et al., 2015). As co-crystallisation is concerned, an introduction of seeding is mean to provide a co-crystal phase in solution during crystal growth and to prevent inconsistent primary nucleation of another solid phase during crystallisation (Gagniere et al., 2012). By considering the different parameters in seeding process such as size of seed, amount of seed, seeding temperature and cooling profile, seeding is therefore believed can expedite the nucleation process, optimise the crystallisation behaviour and ensure the final particle size (Aamir et al., 2010).

2.9.2   Seeding Parameters

2.9.2.1   Seeding Temperature

Addition of seed in crystallisation process is required to shorten the induction time, narrowing the metastable zone width (MSZW), to control the crystal size distribution (CSD) or specifically to reduce the size of broadening the CSD. The time of seed to be added of seeding temperature will reflect the result of CSD. If seeds were added too early, the seed will dissolve in that undersaturated solution. If the seeds were added too late, the secondary nucleation might occur already, in which solute material may have crystallised due to the high supersaturation level. Thus, resulted to the undesired crystal characteristic of the crystal's product. The example of the effect of seeding temperature on the CSD was shown by O'Sullivan, Smith, & Baramidze (2012) and Zhang, Liu, Huo, Guan, and Wang (2016) as listed in the Table 2.2 and Figure 2.12.

Figure 2.12(a) shows the result of seeding experiment of β-LGA crystal by Zhang et al. (2016). The seed of 58-106 μm was added at seeding temperature of 35, 45 and 55 °C. The results showed that, when seed was added at high seeding temperature, the length and width of crystal products increased, and the crystal size distribution became wide. Figure 2.12(b) shows the result of seeding experiment of an organic compound crystallized from water by O'Sullivan et al. (2012). It illustrated that, the nucleation rate increased at low seeding temperature, particle growth reduced, and more fine particles were produced.

Table 2.2   Effect of seeding temperature on CSD from literatures.

Author	(Zhang et al., 2016)	(O'Sullivan et al., 2012)
Compound	β-LGA crystal	an organic compound crystallized from water
Parameter	Seed size range (58-106 μm) Cooling rate (°C/min) = 0.2 Initial supersaturation = 1.2 Seeding temperature (°C) = 35, 45, 55	Amount of seed = 0.25g Cooling is at a fixed linear rate. Seeding temperature (°C) = 20, 22.5, 25
Results	At high seeding temperature increases the length and width of crystal products and widens the CSD.	Low seeding temperature increases nucleation rate, reduces particle growth and results in more fine particles.
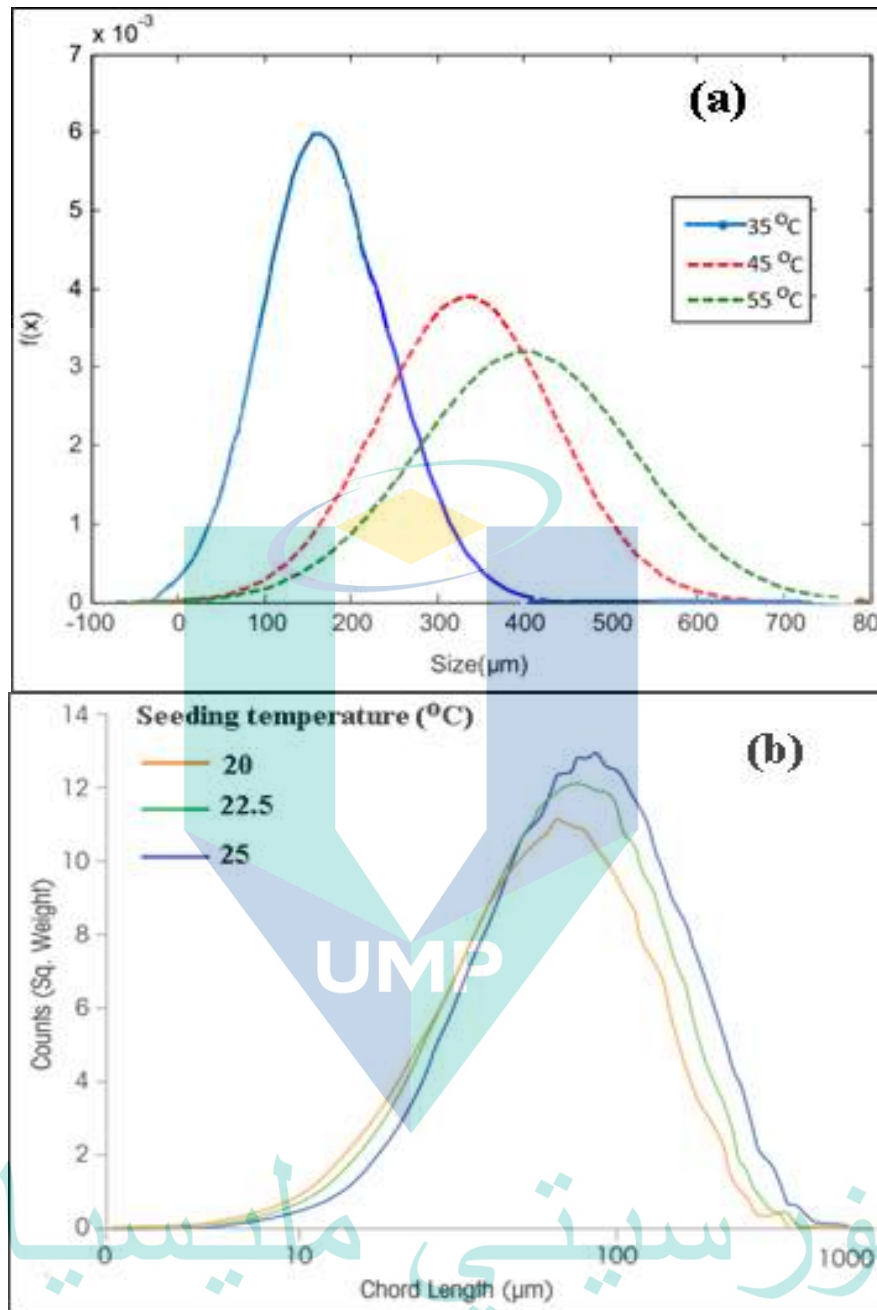
Figure 2.12   Effect of seeding temperature on CSD
(a) Source: Zhang et al. (2016) and (b) Source: O'Sullivan et al. (2012).

2.9.2.2   Seed Load

Seed load is similar as seed surface area indicates the rate at which supersaturation is consumed by the growing homogeneous seeds. Seed load applied to prevent the secondary nucleation to occur. The ratio between seed mass and the crystal yield determines the seed load. In industry, the level of seed loading is normally between 0.5 wt% and 10 wt% (Doki, 2002). High seed loading ratios result in unimodal product CSD. Normally, high seed loading leads to a decrease in mean crystal size, but for silica as heterogeneous seeds, increase in seed load leads to an increase in mean crystal size and CSD (Hayles-Hahn, 2014). The effect of seed loading was described by Hayles-Hahn using silica from Tetraethylorthosilicate (TEOS). Four different silica seed loading (0.25, 0.5, 1.0 and 3.0 wt%) were compared as can be seen in Figure 2.13. The increase in CSD with high seed loads is most clearly observed in a comparison of the 0.25 wt% seeded batch CSD with the 3.0 wt%.
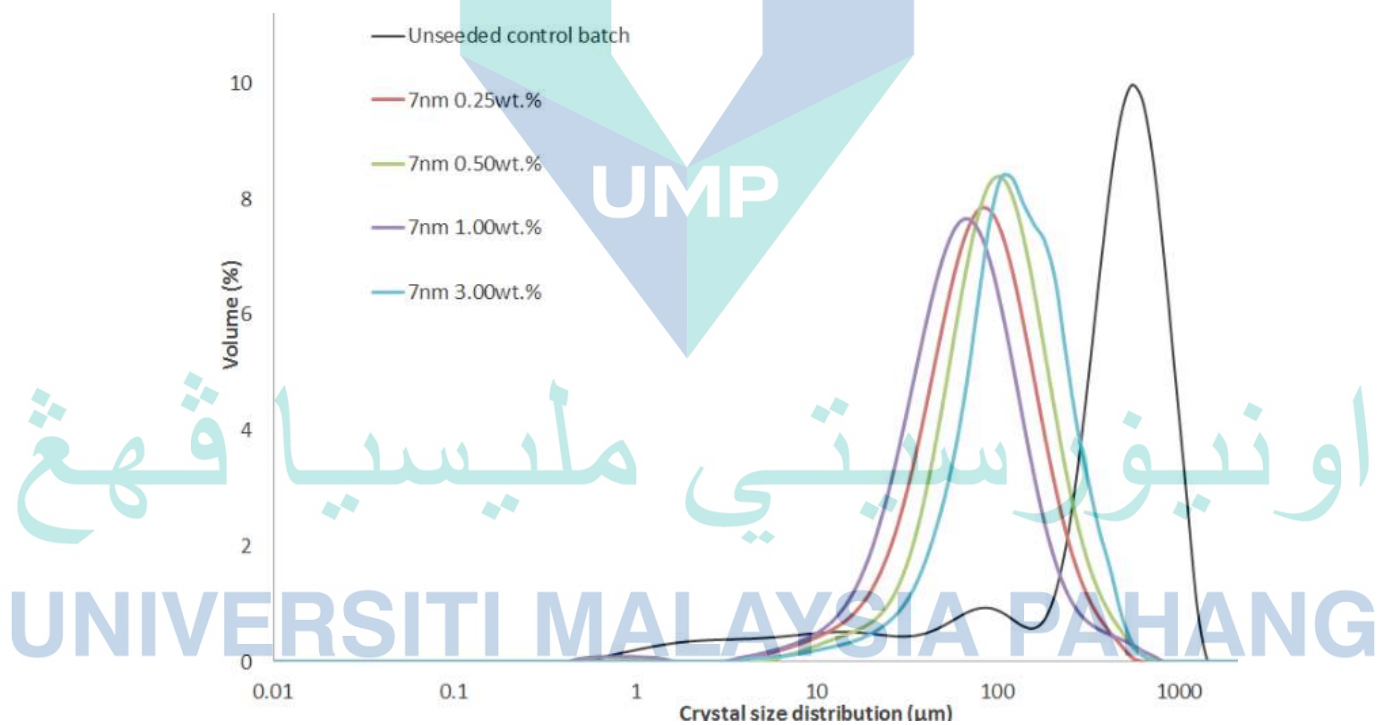
Figure 2.13   CSD of silica at different seed loading.
Source: Hayles-Hahn (2014).

Seed mass is proportional to the surface area of seed crystals and their size. In the ideal case, when the secondary nucleation is suppressed, the number of crystals

36

introduced with seeding should result in the same number of product crystals (Chianese & Kramer, 2012a). Narducci (2012) compares product particle size distributions at three different values of seeding load from cooling crystallization of adipic acid (AA) (Figure 2.14). The cooling speed was constant (0.5 K/min) with initial concentration of 5 g AA/100 g water from 45 ºC to 20 ºC. At low seed loading (1% and 5%), the CSD is widespread and bimodal. The crystals are largely produced by agglomeration and from grown seed crystals, while some crystals generated by secondary nucleation. At 1% seed loading, secondary nucleation occurred due to the bimodal size distribution. High seed load resulted in high presence of fines, which is due to the agglomerative phenomena of fine particles.
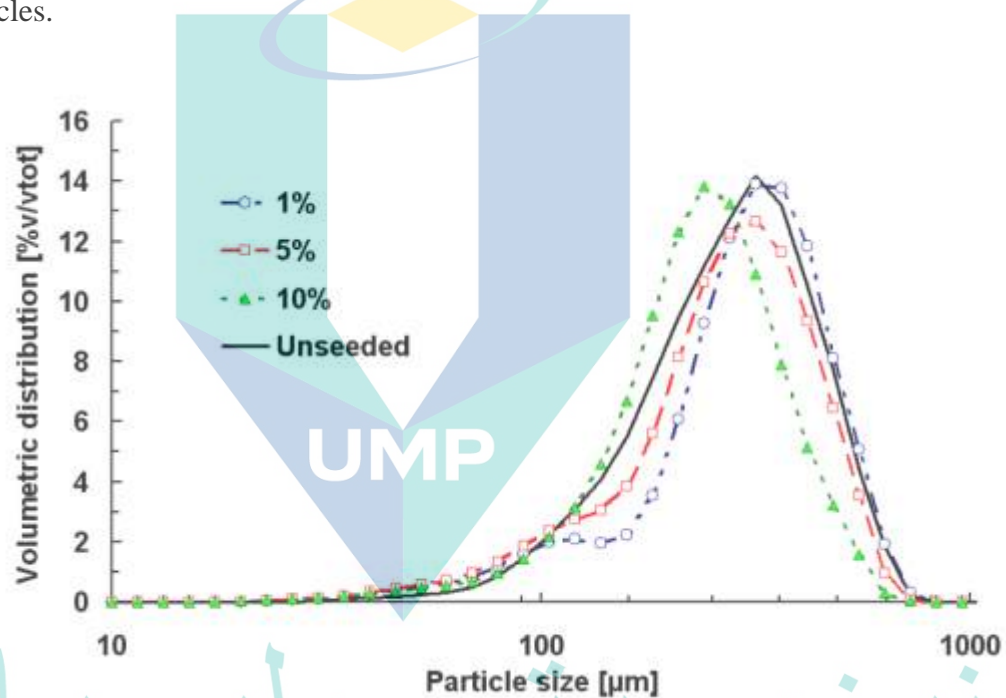
Figure 2.14   Effect of seed loading on CSD.
Source: Narducci (2012).

Another author, Powell (2017) discussed the effect of seed loading (3.5 and 7.0 wt%) on size of product crystals of paracetamol (PCM) from water. Figure 2.15 shows that, the crystal products from seed loading of 3.5 wt% are larger compared with 7.0 wt%. This shows that the amount of seed influences the nucleation and growth kinetics of the system, whereby low seed loading, crystals formed by growth of crystals rather than secondary nucleation.
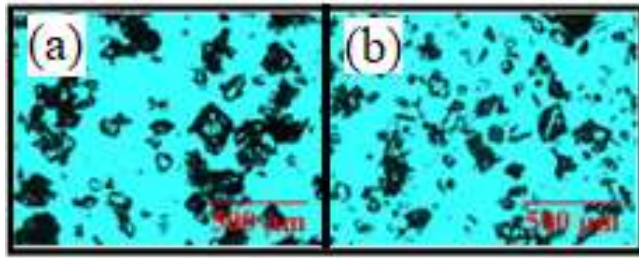
Figure 2.15   Images of PCM product crystals under microscope with seed loading of (a) 3.5 wt%, and (b) 7.0 wt%.

Source: Powell (2017).

Eder et al. (2010) showed in their study that increasing seed loadings resulted in decreased differences between the mean seed and product crystal sizes. This is attributed to the fact that more particles are introduced into the system which leads to increased competition to consume the same amount of supersaturation available.

2.9.2.3   Seed Size

A small seed size provides a large specific surface area for the crystal growth process. An increased surface area results in an increase in supersaturation depletion rate. As a result, supersaturation decreases and the time for nucleation also decreases. In industrial application. small seeds can cause problems such as possibility to agglomerate, difficult preparation and slow growth. Therefore, using of seed size of less than 100 µm is avoidable (Chianese & Kramer, 2012a). The seeds should also be not too large as the required seed mass can be uneconomically large with respect to the process yield. Critical seed size between 200 – 500 µm was enough to produce nuclei in saturated solutions. Seed crystal size is believed to have a significant impact on secondary nucleation. The bimodal distributions in the graph of CSD indicate that significant secondary nucleation. larger crystals cause more secondary nucleation than smaller ones.

2.10   Summary

In the pharmaceutical industry, co-crystals were introduced to improve the physicochemical properties of active pharmaceutical ingredient such as chemical stability, moisture uptake, mechanical behaviour, solubility, dissolution rate, and bioavailability. CBZ is a favourable model in studying of crystal polymorphism due to its five different anhydrous polymorphs. To date, the kinetics of CBZ-SAC co-crystals with enhanced pharmaceutical properties has been poorly characterised. One of the main challenges in the production of CBZ-SAC co-crystals is to identify the metastable zone width, a region in which the supersaturation can be controlled to get the desired co-crystal properties. The kinetics of CBZ-SAC co-crystals can be obtained via slow and fast cooling methods. Furthermore, KBHR method, which reduces the steps in obtaining nucleation kinetics can be applied in co-crystals production. Also, several factors that can affect the nucleation process, such as cooling rate, concentration of compound, ratios between API and co-former and additional of seeds are important to be studied. Finally, the characterisation of the co-crystal needs to be obtained to ensure that the most stable Form I co-crystal are produced.

CHAPTER 3

MATERIALS AND METHODS

3.1   Introduction

This chapter details out the materials and laboratory experimental methods used in this study. The experimental laboratory works performed in this study were divided into three major parts. Section 3.5 and Section 3.6 describes the slow cooling experiments where the effect of cooling and heating rates , SAC/CBZ mole ratios and CBZ concentration on metastable zone width (MSZW) were investigated. From the results, solubility and super-solubility curves were constructed, followed by calculation of nucleation order and nucleation kinetic constant of CBZ-SAC co-crystals. An improved method for determination of dissolution temperature were introduced in this section. Section 3.7 describes the fast cooling experiment of CBZ-SAC co-crystals. The experiments were conducted based on the optimisation of parameters in cooling experiment. In this section, induction time, the radius of the critical nucleus and interfacial energy were calculated. The interfacial energy, critical size nucleus and molecular number of critical of different CBZ concentrations were obtained using Kashchiev–Borissova–Hammond–Roberts (KBHR) method and the results were compared with fast cooling experiments. The details of KBHR method was explained in literature review (Section 2.5.2). Section 3.8 describes the seeding experiment, in which preparation of seed and seeding experiments with different seeding temperature, seed loading and seed size were presented. From this experiment, the crystal size distribution (CSD) of CBZ-SAC co-crystals were constructed using Malvern Mastersizer. Furthermore, the characterisation of CBZ-SAC co-crystal properties using DSC and XRD were done for samples obtained from slow cooling, fast cooling and seeding experiments. The flowchart of research work is provided in Figure 3.1.

- Cooling/heating rate (0.8, 0.6, 0.4, 0.2 ºC/min)
- Determination of cooling temperature
- Determination of dissolution temperature - new technique
- CBZ concentrations (19.14, 17.96, 17.01 and 15.83 mg/ml), mol ratio of SAC to CBZ (3.5, 3.0, 2.5, 2.0, 1.0)
- MSZW and nucleation order are analysed

Slow cooling experiment

- Based on results from slow cooling
- cooling rate (1.0 and 1.2 °C/min)
- Determination induction time, the radius of the critical nucleus and interfacial energy
- temperature within a metastable region (28, 30, 32,34 and 36 °C)

Fast cooling experiment

- Based on results from slow cooling
- Calculation method to determine radius of the critical nucleus and interfacial energy
- Comparison of results from fast cooilng

KBHR method

- Determination induction time, the radius of the critical nucleus and interfacial energy
- temperature within a metastable region (28, 30, 32,34 and 36 °C)
- DSC, powder XRD and Malvern Mastersizer

Seeding experiment

Figure 3.1   Flowchart of research methodology presented in this thesis.

3.2   Materials

Carbamazepine (CBZ) and Saccharin (SAC) were obtained from ECA Corporation USA and Sigma Aldrich, respectively. The solvent used in co-crystals production was an absolute ethanol (EtOH 99.4 %), which was purchased from Fisher Scientific.

3.3   Experimental Setup

Crystalliser with jacketed vessel (Syrris Ltd, Royston, Hertfordshire, United Kingdom) was employed in this work, as seen in Figure 3.2. In this study, the 250 ml vacuum jacketed vessel was equipped with a stirrer, a turbidity probe, and a valve for draining purpose. An analysis software (Globe Reactor Master PC) was connected for automated control and analysis of the operations. Temperature in the jacketed vessel was adjusted via JULABO CF41 circulator, which has an operating temperature between -40ºC to +200ºC. The turbidity sensor was calibrated before each experiment as 100% for a suspension of CBZ-SAC co-crystals and 0% for a clear solution.
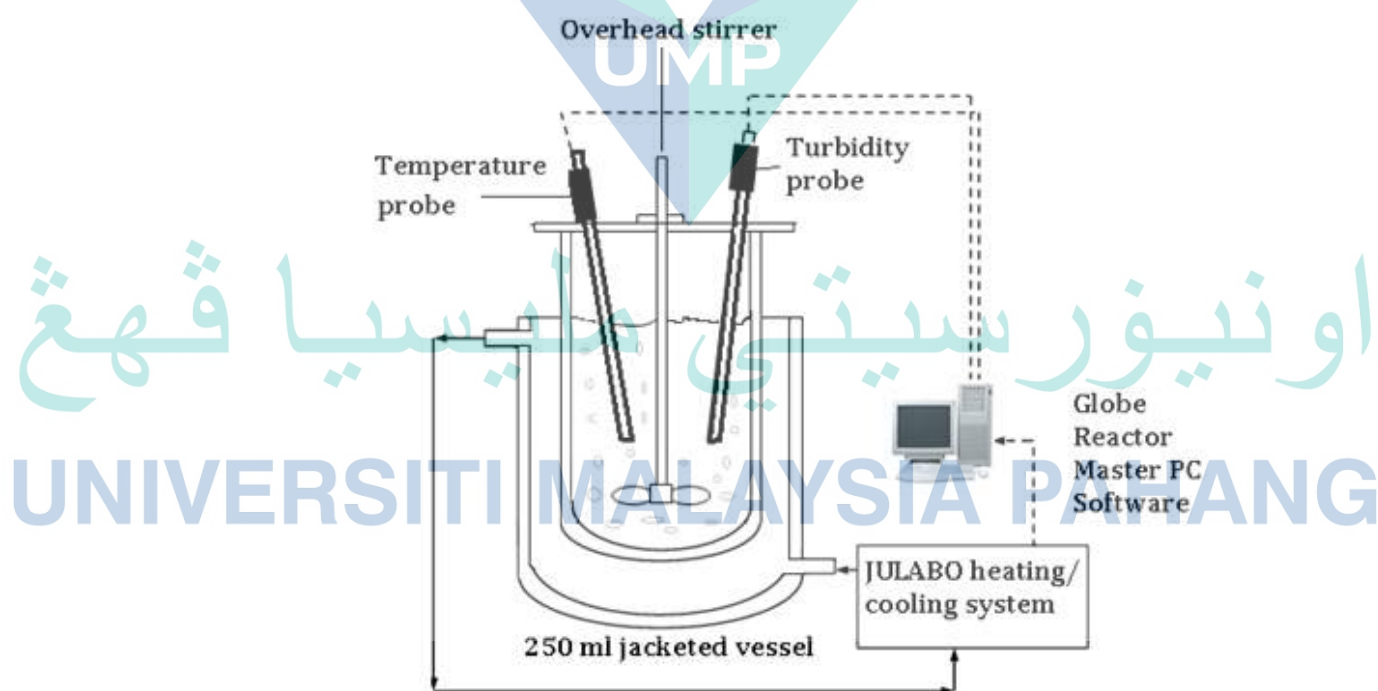
Figure 3.2   Setup of experiment for slow and fast cooling test.

3.4   Crystalliser Calibration and Testing

3.4.1   Turbidity Calibration

Turbidity reader was tested by using two-point calibration. The calibration was done before each experiment to get consistent results of turbidity value. First, the motor was set for the calibration, and the turbidity probe was taken out from the crystalliser. For 0% turbidity, the probe was place in a distilled water, which mean the solution is clear. For the 100% turbidity, the black standard rubber plate was place between the 2 sensors of turbidity, which mean that the solution is fully dark, or in respect to the crystallisation process, this mean the crystal was formed in the solution.

3.4.2   Stirrer Speed Determination

To avoid formation of vortex in the vessel, the stirrer speed must be adjusted accordingly. 200 ml ethanol was added in crystalliser. At the beginning, stirrer speed was set to 400 rpm (fast speed) and was reduced gradually by 20 rpm until it reached zero rpm. The movement of the solution was seen using naked eyes and recorded for each stirrer speed. The fastest stirrer without formation of vortex was chosen for remaining experiments.

3.4.3   Cooling and Heating Rates Determination

200 ml ethanol was added into crystalliser. Carbamazepine and Saccharin with (SAC/CBZ) mole ratio of 2.0 and CBZ concentration of 17.96 mg/ml were added into the solution. Mixture was stirred at 300 rpm continuously while heated to 60 °C. The mixture was kept at 60°C for few minutes until the solid was fully dissolved. Using Syrris crystalliser, only target temperature and time of cooling or heating can be set. Several experiments (Table 3.1) have been done to identify the capability (maximum cooling/heating rate) of the crystalliser to reach the target temperature in required time.

Table 3.1   Experiments to identify the optimum cooling / heating rate with starting and target temperature of 60 and 20 $^{\circ}$C respectively.

Exp. no.	Calculated cooling rate ($^{\circ}$C/min)	Calculated time to reach Target Temp. (min)	Real (measured) time to reach Target Temp. (min)	Target cooling rate achieved?
1	2.0	20.0	27.8	no
2	1.8	22.2	28.2	no
3	1.6	25.0	29.4	no
4	1.4	28.6	30.2	no
5	1.2	33.3	33.3	yes
6	1.0	40.0	40.0	yes

3.5   Preliminary Experiments (Slow Cooling)

In preliminary experiments, 12 set of experiments with different (SAC/CBZ) mole ratios, CBZ concentrations were conducted (Table 3.2). Each experiment was repeated 3 times to get the consistency of the results. As example for experiment No. 1, 3.83 g CBZ and 10.39 g SAC were added into crystalliser with 200 ml ethanol. The mixture was stirred continuously for the whole experiment with propeller at 300 rpm. The mixture was heated to 60°C, which is higher than dissolution temperature for 40 minutes to make sure that the solid was fully dissolved. The mixture solution was afterward cooled at a rate of 1.0 °C /min to a temperature T_2, which is 2-3 °C lower than the crystallisation temperature T_{crys1}. The temperature, in which the turbidity started to increase, serves as crystallisation temperature T_{crys1} of the co-crystal. The solution was again heated to 60°C and left for 40 minutes to get the complete dissolution of solid. The steps were repeated with a new cooling rate (0.75, 0.5, and 0.25 °C/min) to obtain the crystallisation temperature (T_{crys2}, T_{crys3}, T_{crys4}) of the co-crystal. CBZ concentration between 15.83 and 19.14 mg/ml and SAC/CBZ mole ratio between 1.0 and 3.5 were used in this study based on previous research by Abd Rahim (2012).

Table 3.2   Set of experiments for preliminary research in determining crystallisation and dissolution temperatures of CBZ-SAC co-crystals.

Exp. No	(SAC/CBZ) mole ratio	CBZ Conc. (mg/ml)	Amount of CBZ (g)	Amount of SAC (g)	Cooling / heating rate (ºC/min)
1	3.50	19.14	3.83	10.39	1.00, 0.75, 0.50, 0.25
2	3.50	17.96	3.59	9.75	1.00, 0.75, 0.50, 0.25
3	3.50	17.01	3.40	9.23	1.00, 0.75, 0.50, 0.25
4	3.50	15.83	3.17	8.59	1.00, 0.75, 0.50, 0.25
5	3.00	19.14	3.83	8.90	1.00, 0.75, 0.50, 0.25
6	3.00	17.96	3.59	8.35	1.00, 0.75, 0.50, 0.25
7	3.00	17.01	3.40	7.91	1.00, 0.75, 0.50, 0.25
8	3.00	15.83	3.17	7.36	1.00, 0.75, 0.50, 0.25
9	2.50	19.14	3.83	7.42	1.00, 0.75, 0.50, 0.25
10	2.50	17.96	3.59	6.96	1.00, 0.75, 0.50, 0.25
11	2.50	17.01	3.40	6.59	1.00, 0.75, 0.50, 0.25
12	2.50	15.83	3.17	6.14	1.00, 0.75, 0.50, 0.25

3.6   Slow Cooling of CBZ-SAC Co-Crystal

Different mol ratios (3.5, 3.0, 2.5, 2.0 and 1.0) of SAC to CBZ with different concentrations of ethanol solutions containing 19.14, 17.96, 17.01 and 15.83 mg/ml CBZ in 200 ml ethanol were prepared. Four different heating and cooling rates (0.8, 0.6, 0.4, and 0.2 °C /min) were applied in the crystallisation experiments.

Initial suspension (3.5 SAC/CBZ ratio and 19.14 mg/ml CBZ in 200ml ethanol) was heated to 60°C, which is higher than dissolution temperature. The solution was cooled quickly until the crystals formed and heated up again to 60ºC. As can be seen in Figure 3.3, the stirred mixture was kept at 60°C for 40 minutes to make sure that the solid was fully dissolved. The mixture solution was afterward cooled at a rate of 0.8 °C /min to a temperature T_2, which is 2-3 °C lower than the crystallisation temperature T_{crys1}. The temperature, in which the turbidity started to increase, serves as crystallisation temperature T_{crys1} of the co-crystal. The solution was again heated to 60°C and left for 40 minutes to get the complete dissolution of solid. The steps were repeated with a new

cooling rate (0.6, 0.4, and 0.2 °C/min) to obtain the crystallisation temperature (T_{crys2}, T_{crys3}, T_{crys4}) of the co-crystal and then with the different ratios of SAC to CBZ.
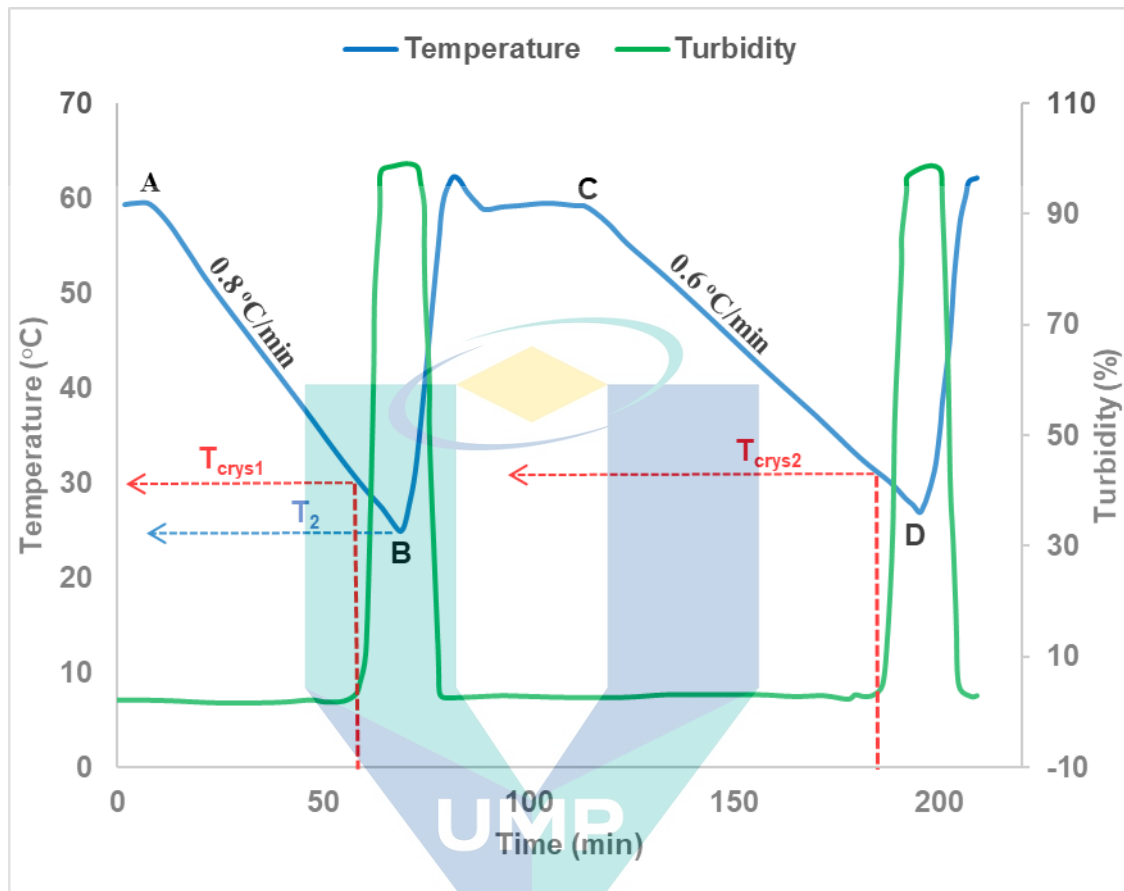
Figure 3.3   Method for determining the crystallisation temperature from the solution. Lines AB and CD are with cooling rate of 0.8°C/min and 0.6°C/min respectively.

There was some modification in the stage to determine the dissolution temperature T_{diss} by comparing with previous researchers (Bernardes & da Piedade, 2010; Bonnin-Paris et al., 2011; Camacho Corzo et al., 2014) as illustrated in Figure 3.4. The solution was dissolved at 60°C for 40 minutes and cooled with a fixed rate of 0.6 °C/min to a temperature T_b, which is 3°C lower than the crystallisation temperature T_{crys3}. The temperature T_b was kept constant for 40 minutes between point b and c. The solution was then heated with the different rate of (0.8, 0.6, 0.4, and 0.2°C/min). Different heating rates resulted in different dissolution temperatures (T_{diss1}, T_{diss2}, T_{diss3}, and T_{diss4}). Solution at point e, f and g follows the same profiles as point a, b, and c that resulted in the similar properties of co-crystal at a point c and g. Therefore, comparison can be done for the effect of different heating rate on MSZW.
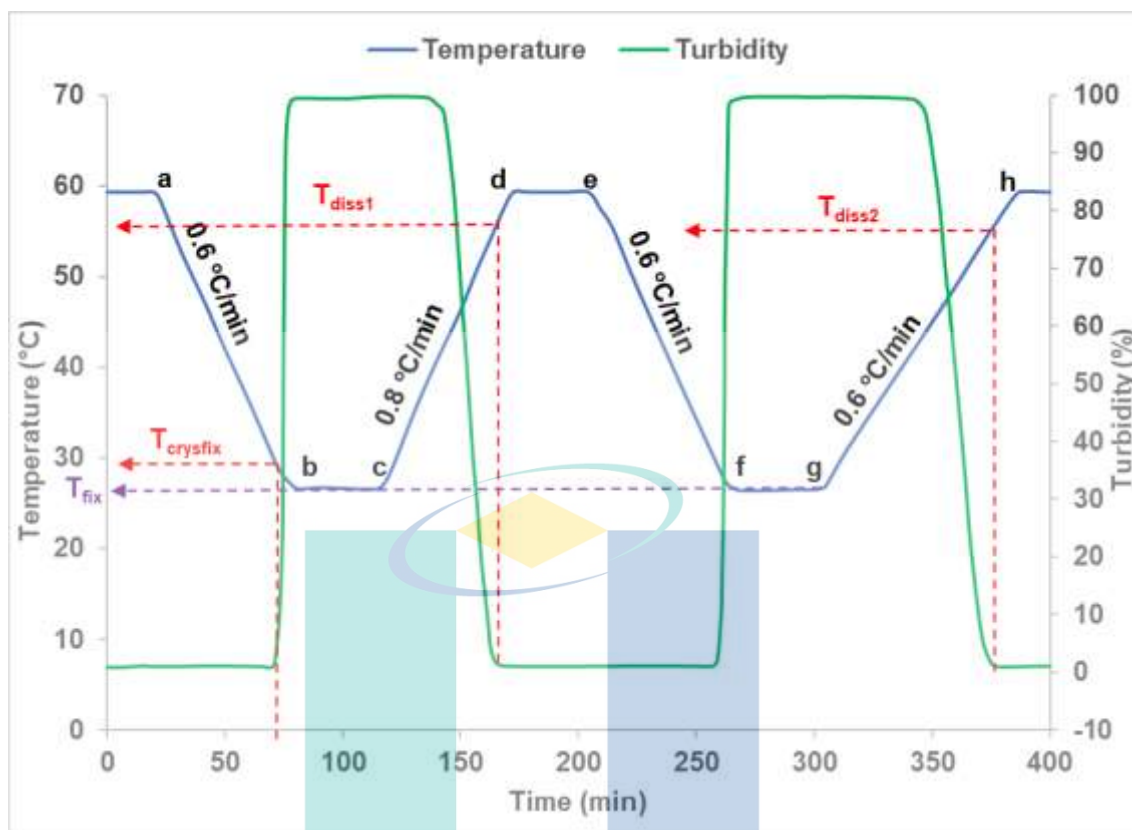
Figure 3.4   New approached method for determining the dissolution temperature of the crystal. Lines abc and efg have the same cooling rate and isothermal temperature. Lines cd and gh are with heating rate of 0.8°C/min and 0.6°C/min respectively.

3.7   Fast Cooling of CBZ-SAC Co-Crystal

Results from slow cooling experiment is further used in the fast cooling experiment. Crystal with CBZ concentration of 17.96 mg/ml and mol ratio (SAC/CBZ) of 2.0 is heated in 200 ml ethanol at 50°C for 40 minutes. The solution is cooled rapidly (line UV) until the crystal is formed (point V) and is heated again to 50°C and left for 40 minutes in order to ensure the complete dissolution of solids (line WX) which is also indicated by a decrease of turbidity (see Figure 3.5). Temperature of the solution is set to 28°C at a rate of 1 °C/min (line XY). Then the temperature is maintained until the crystal is formed. The time between point Y and Z (induction temperature until the forming of crystal) is recorded. The experiments were repeated at a cooling rate of 1.2 °C/min with different induction temperatures of 30, 32, 34, and 36°C. Each experiment was repeated at least three times to get the consistency of the results.

47
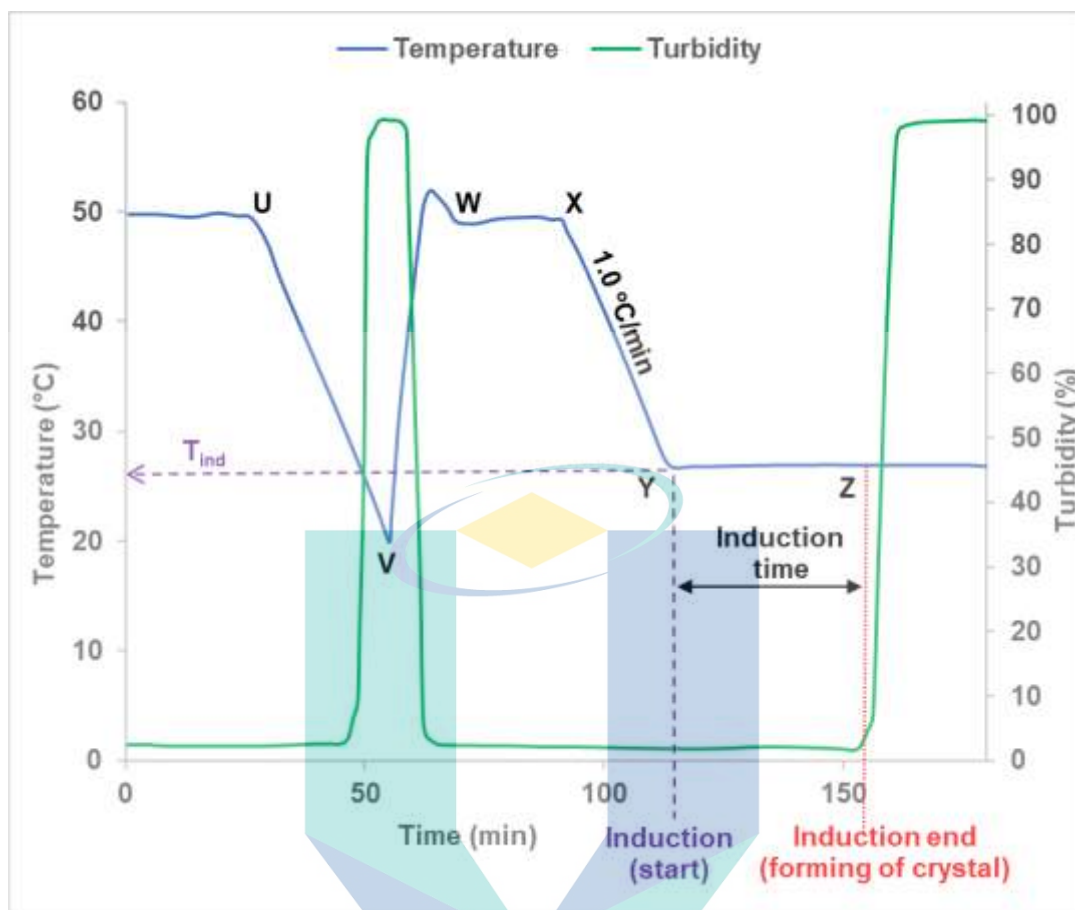
Figure 3.5   Temperature and turbidity profile of fast cooling experiment.

3.8   Seeding Process

3.8.1   Preparation of Sample and Sieve Analysis

The CBZ-SAC cocrystals with SAC/CBZ mole ratio 2.0 and CBZ concentration of 17.96 mg/ml produced from slow cooling experiment were taken as seed for seeding experiment. 20 minutes after the forming of nucleation in the crystalliser, the crystal was drained and filtered. The solid was dried for 60 minutes at 30°C. The produced seed crystal was then collected and sieved using ASTM standard sieve. The sieve of six different sizes from (RETSCH, Germany) were used. Six sizes of sieve were 250, 180, 150, 125, 106 and 63 µm. The sieves were arranged on the shaker in order of larger opening on the top and smaller opening at the bottom. The CBZ-SAC co-crystals were weight and put on the top of the sieve. The sieve shaker machine was run for 10 minutes. As example, the crystals remained on the sieve of 180 µm classified as crystal with the

48

size of bigger than 180 µm, because those seeds cannot pass through the sieve with mesh size of 180 µm. Finally, the CBZ-SAC co-crystals on each sieve was collected and weight.

3.8.2 Seeding Experiments

In this experiment, CBZ-SAC co-crystal solution was prepared, corresponding to a CBZ concentration of 17.96 mg/ml and mole ratio (SAC/CBZ) of 2.0, using a 250 ml jacketed crystallisation vessel equipped with thermocouple, stirrer, and turbidity probe. Seeding experiments can be seen in Figure 3.6. Firstly, the solution was heated to 50°C and the temperature was maintained for 20 minutes to obtain a clear solution (line TU). Then, the clear solution was cooled rapidly until the crystal was formed and was heated again to 50°C (line UVW). Then the temperature was held for 40 minutes to achieve complete dissolution of solids which can be shown by a reduction in turbidity value (line WX). After that, the temperature of the solution was brought down at a rate of 0.6°C/min until it hit the targeted seeding temperature, T_{seed} (line XY), which was shown in Table 3.3. When the temperature of the solution reached 46.56°C (95% of MSZW range), 0.5 wt% seed was added whilst the solution continued to follow the temperature profile with a rate of 0.6°C/min. Seeding temperature was quoted in percent based on MSZW range obtained from slow cooling experiment (section 3.6). Calculated seeding temperature in percent is shown in Table 3.3.

Table 3.3   Calculated seeding temperature (°C) based on percentage of MSZW

Seeding temperature (% of MSZW)	Calculated seeding temperature (°C) based on MSZW range of 47.55 to 27.84 °C), T_{seed}
95	46.56
85	44.59
75	42.62
65	40.65
55	38.68

Figure 3.6   Seeding experiment with 0.5 wt% of CBZ-SAC co-crystals at seeding temperature of 46.05°C.

Once the nucleation started (point Z), which can be indicated by the changes of turbidity value, the temperature was maintained for 20 minutes before the solution was drained and seed crystal was filtered and collected. The experiment was repeated with different temperature of seeding (85, 75, 65 and 55% of MSZW range) and different amount of seed loading (1.0 and 1.5 wt%). Each experiment of different seeding temperature and seed loading was repeated at least three times to get the consistent results. The number of the experiments can be seen in Table 3.4.

Table 3.4   Parameters for seeding experiment

Experiment no.	Seeding temperature (ºC)	Seed wt%
1	46.56	0.5
2	44.59	0.5
3	42.62	0.5
4	40.65	0.5
5	38.68	0.5
6	46.56	1.0
7	44.59	1.0
8	42.62	1.0
9	40.65	1.0
10	38.68	1.0
11	46.56	1.5
12	44.59	1.5
13	42.62	1.5
14	40.65	1.5
15	38.68	1.5

3.8.3   Crystal Size Distribution (CSD) of CBZ-SAC Co-Crystal

The crystal size distribution was obtained using laser scattering particle size analyser (Mastersizer 2000®, Malvern Instruments Ltd., Malvern, UK) equipped with Scirocco 2000 for dry particle at an air pressure of 3 bar. The particle size distribution was evaluated by cumulative distribution data. The median diameter was taken for evaluating the particle size of the seeded and unseeded CBZ-SAC cocrystals.

3.9   Characterisation of Co-Crystals Properties

3.9.1   Differential Scanning Calorimetry (DSC)

DSC is the most popular technique to determine the thermal property of co-crystals. It monitors the difference in melting point between sample and an inert reference material during heating and cooling cycle with a constant rate.   The DSC curve was obtained with the Y-axis as the differential rate of heat flow (in W/g) and the X-axis as temperature (in ºC). The peak was shown as melting, polymorphic transformation and crystallisation took place.

The thermal property of CBZ-SAC co-crystals was characterised by DSC model of TA- Instrument DSC/Q 1000 (V9.6, Build 290). A sample of the crystal (about 0.05g) was studied under a nitrogen purge and heated from 40°C to 200°C at a scanning rate of 10°C/min. The sample was placed in an aluminium pan and an empty pan was used a reference. The melting point, heat of fusion and the onset temperature were obtained.

3.9.2 X-ray Diffraction (XRD)

The phase compositions and crystallinity of the compounds were characterized and identified using XRD analysis. The data were collected using RIGAKU, model Miniflex II diffractometer equipped with Cu Kα radiation of (λ=1.54Å), a tube voltage of 40kV and a tube current of 100mA. Scanning was generally done between $3° < 2\theta < 40°$. The measurements were performed with continuous step size of 0.01 degree/s, and the step time of 1 second/step. The patterns or profiles of co-crystals were then obtained.

3.9.3 Malvern Mastersizer

Malvern Mastersizer 2000 particle size analyser was used to determine the particle size of CBZ-SAC co-crystal compounds obtained using sucrose, urea and water. Uniformity of particle size distribution and surface area of the samples could be also determined by the analyser. Measurement of sample using Malvern Mastersizer consist of three steps. At first, the sample was prepared and delivered to the optical bench. Then, the scattering pattern of sample was captured by detectors in optical bench. Standardly over 2000 snapshots of the scattering pattern were captured by detector for the representative reading. Finally, the raw data from the optical bench was analysed by Malvern software to calculate a particle size distribution (Malvern Instruments, 2007).

3.9.4 Sieve Shaker

The sieve shaker machine was used to sieve the seed crystals. Seven sieves with opening of 63, 100, 125, 150, 200, 425 and 500 μm were cleaned and weighted. The sieves were arranged on the shaker in order of larger opening on the top and smaller opening at the bottom. The CBZ-SAC co-crystals were weight and put on the top of the sieve. The sieve shaker machine was run for 10 minutes. Finally, the weight of the crystal

on each sieve was recorded and distribution of CBZ-SAC co-crystal for each sample was obtained.
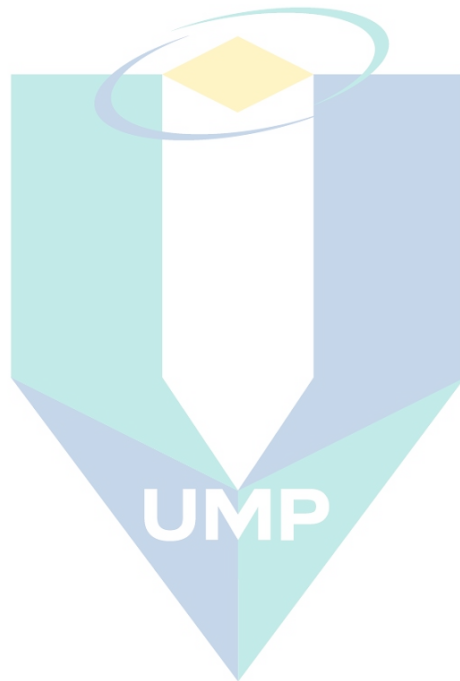
CHAPTER 4

NUCLEATION KINETICS OF CBZ-SAC CO-CRYSTAL

4.1 Introduction

Nucleation kinetics play a significant role in manufacturing required co-crystals product. In this chapter, the effect of the heating and cooling rate of various CBZ-SAC mixture in ethanol was investigated in order to deduce the metastable zone width (MSZW) and the nucleation order. The preliminary experiment was conducted, to get the optimum range of parameter for the experiment and to know the trend of the graph. A fast cooling experiment was conducted to evaluate the induction time, the radius of the critical nucleus and interfacial energy of the co-crystal. In addition, an application of Kashchiev–Borissova–Hammond–Roberts (KBHR) Technique to deduce the induction time, the radius of the critical nucleus and the interfacial energy of the CBZ–SAC co-crystals were conducted. The results from KBHR technique were compared with isothermal method.

4.2 Polythermal Crystallisation of CBZ-SAC Co-Crystal

Cooling rate, initial concentration, agitation and impurities are the main contribution to the shape of metastable zone in crystallisation (Nývlt, 1968). MSZW of CBZ-SAC co-crystals were defined by polythermal method, in which the experiments were run with different concentrations of CBZ and different mole ratios of SAC/CBZ in ethanol solution at different cooling and heating rates. Sample calculation for amount of CBZ and SAC needed in the experiment was shown in the Appendix A.

4.2.1 Effect of Cooling and Heating Rates on MSZW of CBZ-SAC Co-Crystal

The raw data of MSZW measurements for all CBZ concentrations were presented in Appendix B and values for 1.0 SAC/CBZ mole ratio were shown in Table 4.1.

Table 4.1   Average crystallisation temperature, average dissolution temperature and MSZW at different cooling/ heating rates for 1.0 SAC/CBZ mole ratio and different CBZ concentrations.

CBZ concentration (mg/ml)	Cooling/ heating rate R (ºC/min)	T_{crys} (ºC)	T_{diss} (ºC)	MSZW (ºC)
15.83	0.20	4.38	34.96	30.58
	0.40	0.32	35.26	34.94
	0.60	0.06	35.85	35.79
	0.80	-4.53	35.17	39.70
17.01	0.20	9.88	36.87	26.99
	0.40	7.08	37.03	29.95
	0.60	3.32	37.24	33.92
	0.80	1.19	37.34	36.15
17.96	0.20	10.96	37.00	26.04
	0.40	7.92	38.34	30.42
	0.60	4.26	37.39	33.13
	0.80	2.17	37.93	35.76
19.14	0.20	15.11	40.29	25.18
	0.40	10.07	40.17	30.10
	0.60	7.50	40.41	32.91
	0.80	5.94	40.18	34.24

Figure 4.1 and Figure 4.2 show the graphs of dissolution temperature and crystallisation temperature for CBZ concentration of (19.14, 17.96, 17.01, and 15.83 mg/ml) with SAC/CBZ molar ratio of 1.0. The graphs for molar ratios of 2.0, 2.5, 3.0 and 3.5 can be found in Appendix C. It can be seen from Figure 4.1 that, there is a small variation in dissolution temperature in relation to the changes in CBZ concentration. Small variation here means that, the temperature difference is small as the CBZ concentration changes. As example, the dissolution temperature different between CBZ concentration of 19.14 mg/ml and 15.83 mg/ml for SAC/CBZ mole ratio of 1.0 at heating

rate of 0.8 ºC/min is only 5.01 ºC. Whereas, in Figure 4.2 can be seen that, large variation of crystallisation temperature was noted with the changes in CBZ concentration. For the comparison, the crystallisation temperature of co-crystal at cooling rate of 0.8 ºC/min with 1.0 SAC/CBZ mole ratio for CBZ concentration of 19.14 mg/ml and 15.83 mg/ml is 5.94 ºC and -4.53 ºC respectively, which resulted in temperature different of 10.47 ºC. This shows that changes in CBZ concentration gave huge different in nucleation process, due to high concentration of CBZ leads to high supersaturation of solution and therefore enhanced the nucleation process of CBZ-SAC co-crystals. Park & Yeo (2012) suggested that, nucleation rate increased with high supersaturation of solution, which was generated by high concentration of solution. At high concentration, more solute molecules are available for solute/solute interaction, which are important for the nucleation process to occur (Borissova et al., 2009).
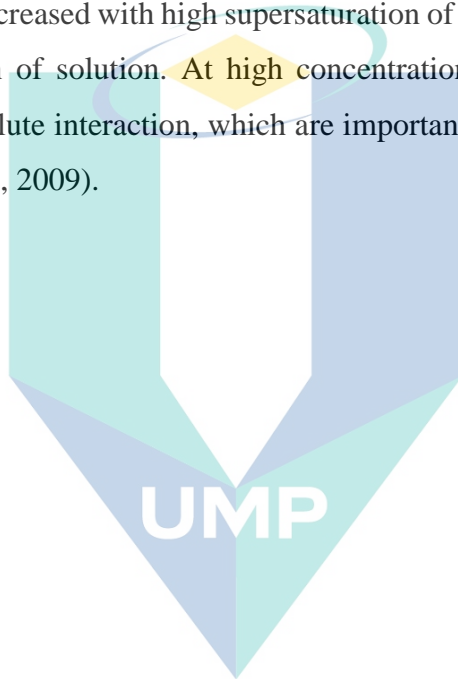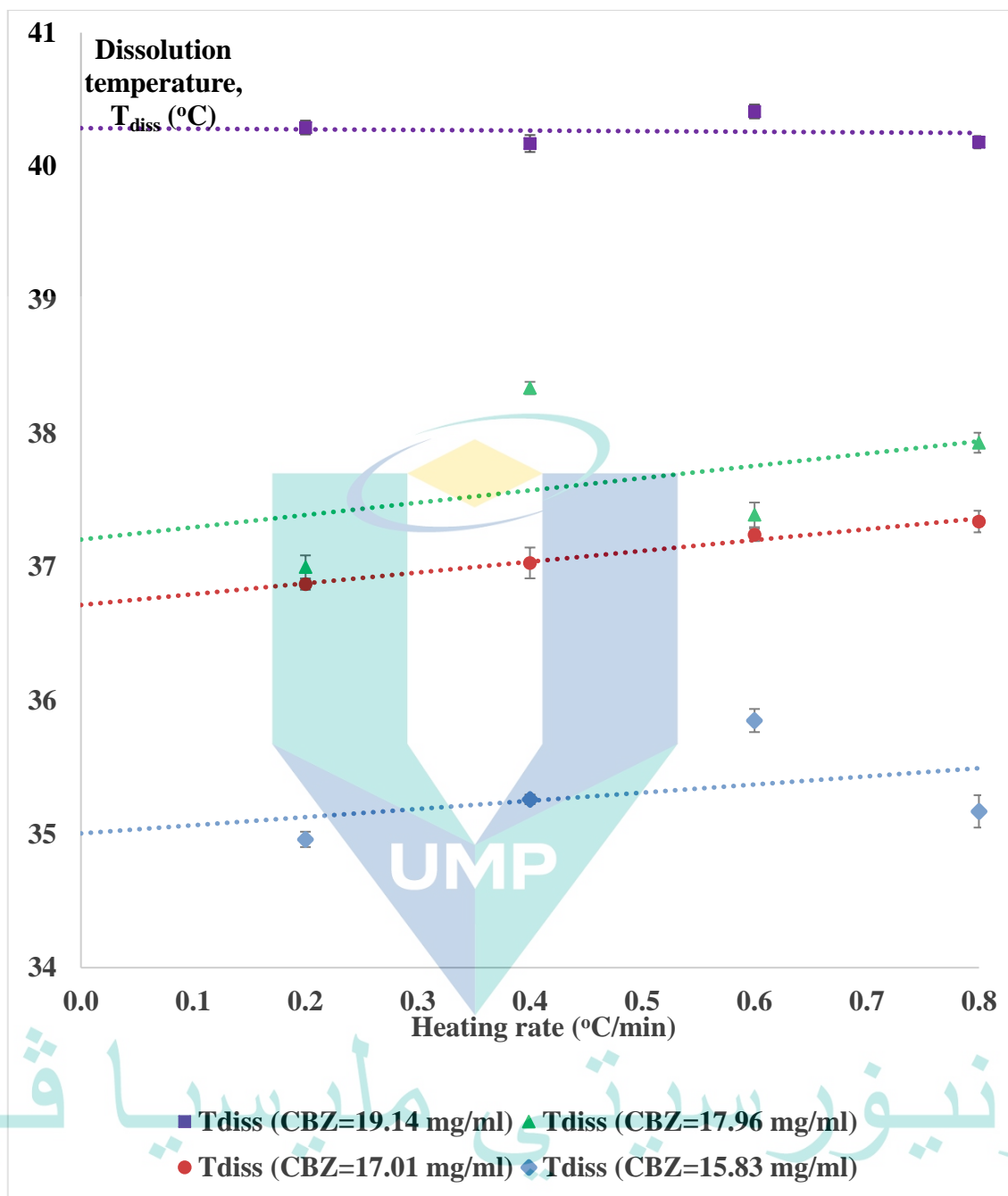
Figure 4.1 Dissolution temperature of CBZ-SAC co-crystals at different CBZ concentrations and SAC/CBZ molar ratio of 1.0.

The cooling rate is extremely affecting the crystallisation temperature. For example, the crystallisation temperature of co-crystal with 1.0 SAC/CBZ mole ratio and CBZ concentration of 19.14 mg/ml at 0.2 ºC/min and 0.8 ºC/min is 15.11 ºC and 5.94 ºC respectively, which indicates that the crystallisation is highly dependent on cooling rate, which leads to the changes in temperature. The changes in temperature is an

indication that, crystallisation is kinetically controlled (Toroz et al., 2015). From the Figure 4.3 and Appendix D, it can be seen that, the MSZW increased with cooling rate for all CBZ concentrations and SAC/CBZ ratios, these observations have also been recorded from the preliminary experiments. The finding is also consistent with findings of past studies (Camacho Corzo et al., 2014; Qian et al., 2014; Toroz et al., 2015). For example, MSZW of SAC/CBZ mole ratio of 1.0 and CBZ concentration of 15.83 mg/ml changes from 30.58 ^{o}C to 39.70 ^{o}C as the cooling rate increases from 0.2 ^{o}C/min to 0.8 ^{o}C/min. The results for all MSZW at cooling rates of (0.2, 0.4, 0.6 and 0.8) ^{o}C/min for CBZ concentration of (19.14, 17.96, 17.01, and 15.83 mg/ml) with SAC/CBZ molar ratio of (1.0, 2.0, 2.5, 3.0 and 3.0) are presented in Appendix B. Nucleation theory by Mullin stated that, at high cooling rate, longer relaxion time needed to reach the quasi-steady-state distribution of molecular cluster to allow the formation of first nuclei. As a result, the MSZW widen with the cooling rate (Mullin, 2001). In addition, Qian et. al (2014) and Sun et. al (2015) presented similar explanation that, during crystallisation process, the saturation gradually reached, and the system creates supersaturation due to cooling. The first nuclei will not be formed until supersaturation of solution reaches solubility (Qian et al., 2014; X. Sun et al., 2015). The time lag between saturation and supersolubility is known as induction period. Thus, by increasing the cooling rate resulted in wider MSZW due to the delaying of onset nucleation (Rajoub, 2014). Furthermore, Wang et. al has explained that a high cooling rate led to a high supply of supercooling, which enhanced the MSZW (Wang et al., 2015).
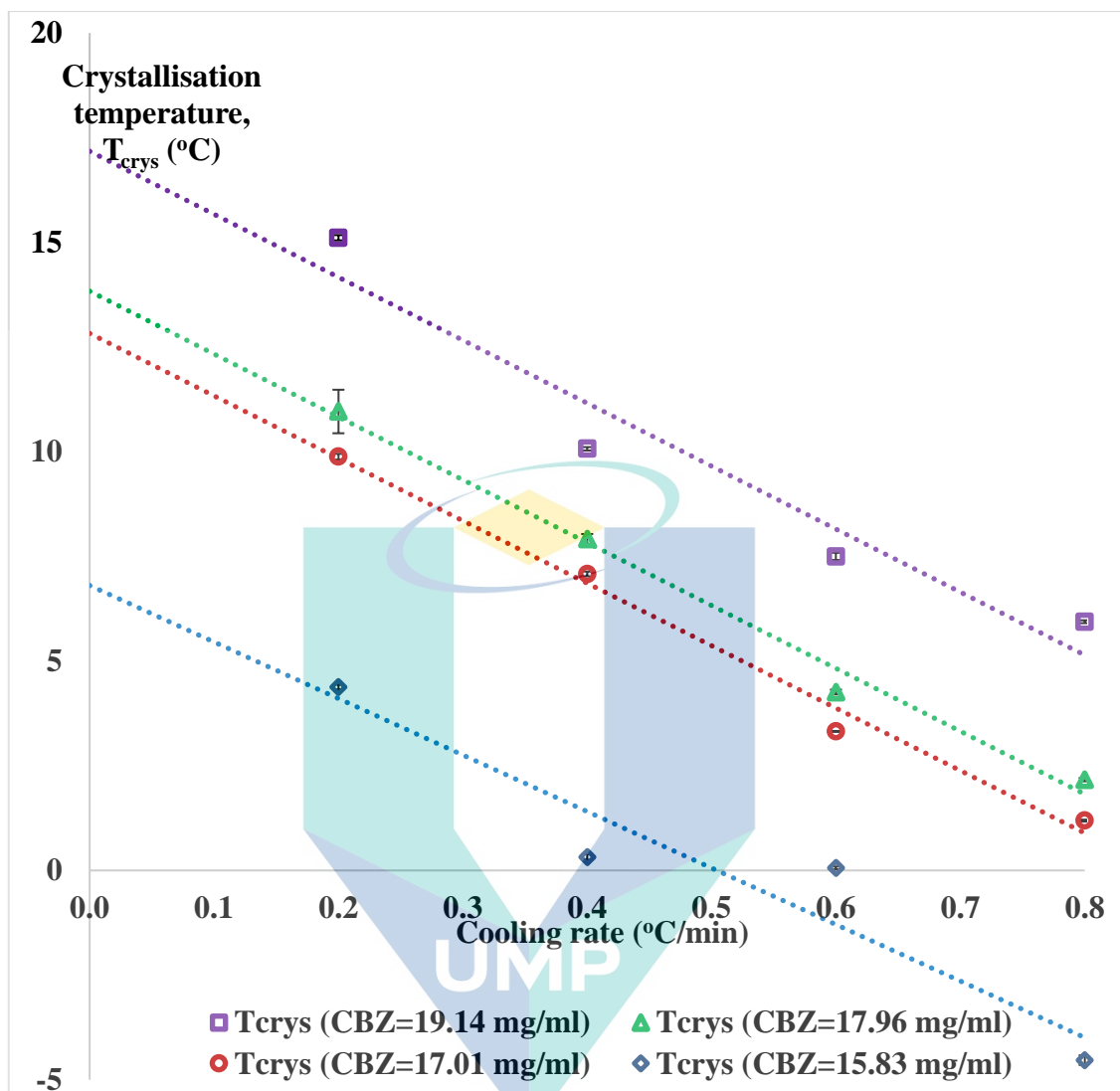
Figure 4.2   Crystallisation temperature of CBZ-SAC co-crystals at different CBZ concentrations and SAC/CBZ molar ratio of 1.0.

A point to note that, the data of crystallisation temperatures for all concentrations are inconstantly scattered and produce a relatively high standard deviation, which is not the case for data of dissolution temperatures. This is supported by Parsons, Black and Colling (2003)'s study which reveal that the crystallisation temperature is influenced by kinetic parameters such as stirring speeds, cooling profiles and solution concentrations.

As MSZW was defined as different between dissolution temperature and crystallisation temperature, the plot of MSZW of CBZ-SAC co-crystals at different CBZ concentrations and SAC/CBZ molar ratio of 1.0 was obtained as can be seen in Figure 4.3. The graph showed clearly that the MSZW increased with cooling rate. As explained

earlier, low cooling rate resulted to narrow MSZW due to the system has more time to reach supersaturation and formed the nucleus. In theory, if solution is cooled infinitely slow, formation of first nuclei could be seen at the solubility temperature (equilibrium state) (Randall et al., 2012). The same observation was obtained for SAC/CBZ mole ratio of 2.0, 2.5, 3.0 and 3.5 (Appendix D), where the MSZW for all SAC/CBZ mole ratio increased with cooling rate. An increase in SAC/CBZ mole ratio led to an increase in hydrogen bonding interaction, thus increased the possibility of producing stable CBZ-SAC co-crystals form I.
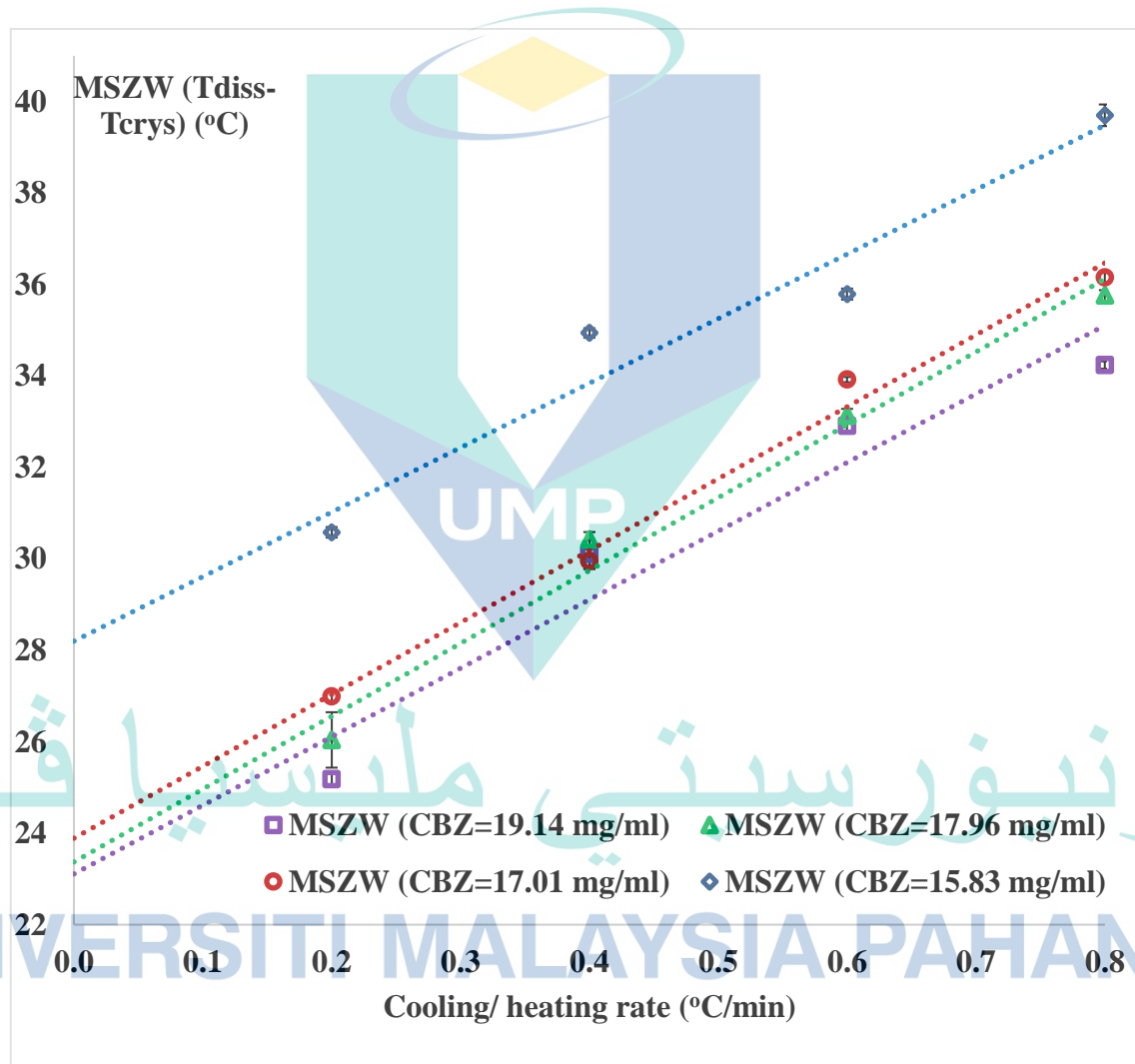
Figure 4.3   MSZW of CBZ-SAC co-crystals at different CBZ concentrations and SAC/CBZ molar ratio of 1.0.

The value of T_{diss0} corresponds to the apparent dissolution temperature down to a zero heating rate, which is in fact the equilibrium dissolution temperature (Arunmozhi et al., 2004). Same goes with crystallisation temperature, which extrapolated to zero heating rate for getting the equilibrium crystallisation temperature, T_{crys0}. The values of these temperatures are presented in Table 4.2. The different between these equilibrium temperatures is MSZW, which is also shown in Table 4.2. The data from Table 4.2 are plotted in a graph MSZW at equilibrium versus SAC/CBZ mole ratio for all CBZ concentrations in order to see the relation between them (Figure 4.6) . The explanation about effect of SAC/CBZ mole ratio on MSZW is in section 4.2.3.

Table 4.2   The crystallisation temperature, dissolution temperature at equilibrium (zero colling rate) and MSZW for all SAC/CBZ molar ratios and CBZ concentrations.

SAC/CBZ mole ratio	CBZ concentration (mg/ml)	Tcrys0 (ºC)	Tdiss0 (ºC)	MSZW (ºC) (Tdiss0-Tcrys0)
1.0	15.83	8.26	35.01	26.75
	17.01	12.83	36.72	23.89
	17.96	13.83	37.21	23.37
	19.14	17.18	40.29	23.11
2.0	15.83	21.95	43.43	21.48
	17.01	23.98	44.68	20.70
	17.96	27.84	47.55	19.72
	19.14	27.54	48.72	21.18
2.5	15.83	26.14	46.35	20.22
	17.01	29.38	47.99	18.61
	17.96	32.59	49.88	17.29
	19.14	33.05	51.15	18.09
3.0	15.83	27.48	48.64	21.16
	17.01	30.39	48.25	17.86
	17.96	33.39	51.49	18.10
	19.14	35.38	51.87	16.50
3.5	15.83	34.05	51.80	17.75
	17.01	32.85	51.88	19.03
	17.96	34.53	52.38	17.85
	19.14	36.13	52.76	16.63

4.2.2 Effect of CBZ Concentrations on MSZW of CBZ-SAC Co-Crystals

Figure 4.4 shows the effect of CBZ concentration on MSZW of CBZ-SAC co-crystals for SAC/CBZ mole ratio of 3.5 at different cooling rates and Figure 4.5 shows effect of CBZ concentration on MSZW at equilibrium of CBZ-SAC co-crystals for all SAC/CBZ mole ratio respectively. It was seen from all experiments with different CBZ concentrations that the high concentrated solution (19.14 mg/ml) had a higher probability to nucleate from the less concentrated solution (15.86 mg/ml). This results is in accordance to previous study on the effect of initial concentration and saturation concentration on MSZW, where the MSZW narrows with an increase of concentration (Abdul Mudalip, 2016; Kadam, 2012; Mao, Zhang, Rohani, & Ray, 2010; Md Azmi, Anuar, Abu Bakar, & Zakaria, 2015; Mohod & Gogate, 2018; Ramisetty, Pandit, & Gogate, 2013; Wang et al., 2016). Wang et al. (2016) studied the factors affecting MSZW of sodium dichromate dihydrate suggested that, the saturation temperature increased with an increase in initial concentration, thus the probability for diffusion and collision of solute improved and led to faster nucleation. The probability of molecular collision is the pre-exponential factor, A defined in crystallisation nucleation theory as explain in section 2.3.1.1 (Equation 2.10). In addition the results are following to the conventional crystallisation theory, in which the crystallisation is driven by supersaturation level of solution: a higher concentrated solution attains supersaturation earlier than the solution with less concentration level (A.-Z. Chen, Chen, S. Wang, Wang, & Zha, 2015). Research finding by Ramisetty et al. (2013) on antisolvent crystallization of benzoic acid also points out that, as the initial concentration increased, the solution become more saturated resulting the high number of crystal produced, thus the MSZW narrowed. Recent paper by Mohod and Gogate (2018) on the crystallization of ammonium sulphate using ultrasound assisted approach confirmed that, the high initial concentration led to the solution became more supersaturated and reduced the limit of metastable zone. In addition, by increasing the solution concentration, the induction time or the time required for precipitation after reaching supersaturation, reduced due to the more supply of particles in the solution, which enhanced the crystal growth due to the prolonged lifetime of nuclei (Md Azmi et al., 2015). However, a number of studies show that significant differences do exist, albeit findings are somewhat contradictory. As example, the research

by Smith and Wohlgemuth stated that, the correlation between MSZW and concentrations is insignificant. This might be due to the accuracy of the results (Smith et al., 2001; Wohlgemuth, 2012). The graphs of MSZW against CBZ concentration for SAC/CBZ mole ratio of 3.0, 2.5, 2.0 and 1.0 with similar trends can be seen in Appendix E, where high CBZ concentration enhances nucleation of CBZ-SAC co-crystals for all SAC/CBZ mole ratios. In Figure 4.5, SAC/CBZ mole ratio 1.0 has very different trend as compared to the other mole ratio. The CBZ-SAC co-crystal is in solid form as the ratio of SAC to CBZ is one to one, thus the SAC/CBZ mole ratio 1.0 did not have any excess of saccharin molecule in the solution.
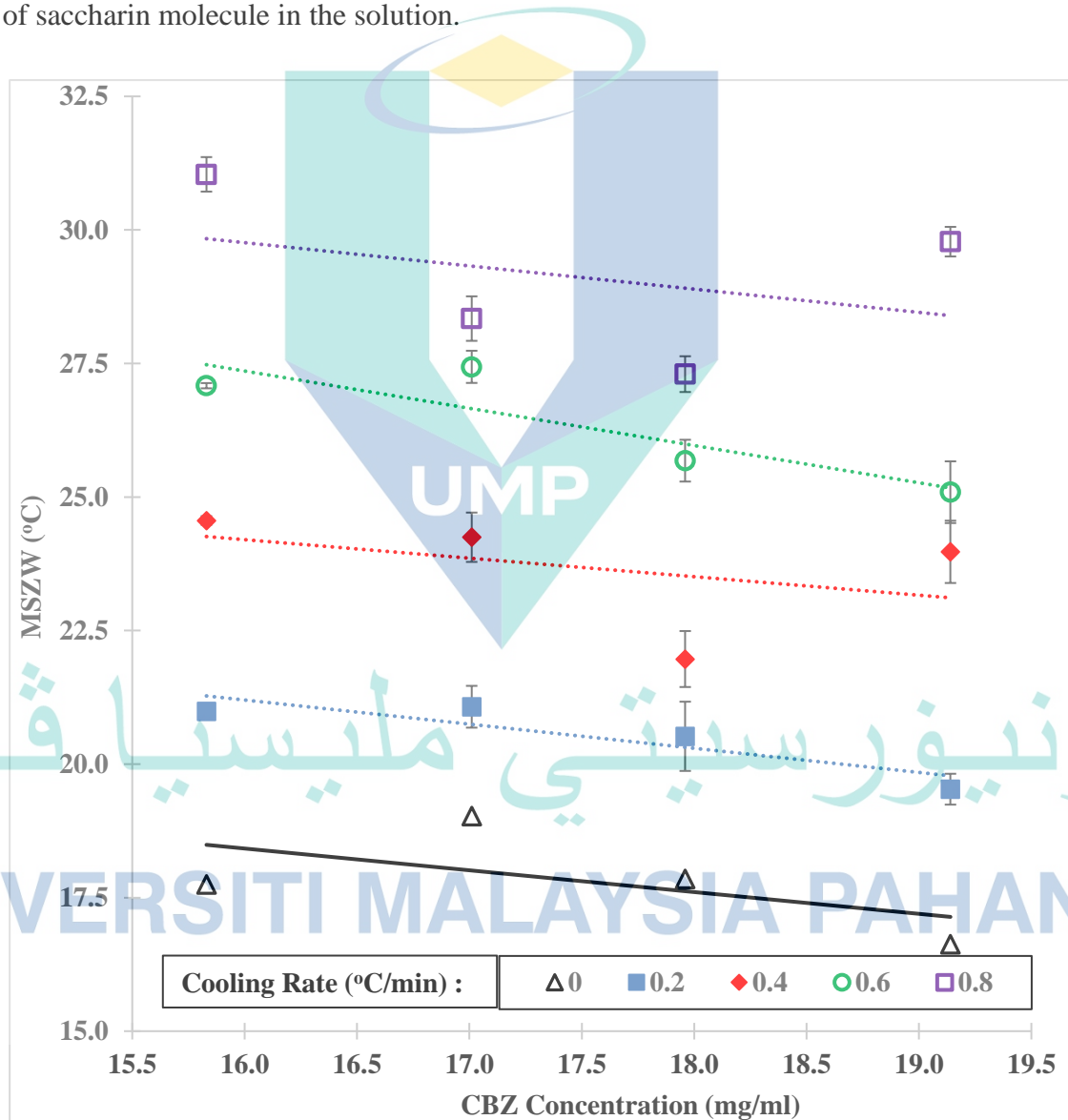
Figure 4.4   MSZW vs CBZ concentration for SAC/CBZ mole ratio of 3.5.
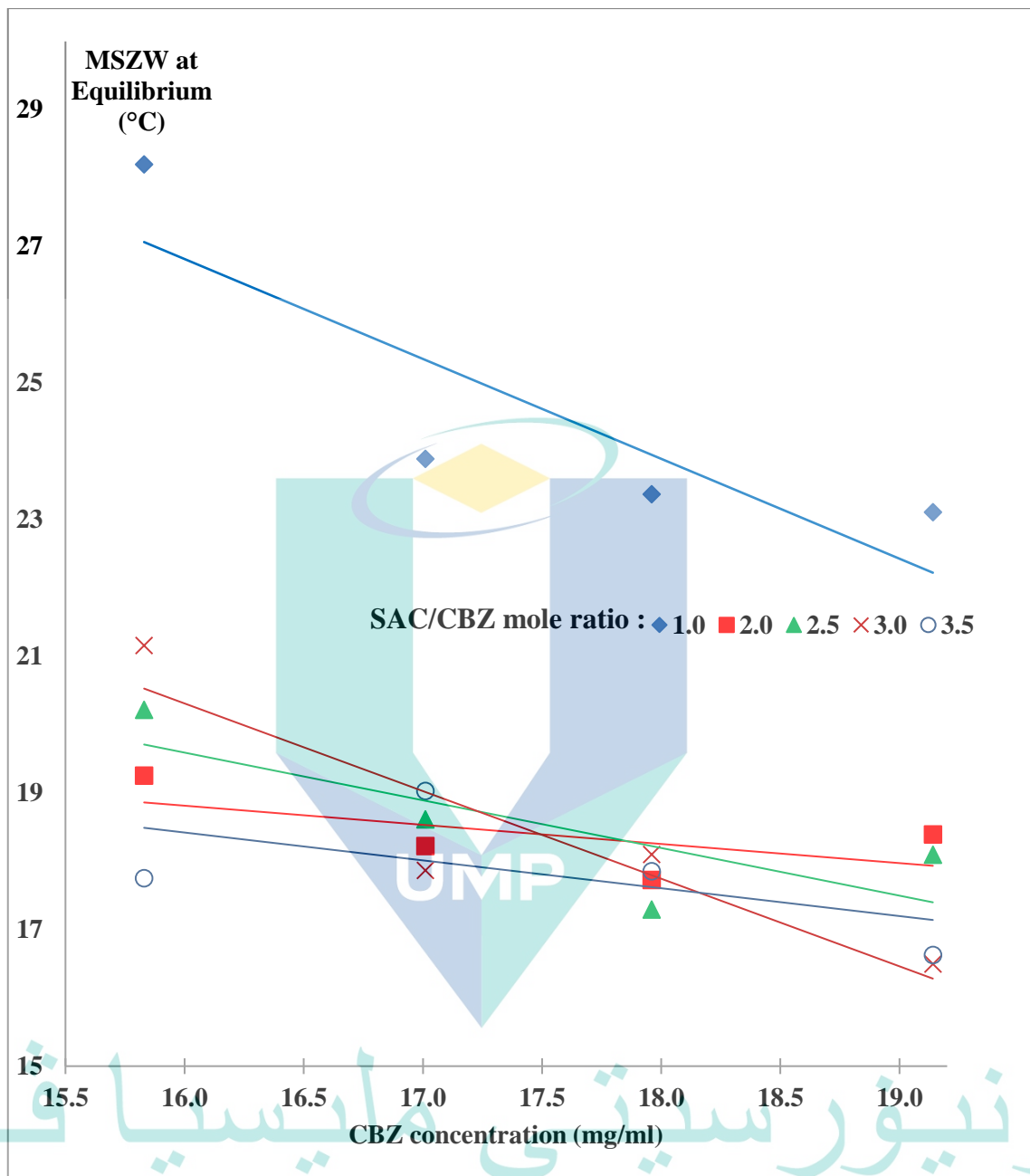
Figure 4.5　　Effect of CBZ concentration on MSZW for all SAC/CBZ mole ratio.

4.2.3 Effect of SAC/CBZ Mole Ratios on MSZW of CBZ-SAC Co-Crystal

In general, CBZ-SAC cocrystals formulated by mixture of API (CBZ) and co-former (SAC) with a certain mole ratio and concentration. As described in chapter 2, forming of nucleus occurs after the supersaturation level surpass the solubility limit if considering no foreign particles exist in the system. In co-crystals, supersaturation is dependent on the composition of solution. From the equation derived by Jayasankar, Good and Rodríguez-Hornedo (2007), increase the concentration of individual component in co-crystal , leads to the high degree of supersaturation and crystallisation rate.

In this study, API component (CBZ concentration) was remained constant and only concentration of SAC was adjusted to suit the ratio of SAC/CBZ to 1.0, 2.0, 2.5, 3.0 and 3.5. As the concentration of SAC or written as molar ratio of (SAC/CBZ) increased, the initial supersaturation also increased. Thus, the solution became more supersaturated and produced high degree of nucleation. As a result, the MSZW was narrower. This can be seen in, Figure 4.6, where for all CBZ concentrations, the MSZW reduced with the increased of molar ratio of SAC to CBZ. Overall, the trend shows a decreased on MSZW value with the SAC/CBZ mole ratio, except for the graph of CBZ concentration of 15.83 mg/ml. From the data, MSZW values from SAC/CBZ mole ratio of 2.0 were too low compared to the values from other SAC/CBZ mole ratios, thus caused the trend of the graph from CBZ concentration of 15.83 mg/ml to be inconsistent. This finding was in accordance to the previous research by Li, Sun, Jin and & Li (2015), which studied the hydrothermal growth of ZnO nanocrystals. In that study, the crystallisation was observed, by changing the NaOH/ZnAc molar ratio and found that high degree of supersaturation attained by lowering the molar ratio. Study by Vasenko and Qu (2017) on precipitation of calcium phosphate has also affirming the result, in which the increase of mole ratio enhanced the nucleation due to the most of supersaturation consumed in the solution.
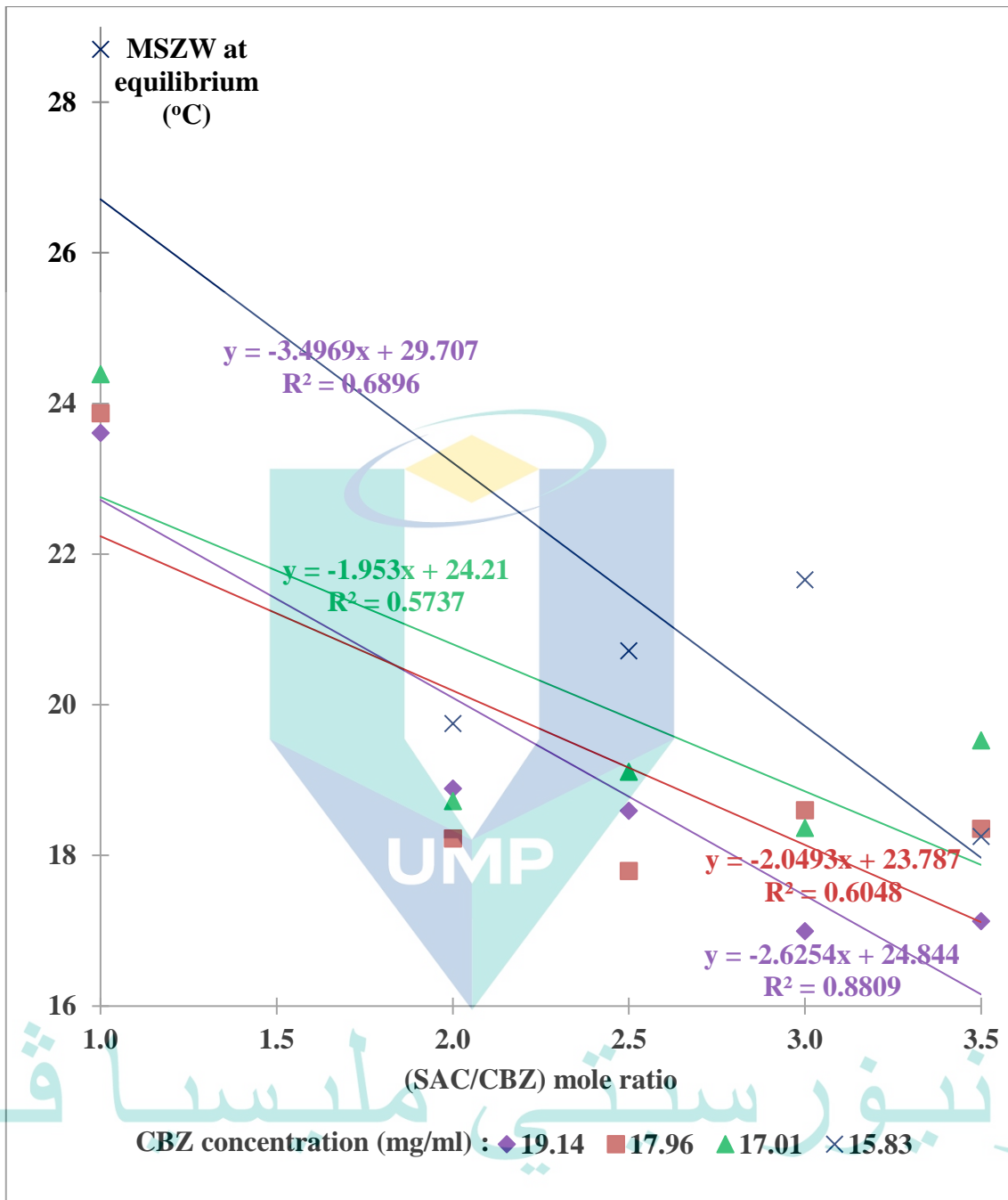
Figure 4.6   MSZW at equilibrium versus SAC/CBZ mole ratio for all CBZ concentrations.

4.2.4 Solubility and Super-Solubility Curves of CBZ-SAC Co-Crystal

Figure 4.7 depicts the variation of solubility and supersolubility curves of CBZ-SAC co-crystals under different experimental conditions. It can be seen that, the curve shifted to the right as the mole ratio of SAC to CBZ increased from 1.0 to 2.5. As mention in section 4.2.3, an increase in SAC/CBZ mole ratio caused an increase in supersaturation, thus enhanced the nucleation. Furthermore, this means less driving force for nucleation to occur is required for the higher SAC/CBZ mole ratio. The MSZW, which can be defined as the region between solubility and super-solubility curve, is found to be narrow with the increase of mole ratio from 1.0 to 2.5. It is suggested that, by increasing the amount of saccharin in a co-crystal, allows the earlier forming of the nucleus, which can be detected faster by turbidity probe. As amount of saccharin increased, more solute molecules are available for solute/solute interaction, thus increased the chance of nucleation (Borissova et al., 2009).
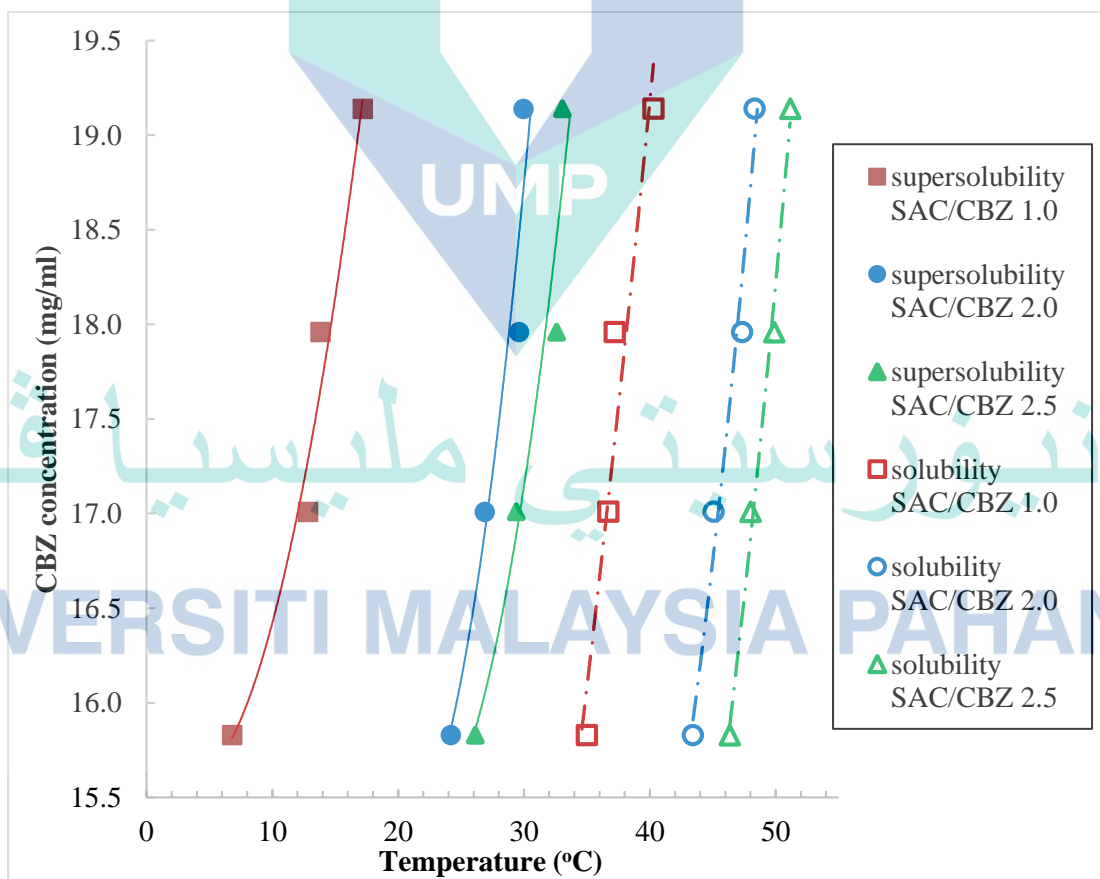
Figure 4.7   Solubility and supersolubility curve for SAC/CBZ mole ratio of 1.0, 2.0 and 2.5

4.2.5 Nucleation Order and Nucleation Kinetic Constant of CBZ-SAC Co-Crystal

Main kinetic parameters governing nucleation include nucleation rate, nucleation order which represents dependence of MSZW on cooling rate and the nucleation rate constant which gives dependence of nucleation rate on MSZW (Hammond et al., 2016). Following the equation (log R vs log MSZW), the straight line was constructed, and the slope of the graph defined as nucleation order, m. The construction of the straight-line graph for CBZ-SAC co-crystals with SAC/CBZ mole ratio of 1.0 and different CBZ concentrations can be seen in Figure 4.8. Graphs for (2.0, 2.5, 3.0 and 3.5) SAC/CBZ mole ratio are presented in Appendix F. The values of nucleation orders for all CBZ concentrations and SAC/CBZ mole ratios are listed in Table 4.3.
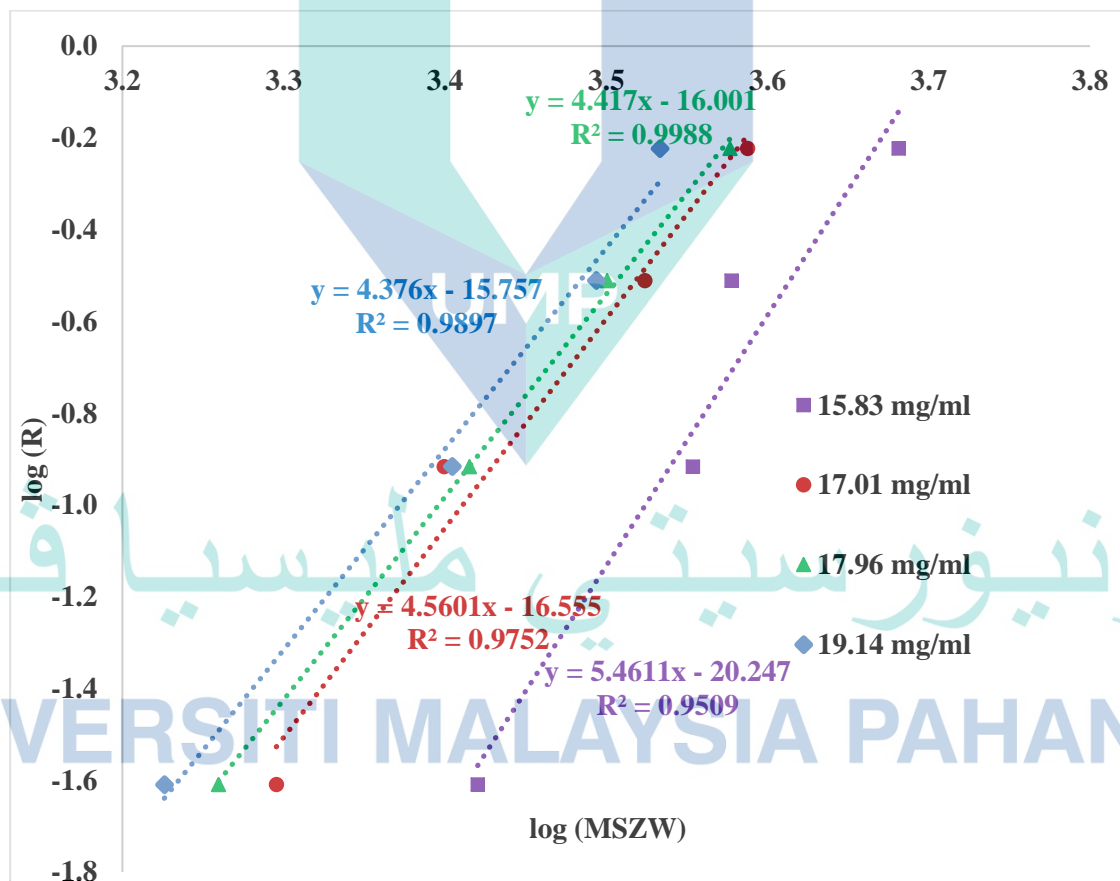
Figure 4.8   log R versus log MSZW for CBZ-SAC co-crystals with SAC/CBZ mole ratio of 1.0 and different CBZ concentrations. Slope of the graph is the nucleation order, m.

The values of nucleation order depend on the processes of formation of the nuclei and how the nuclei that grow into stable nuclei was detected, which means methods of determining the nucleation process and measurement of metastable zone width is extremely effecting the value of nucleation order (Sangwal, 2009). The nuclei is stable if the nuclei reaches the critical size of nucleus, r_c as mention in section 2.3.1.1. Wider MSZW results in high value of MSZW, which means the system is easier to control (Nagy et al., 2007).

The results from Table 4.3 shows that, the nucleation order has no association with the changes in CBZ concentration for all SAC/CBZ ratios. This is in consistent with the finding by Abd Rahim (2012), which studied the effect of concentration on nucleation order for CBZ-SAC cocrystals in a small scale (1ml). Figure 4.9 shows the graphs of ln(R) vs. ln MSZW for CBZ concentration of 19.14 mg/ml and different ratio of (SAC/CBZ). Values of m are shown in Table 4.3 and the calculated nucleation kinetics k is given in Table 4.4. The analysis reveals that the nucleation order, m for CBZ-SAC co-crystals increases with the SAC to CBZ ratio and have the average value of 3.44. This value is acceptable as reported in the literature that, the values of nucleation order, m are usually in the range of 1.65–4.9 for organic compounds (Arunmozhi et al., 2004).The low value of m (3.44) indicated that there is a strong solute-solvent interaction which induced the formation of stable CBZ-SAC cocrystal (Form I).
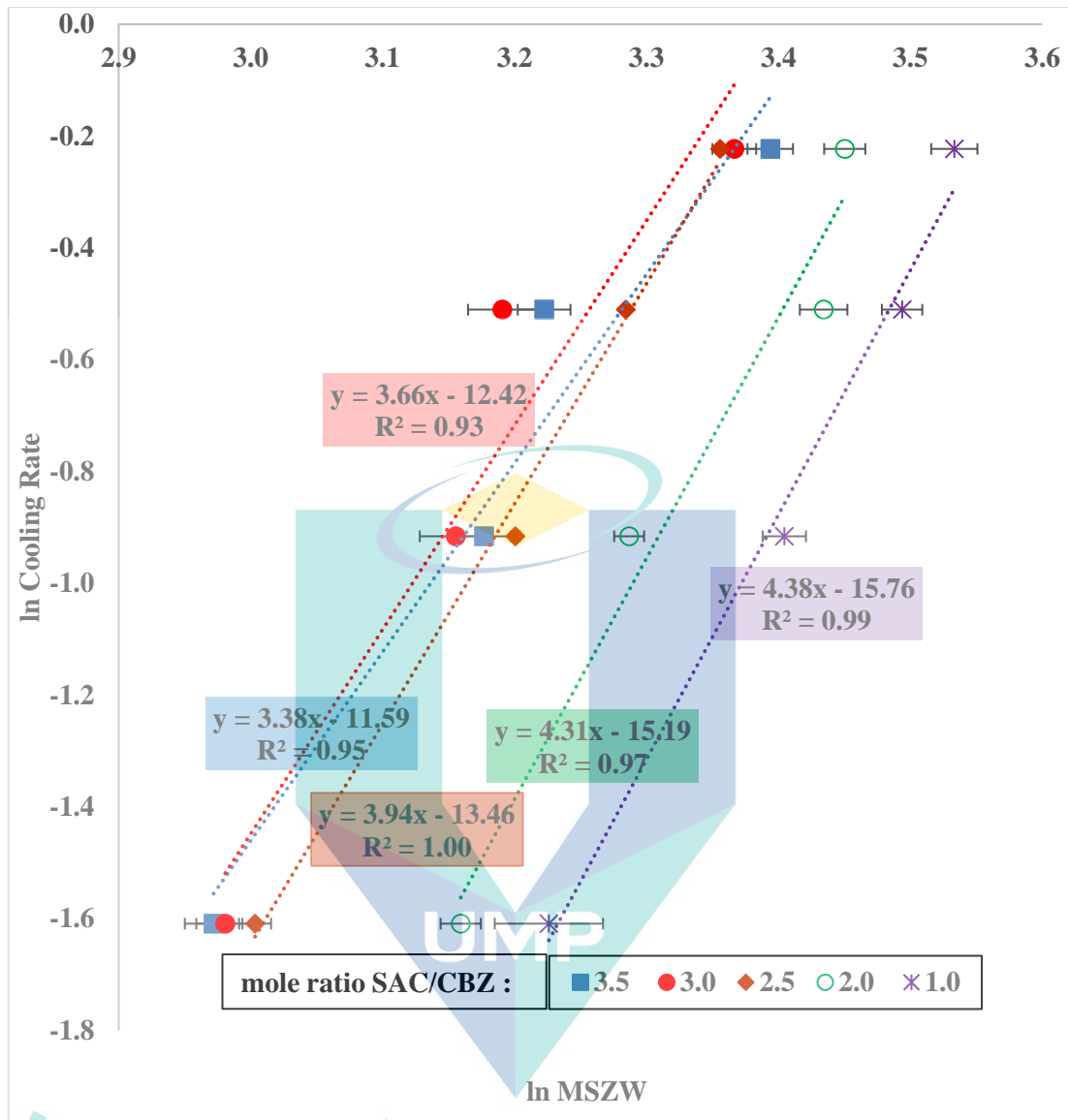
Figure 4.9   ln R vs. ln MSZW for CBZ concentration of 19.14 mg/ml.

Same goes with the effect of mole ratios to the nucleation order. Table 4.3 shows, there is no trend of nucleation order can be recognised for all CBZ concentration with the increase of mole ratio. Howard (2011) suggested that, the nucleation orders varied with the different set-ups of the systems such as distinct size of reactor and different mixing conditions. In this case, the size of vessel was fixed at 250ml and the steps of mixing process for each SAC/CBZ mole ratio and CBZ concentration were similar.

Table 4.3   Nucleation order, m for all CBZ concentrations and SAC/CBZ mole ratios.

CBZ concentration	SAC/CBZ mole ratio				
(mg/ml)	1.0	2.0	2.5	3.0	3.5
15.83	5.46	3.14	4.58	5.38	3.60
17.01	4.56	3.12	3.97	4.34	4.43
17.96	4.42	4.35	3.35	5.40	4.35
19.14	4.38	3.70	3.94	3.56	3.38

Table 4.4 shows the results of nucleation kinetic constant derived from the interception of the straight-line graph of ln R versus ln MSZW. The data shows no trends effected from different CBZ concentration and SAC/CBZ mole ratios. Only at SAC/CBZ mole ratio of 1.0, the nucleation kinetic constants seem to be increased with the CBZ concentration. Nývlt (1968) derived an equation 2.22 in section 2.5.1 that, the nucleation rate constant, k increased with an increase in nucleation order, m. Therefore, high value of k means that, the formation of stable CBZ-SAC co-crystals (Form I) is easier. From the results in Table 4.4, only SAC/CBZ mole ratio of 1.0 shows an increase in k with CBZ concentration, which is in accordance with previous finding (Abdul Mudalip, 2016; Kobari et al., 2011). The k-values from SAC/CBZ mole ratios of 2.0, 2.5, 3.0 and 3.5 show no linear correlation with CBZ concentration. These similar findings were also reported by Abd Rahim (2012)

Table 4.4   Nucleation kinetic constant, k x 10^{-7} for all CBZ concentrations and SAC/CBZ mole ratios.

CBZ concentration	SAC/CBZ mole ratio				
(mg/ml)	1.0	2.0	2.5	3.0	3.5
15.83	0.14	295.45	6.46	0.66	2.13
17.01	3.59	372.21	37.30	22.82	0.06
17.96	5.84	21.45	235.07	1.40	0.12
19.14	7.31	91.17	47.56	179.25	6.71

4.3 Fast Cooling Analysis

In fast cooling experiments, induction time, t_{ind}, which was time taken to create first nuclei at a specific temperature (see induction temperature in Table 4.5) in supersaturation state, was recorded. In this experiment, the suspension with the CBZ concentration of 19.76 mg/ml and SAC/CBZ mole ratio of 2.0 was chosen due to the range of T_{crys} and T_{diss} value (MSZW between 47.55 and 27.84 °C). The isothermal temperature in this experiment was within the MSZW region or supersaturated solution, in which the nucleation has a possibility to occur.

The raw data of induction times of CBZ-SAC co-crystal with SAC/CBZ mole ratio of 2.0 and CBZ concentration of 19.76 mg/ml in ethanol solution for cooling rate of 1.0 °C/min and 1.2 °C/min are shown in Appendix G. An example of result during fast cooling experiment to find the induction time of CBZ-SAC co-crystal in ethanol is shown in Figure 4.10.

As can be seen from Figure 4.10, forming of nuclei identified by the sharp increase of turbidity value from 0 to 100. Time taken between the fixed desired temperature and the forming of nucleus known as induction time, τ. The value of supersaturation is a function of temperature and concentration. Calculated supersaturation values, induction times for cooling rates of 1.0 and 1.2 °C/min and the average of induction time were presented in Table 4.5. The correlation between induction times and supersaturation shown by the graphs plotted in Figure 4.11.
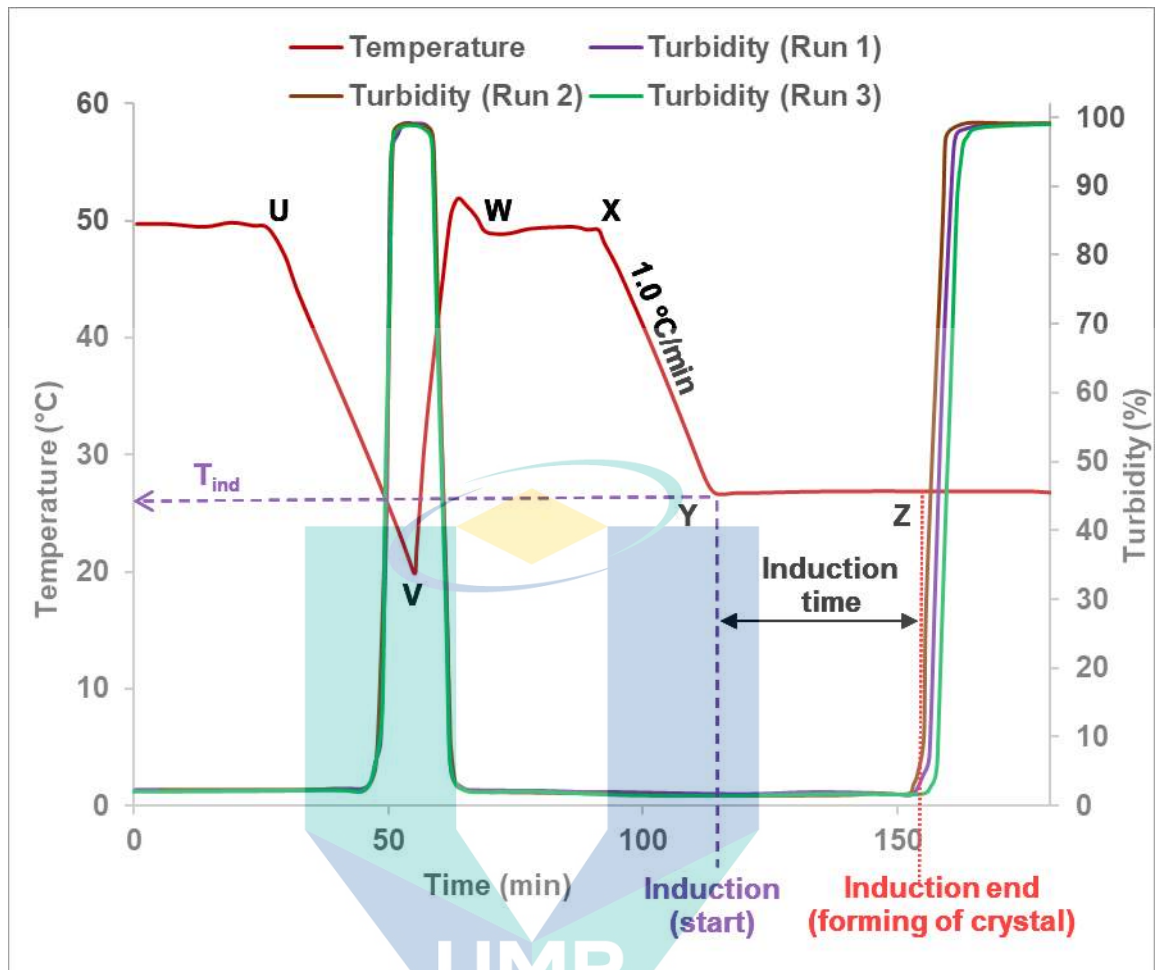
Figure 4.10   Experiment on induction time of CBZ-SAC co-crystals with SAC/CBZ
mole ratio of 2.0 and CBZ concentration of 19.76 mg/ml in at supersaturation, S = 1.63.

Table 4.5Induction times of CBZ-SAC co-crystals with SAC/CBZ mole ratio of 2.0 and CBZ concentration of 19.76 mg/ml for two different cooling rates.

Cooling rate = 1.0 °C/min

Induction temperature (°C)	Supersaturation, S	Average induction time (min)
28	1.87	35.54 ± 2.00
30	1.75	47.33 ± 0.76
32	1.63	87.22 ± 2.78
34	1.53	110.43 ± 7.81
36	1.43	142.17 ± 9.00

Cooling rate = 1.2 °C/min

Induction temperature (°C)	Supersaturation, S	Average induction time (min)
28	1.87	48.37 ± 6.67
30	1.75	59.79 ± 9.42
32	1.63	76.95 ± 6.74
34	1.53	95.96 ± 7.23
36	1.43	171.06 ± 5.46

4.3.1 Effect of Supersaturation on Induction Time

Figure 4.11 shows that the induction time decreases with supersaturation. As expected, longer time was needed to create nuclei if the target (isothermal) temperature is close to solubility curve, whereas the induction time was shorter as the target temperature approached the supersolubility curve. In respect with the effect of cooling rate, cooling rate of 1.2 °C/min shows large error in the results. This may due to the limited ability of the machine (temperature regulator), which cannot provide the consistency of the temperate profile during heating and cooling at higher rate. This large error could be overcame by controlling the parameter and the evaporated solvent could be condensed by adding a condenser in the system.   Since the error was huge, and the results was inconsistent for fast cooling experiment with cooling rate of 1.2 °C/min, only result from fast cooling experiment of 1.0 °C/min was further analysed. In general, fast cooling experiment with faster cooling rate showed higher induction time, which is in accordance to the literature (Dasgupta et al., 2016; Martini et al., 2001). This finding is also supported by the study from Martini et al. (2001) on nucleation of sunflower oil,

where lower degree of cooling rate reduced induction time due to the molecular organisation already occurred before the formation of nuclei (Herrera et al., 2015; Martini et al., 2001).
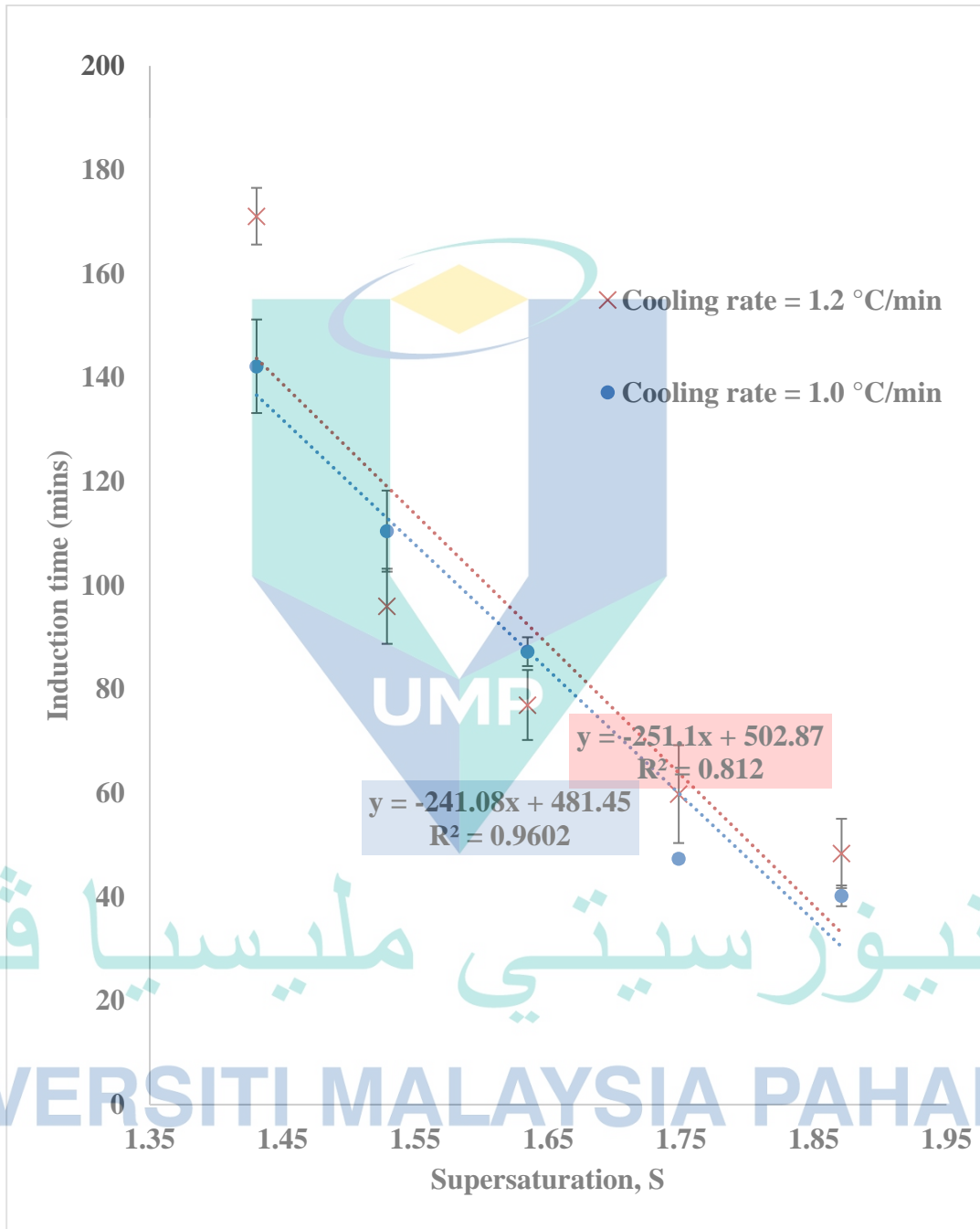
Figure 4.11   Induction times of CBZ-SAC co-crystals with SAC/CBZ mole ratio of 2.0 and CBZ concentration of 19.76 mg/ml versus supersaturation for two different cooling rates.

4.3.2 Determination of Interfacial Energy and the Critical Size Nucleus

Interfacial energy, γ is a significant parameter in initial forming of stable nuclei. It is a measure of difficulty for formation of nucleation in solution (Ma et al., 2014; Y. Zhang et al., 2015). Low value of interfacial energy means that the solute can crystallise easily and high value of interfacial energy indicates that the solute is difficult to crystallize (Lenka & Sarkar, 2014; Nguyen & Kim, 2008). According to the equation 2.36 in section 2.5.3, graph of ln (induction time,t_{ind}) against $1/(\ln$ (supersaturation, S$))^2$ was plotted over a range of supersaturation at fixed temperature of 28, 30, 32, 34 and 36 °C to estimate the value of interfacial tension,γ (Figure 4.12).

From Figure 4.12, it can be seen that the trend of the graph of ln t_{ind} vs (ln S)$^{-2}$ follows the straight line, which is consistent with the literatures (Du et al., 2016; Gherras & Fevotte, 2012; Kubota et al., 2014). The slope was obtained and substituted in Equation 2.38 to calculate the value of interfacial energy,γ. The molecular volume, V_m of CBZ-SAC co-crystal taken as $957\text{Å}^3 \approx 9.57 \times 10^{-28}$ m^3 and the Boltzmann constant K as $1.3805*10^{-23}$ J/K (Abd Rahim, 2012). Following the Equation 2.39 and 2.40, the values of critical size nucleus and the molecular number of critical nucleus were calculated respectively. The values of all interfacial energy, critical size nucleus and the molecular number of critical nucleus were presented in Table 4.6
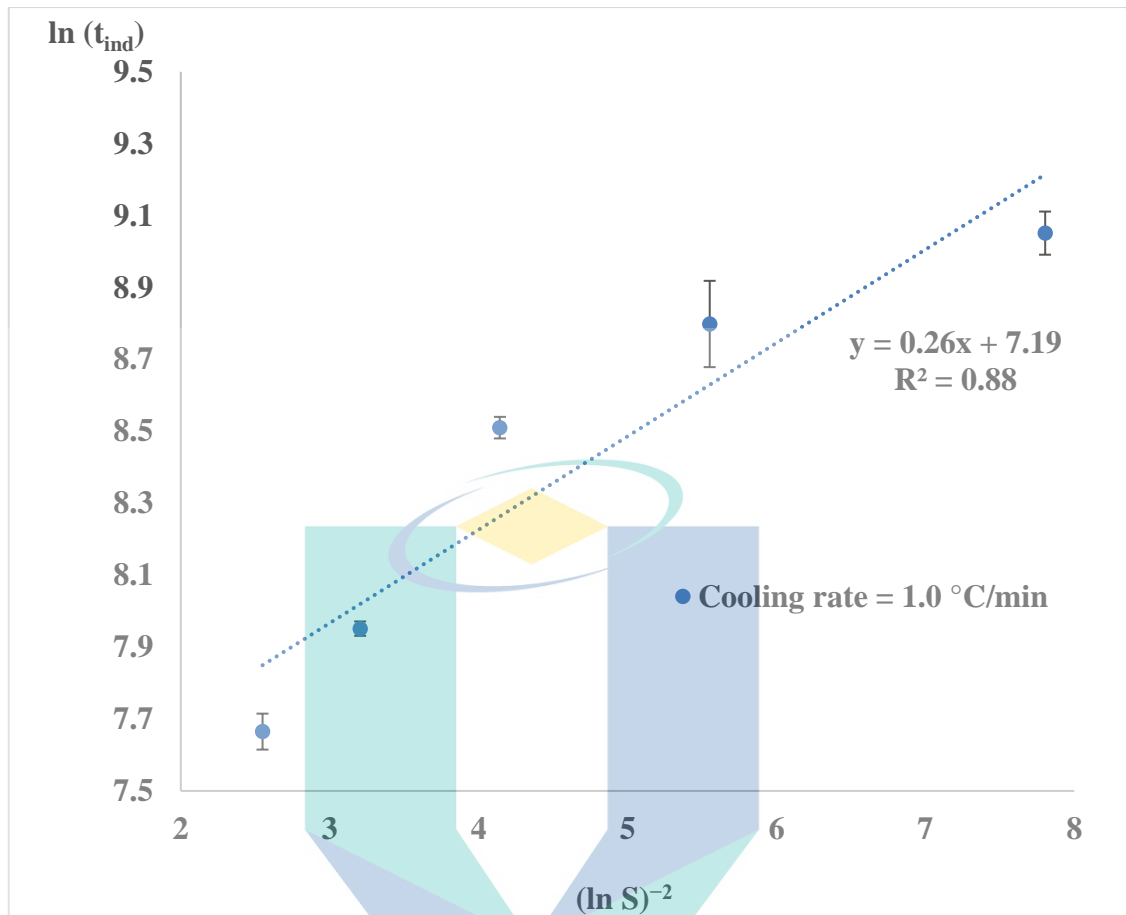
Figure 4.12   ln t_{ind} vs (ln S)$^{-2}$ for CBZ-SAC co-crystal of CBZ concentration, ρCBZ of 17.96 mg/ml and SAC/CBZ mole ratio of 2.0.

Table 4.6   Calculated values of interfacial energy (γ), critical size nucleus (r*) and the molecular number of critical nucleus (i*) with fast cooling rate of 1.0 °C/min.

Supersaturation ratio S	Slope of ln t_{ind} vs (ln$S$)$^{-2}$	γ /mJm^{-2}	r* /nm	i*
1.871		1.067	0.784	2.11
1.748		1.074	0.880	2.98
1.634	0.260	1.081	1.000	4.38
1.529		1.088	1.158	6.79
1.430		1.095	1.373	11.32

77

It can be seen from Table 4.6 that, the value of interfacial energy decreased with supersaturation ratio or increased with temperature ranging from 1.067 to 1.095 mJm^{-2}. It shows the interfacial energy is highly dependence on temperature. High degree of temperature leads mostly to lower supersaturation value, which resulting in lower interfacial energy. Increased temperature usually increases the solubility of solids in solution. From Second Law of Thermodynamics, the movement of particles in solution increased with temperature, thus the system can change the system easily. Temperature of solutions, degree of supersaturations and interfacial tensions are three factors that affecting the nucleation rate (Nguyen, 2013). Besides other factors can reduce the nucleation energy barrier, such as introducing of ultrasound in the system and addition of substance in the solution (Jiang et al., 2012). Abd Rahim (2012) and Nguyen (2013) described that, the reducing of supersaturation bring to the reduction in interfacial energy because of favourable interaction between solid and liquid (solute-solvent interaction). Few solvent-solute intermolecular interactions reduced the energy for nucleation on crystal surface. The calculated critical size nucleus was plotted in graph as a function of supersaturation and temperature (Figure 4.13).

Figure 4.13 shows clearly that the critical size nucleus of CBZ-SAC co-crystals increased with temperature and gradually decreased with supersaturation ratio. As the supersaturation ratio decreased from 1.871 to 1.430, the critical size of nucleus increased from 0.784 to 1.373 nm. According to classical nucleation theory, an increase in supersaturation ratio leads to a decrease in energy barrier for nucleation, resulted to a decrease in critical size of nucleus (Du et al., 2016; Jiang et al., 2012). Thus at high supersaturation ratio, a smaller nucleus were produced (Sun, Wang, & Gong, 2010). This phenomenon was explained by Du et al. (2016) as theory of Gibbs-Thomson effect. If nucleus reaches the critical size, the free energy decreases in the system, resulting only the growth of the crystal, if not, no growth occurs, and crystals dissolves in the solution. The cluster smaller than critical size tends to re-dissolve due to the high interfacial tension in the system, in which the energy barrier need to be overcome for the complete formation of the crystal (Turner, 2015). In addition, high value of critical size of nucleus caused a slow growth of crystal, which was due to the less solute-solvent interaction in the system (Abd Rahim, 2012).
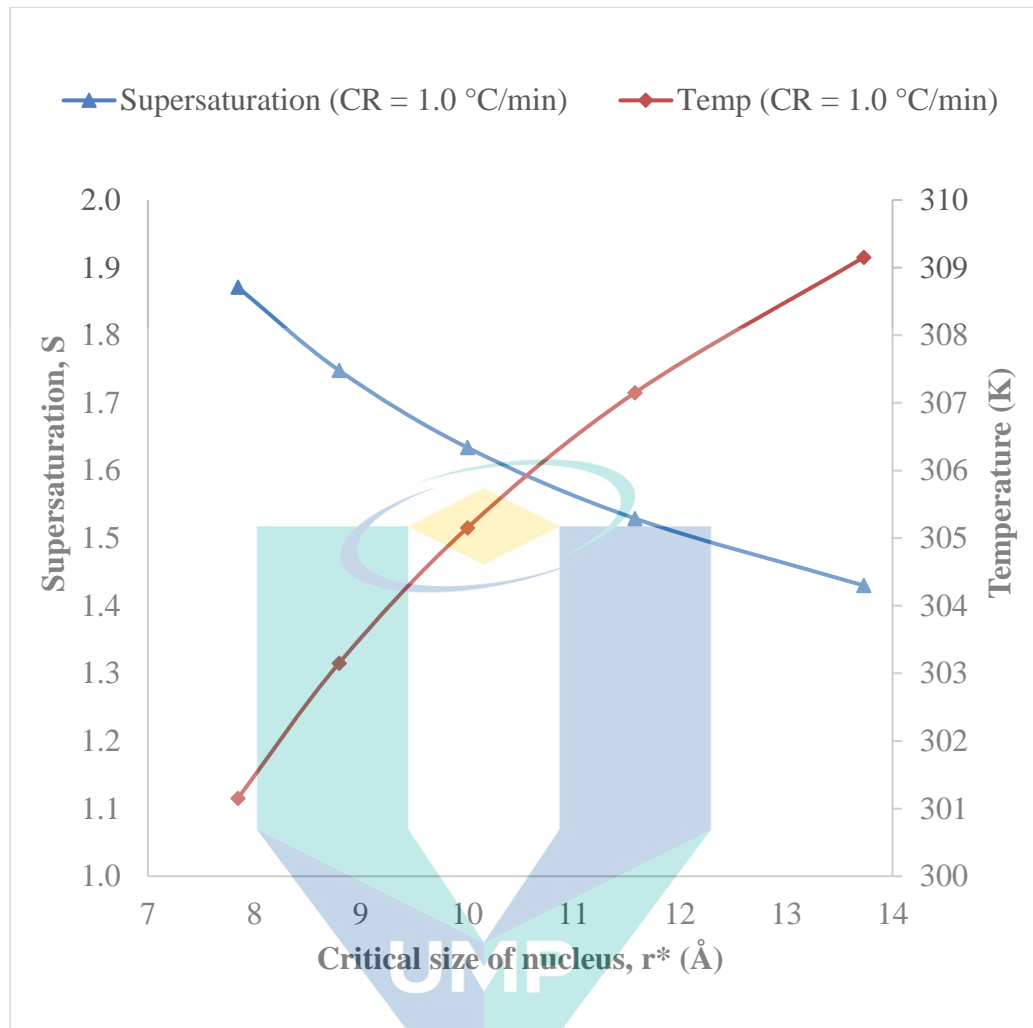
Figure 4.13   Graph of critical size of nucleus as a function of supersaturation and temperature .

4.4   Determination of Nucleation Kinetics Using KBHR Method

Results from slow cooling experiments were further analysed using KBHR method as described in Chapter 2, Sections 2.5.2. The values of T_{crys}, T_{diss}, T_e, ΔT_c and u_c for SAC/CBZ mole ratio of 2.0 at CBZ concentrations of 15.83, 17.01, 17.96 and 19.14 mg/ml were shown in Table 4.7. Flowchart for KBHR method can be seen in Appendix H . The value of T_{crys}, T_{diss}, T_e, ΔT_c and u_c for others SAC/CBZ mole ratios (1.0, 2.5, 3.0 and 3.5) were presented in Appendix I. Following the method, the graph ln R against ln u_c resulted in a straight line as evident in Figure 4.14. The slope of the best fit straight line for the graphs for all concentrations was presented in Table 4.8.

Table 4.7 T_{crys}, T_{diss}, T_e, ΔT_c and u_c for SAC/CBZ mole ratio of 2.0.

CBZ concentration (mg/ml)	Cooling rate, R /°C min⁻¹	T_{crys} /°C	T_{diss} /°C	T_e /°C	ΔT_c /°C	u_c /K
15.83	0.20	20.52	43.55	43.43	22.92	0.07
	0.40	16.40	44.10		27.04	0.09
	0.60	11.37	44.26		32.06	0.10
	0.80	9.07	44.33		34.36	0.11
17.01	0.20	23.98	45.67	45.09	19.45	0.06
	0.40	19.10	46.40		24.34	0.08
	0.60	17.20	47.05		26.23	0.08
	0.80	13.33	47.58		30.10	0.09
17.96	0.20	27.43	47.68	47.33	16.00	0.05
	0.40	25.19	47.85		18.24	0.06
	0.60	22.99	48.39		20.44	0.06
	0.80	20.85	48.55		22.58	0.07
19.14	0.20	27.61	48.75	48.34	15.82	0.05
	0.40	24.34	49.35		19.09	0.06
	0.60	22.59	51.19		20.84	0.06
	0.80	19.66	50.17		23.77	0.07
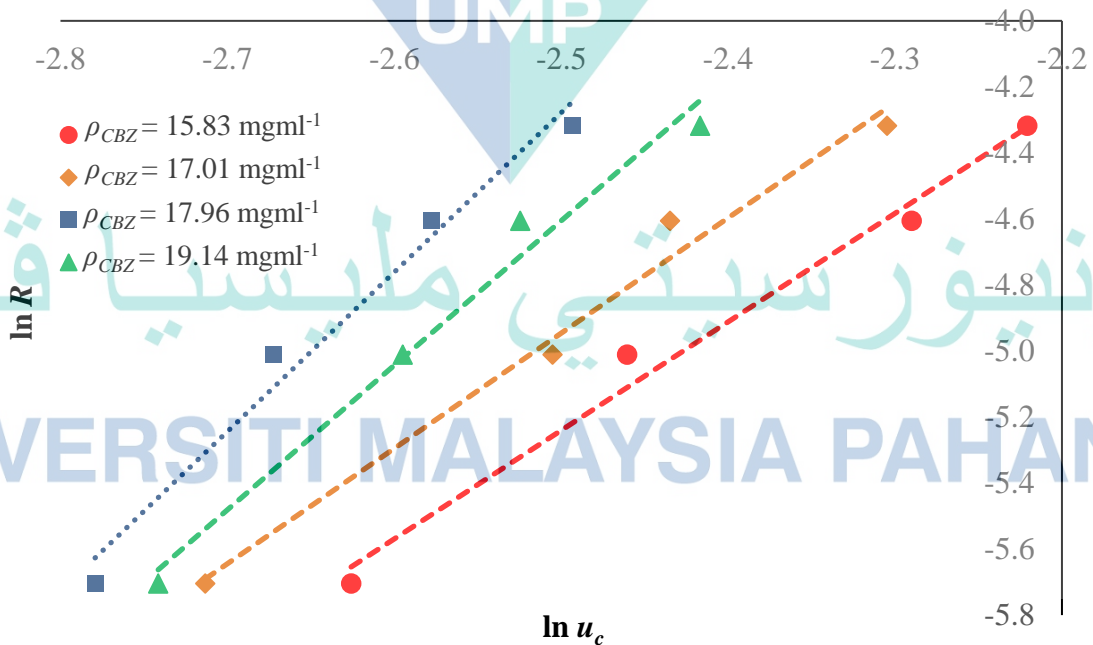
Figure 4.14   ln R vs ln u_c for all CBZ concentration, ρ$_{CBZ}$ and SAC/CBZ mole ratio of 2.0.

Table 4.8   The values of slope (ln R vs ln u_c), a_1, a_2, ln $R0$ and $R0$.

CBZ conc. (mg/ml)	T_e /K	Slope of best-fit straight line of ln R vs ln u_c	Nucleation mechanism	a_1	$a_2 = b$	ln R0	R0/Ks^{-1}
15.83	316.6	3.287	PN	3	0.002	2.381	30.978
17.01	318.2	3.266	PN	3	0.003	3.087	24.123
17.96	320.5	4.009	PN	3	0.001	3.346	21.098
19.14	321.5	3.491	PN	3	0.002	3.593	10.793

All values of slope were greater than 3, which indicated progressive nucleation. In progressive nucleation, the outcoming crystal were in a various size, due to the forming of new nuclei alongside with the older one. To proceed further, the inequalities $u_c < 0.1$ and $au_c < 1$ must be met. The value of the dimensionless, molecular latent heat of crystallisation, a was obtained from equation (2.29), where $\lambda = 8.98 \times 10^{-20}$ J, and K = 1.38×10^{-23}. Since the inequalities were met, the values of ln R0 and a_2 were determined from equation 2.30 and 2.31 respectively. The least square method yielded the values of ln R0 and a_2, given $a_1 = 3$ and $k_n = 16\pi/3$ for spherical nuclei. The values of a_2 and R0 were listed in Table 4.8. Then, the interfacial energy, γ_{eff}, was calculated following equation (2.38) with the molar volume, $V_m = 9.57 \times 10^{-28}$ nm^3. Lastly, the values of r* and i* were calculated based on the maximum and the minimum value of relative critical undercooling, u_c, for each concentration. The values of γ_{eff}, r* and i* were recorded in Table 4.9.

From Table 4.9 can be seen that, the critical size nucleus of CBZ-SAC co-crystals interfacial energy has no correlation with CBZ concentration. The value of interfacial energy is between 1.95 and 1.46 mJm^{-2}, which is from CBZ-SAC co-crystals with CBZ concentration of 17.01 and 17.96 mg/ml respectively.

Table 4.9   The value of γ_{eff}, r* and i* for low (L) and high (H) critical undercooling.

CBZ concentration, (mg/ml)	γ_{eff} /mJm^{-2}	r*(L) /nm	r*(H) /nm	i*(L)	i*(H)
15.83	1.69	0.4982	0.3323	0.5414	0.1606
17.01	1.95	0.6798	0.4393	1.3749	0.3710
17.96	1.46	0.6250	0.4428	1.0688	0.3800
19.14	1.62	0.7000	0.4658	1.5014	0.4424

4.5   Comparison of Results from Fast Cooling with KBHR Technique

When comparing the values from KBHR and fast cooling method, the values of interfacial energy (1.46 – 1.95 mJm^{-2}) from KBHR method were similar with a slightly lower value from the fast cooling method (1.067 – 1.095 mJm^{-2}). Critical radius of nucleus, r* from KBHR method gave value of (0.33 – 0.70 nm) and values fast cooling method were 2-fold higher (0.78 – 1.37 nm). Furthermore, molecular number of critical nucleus, i* in KBHR method were (0.16 – 1.50) and (2.11 – 11.32) in the fast cooling method, which were 2 to 10 times higher, which meant multi-fold numbers of nuclei created via isothermal method (Qiu, 2015).

4.6   Characterisation of CBZ-SAC Co-Crystal

4.6.1   Introduction

Cocrystal characterisation is an important constituent part within cocrystal research. The basic physicochemical properties of cocrystal can usually be characterised by X-ray diffraction (XRD), single crystal X-ray diffraction (SXRD), infrared spectroscopy (IR), Raman spectroscopy, differential scanning calorimetry (DSC), scanning electron microscopy (SEM), and terahertz spectroscopy. In this research, CBZ-SAC co-crystal screening products were characterized by Differential Scanning Calorimetry (DSC), and X-ray Diffraction (XRD) techniques. CBZ-SAC co-crystals

were compared with pure compound of CBZ and SAC and the properties were later confirmed with literature.

4.6.2 Characterisation of CBZ-SAC Co-Crystal by Differential Scanning Calorimetry (DSC)

Figure 4.15 shows DSC thermograms of CBZ-SAC co-crystals with CBZ/SAC ratio of 1.0 and CBZ concentration of 17.96 mg/ml compared with pure CBZ, and pure SAC specimens. The CBZ powder was characterized by a major peak at 191 ∘C and a small peak at 170 ∘C, corresponding to form III (the stable polymorph) and form I, respectively. SAC was verified by a single peak at 227 ∘C. The DSC of CBZ-SAC co-crystals peaks at 177°C correlates with co-crystals form I. This can be seen from Figure 4.15, in which 2 samples of CBZ-SAC co-crystal of Form I and Form II by Pagire et al.(2017) were taken as comparison to this results. Analysis by Pagire et al stated that, CBZ-SAC of Form I and Form II exhibit a peak of 177 °C and 165 °C respectively (Pagire et al., 2017). Thus CBZ-SAC co-crystal in this study correlates to co-crystal of form I. This is in accordance to the finding of Lee et al. (2015), in which at the end of the CBZ-SAC antisolvent crystallisation process, one prominent peak was left, which belongs to co-crystals form-I (Lee et al., 2015). In addition, studies from previous researches suggested that CBZ-SAC of form I has a single peak in the range of 176-178°C (Abd Rahim & Amanina Mohamad Adaris, 2018)
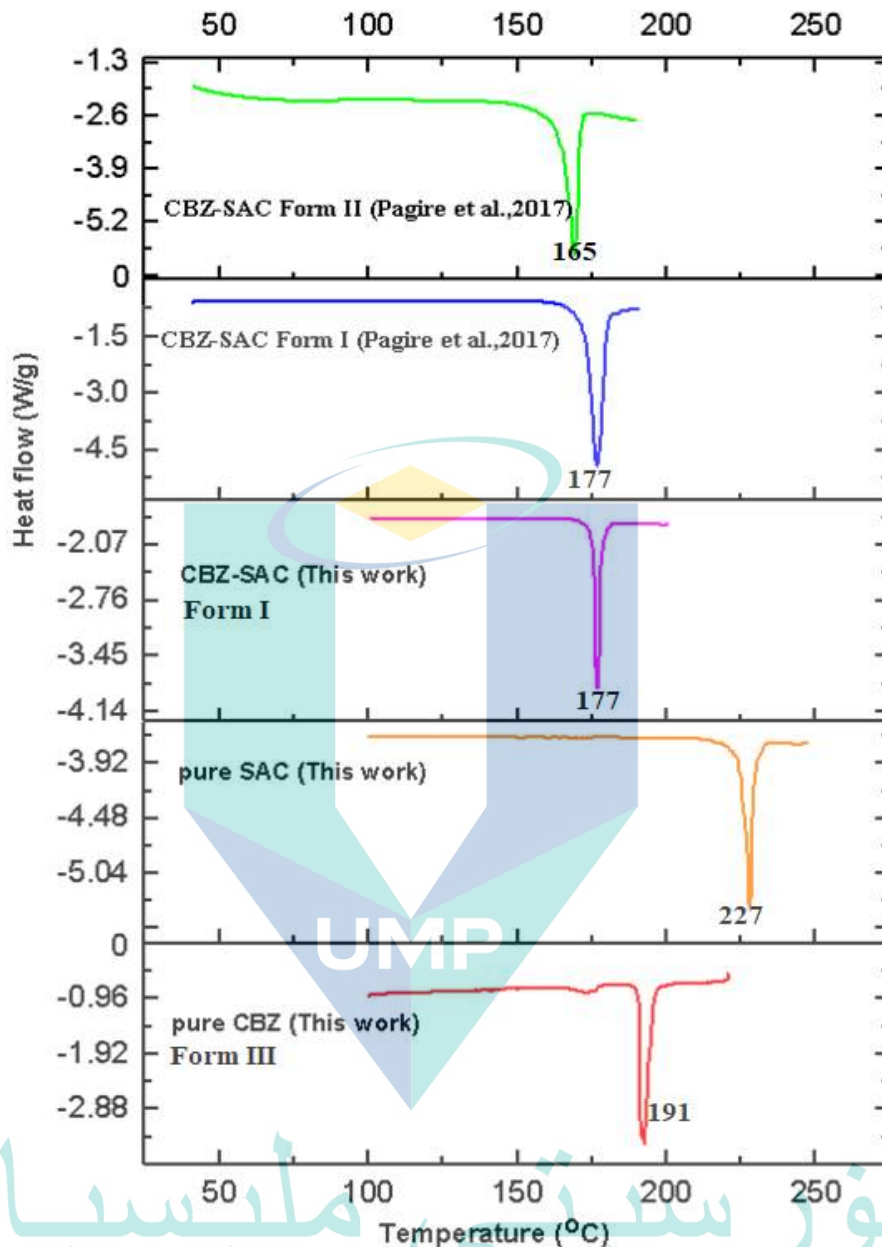
Figure 4.15   DSC of pure CBZ, pure SAC, CBZ-SAC co-crystals in this work and CBZ-SAC form I and II by Pagire et al. (2017).

Figure 4.16 showed the results from DSC of CBZ-SAC co-crystals produced by initial CBZ concentration of 17.96 and 19.14 mg/ml, SAC/CBZ molar ratio of 1.0 and 2.0 at cooling rate of 0.06, 0.08 and 0.1 °C/min. All profiles showed that the CBZ-SAC co-crystals exibit as a Form I, since the value of peaks were in between 176.96 and 178.47 °C, which was in the range of Form I CBZ-SAC co-crystals as stated from the literature (Pagire et al., 2017).

For the case of CBZ-SAC co-crystals by CBZ concentration of 17.96 mg/ml and molar ratio of SAC to CBZ of 1.0, an increased in cooling rate from 00.6 to 0.1 °C/min, resulted in the shifting of CBZ-SAC peak profile slightly to the right by 0.74 °C. The rest of the samples showed no correlation in changing of melting point as the cooling rate changed. As molar ratio of SAC to CBZ increased from 1.0 to 2.0, the melting point increased by 0.77 °C.
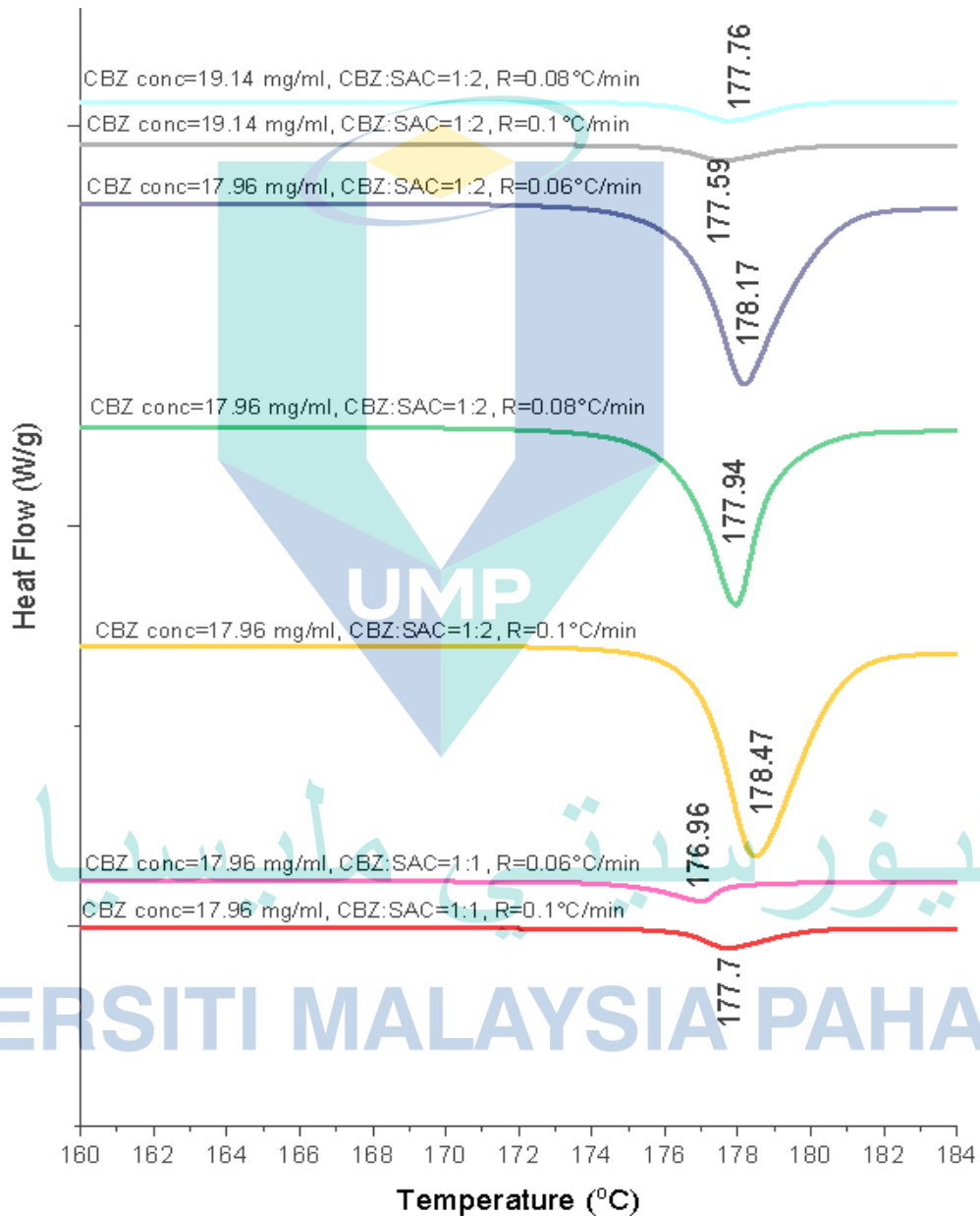
Figure 4.16   DSC of CBZ-SAC co-crystals from CBZ concentration of 17.96 and 19.14 mg/ml, SAC/CBZ molar ratio of 1.0 and 2.0 at cooling rate of 0.06, 0.08 and 0.1 °C/min.

4.6.3   Characterisation by X-ray Diffraction Spectra (XRD)

Figure 4.17 shows XRD pattern of CBZ-SAC co-crystals compared with pure component of CBZ and SAC as stated in the literature. The pattern shows three characteristic peaks of CBZ- SAC cocrystal Form I at 7°, 14° and 28° The finding is consistent with findings of recent studies by (Abd Rahim & Amanina Mohamad Adaris, 2018), in which the formation of CNZ-SAC co-crystals of Form 1 and Form II depending on method used in co-crystal formation and mol ratio of SAC to CBZ. Rahim et al. (2013) suggested that, with mole ratio of SAC/CBZ below than 1.5 for solvent of ethyl acetate, co-crystal of Form II instead of Form I was formed. In addition, according to Rahim, Hammond, Sheikh, & Roberts (2013) and Wang et al. (2013), the forming of different type of polymorphs influenced by different methods, antisolvent flowrate and addition of polymer additive.
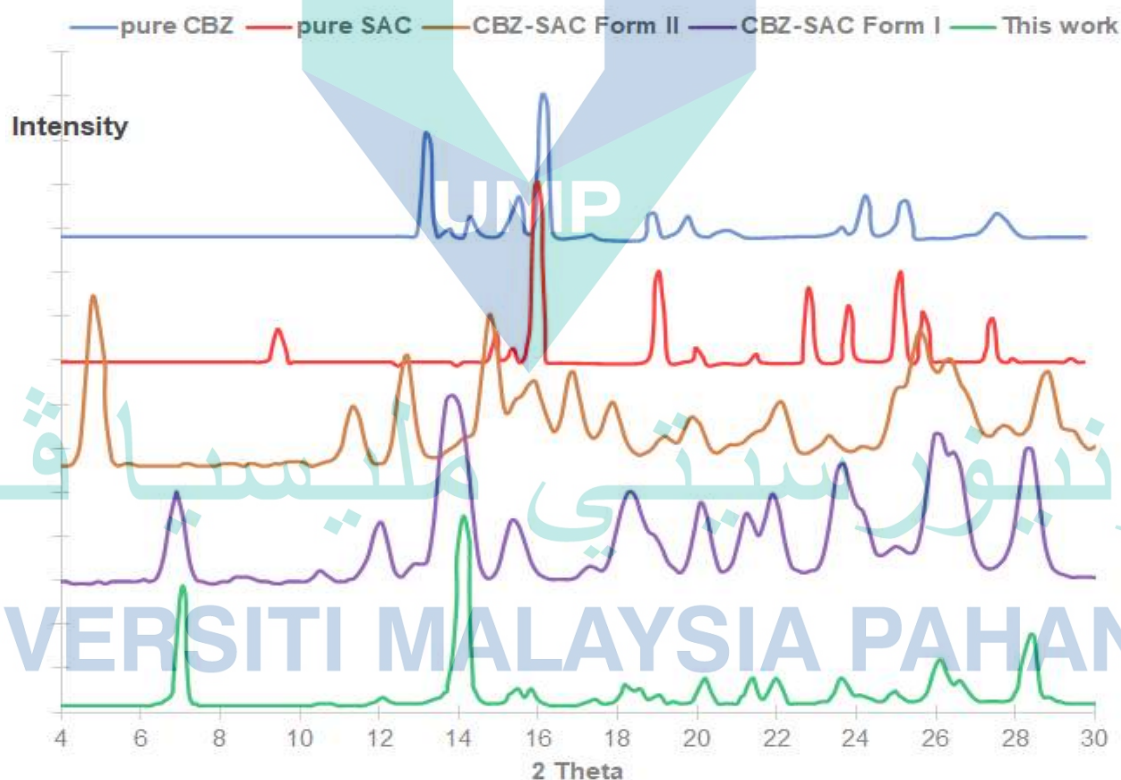
Figure 4.17   Comparison of XRD of CBZ-SAC co-crystal with literature.

Data pure CBZ and pure SAC. Source: Lu, Rodríguez-Hornedo, & Suryanarayanan (2008) and CBZ-SAC Form I and II. Source: Porter III, Elie, & Matzger (2008).
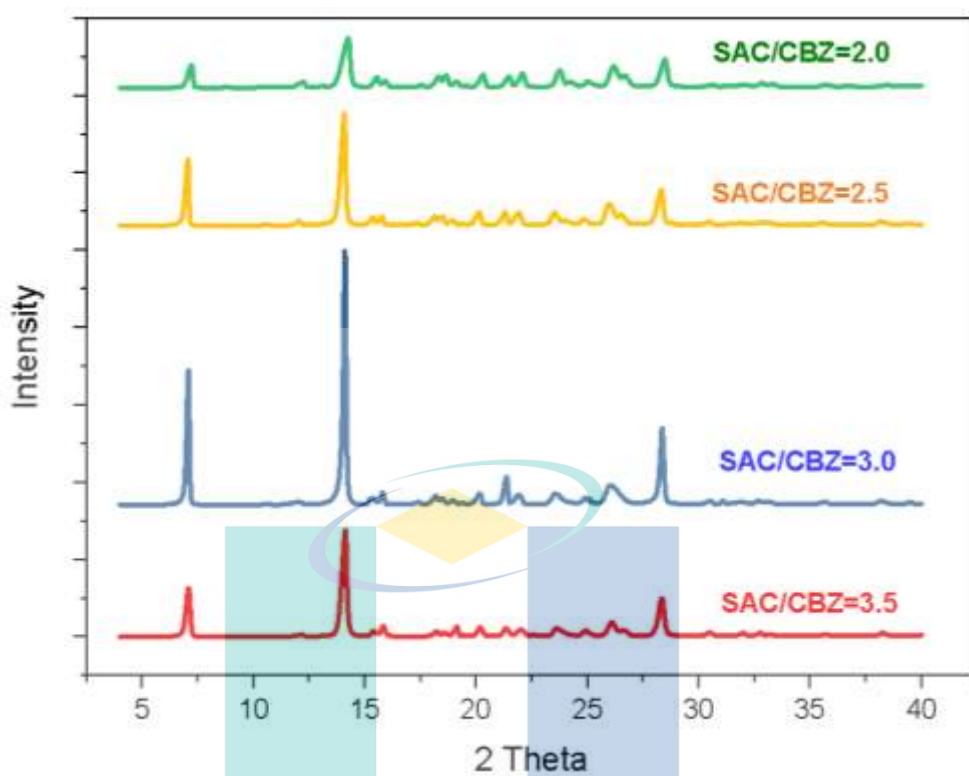
Figure 4.18   XRD of CBZ-SAC co-crystals with molar ratio SAC/CBZ of 2.0, 2.5, 3.0 and 3.5

Figure 4.18 showed the XRD pattern of CBZ-SAC co-crystals with SAC to CBZ molar ratio of 2.0, 2.5, 3.0, and 3.5. From the graph, the pattern showed that, all ratios of SAC to CBZ produced the CBZ-SAC of Form I, which can be indicated by three prevalence peaks at 7°, 14° and 28°. The changes in molar ratio had only affected the intensity of the profile, which was not an important factor to be discussed. But different intensity of same materials was due to the different size or height of the sample. The sample was in powder form, which was compacted on the sample holder, this process was also give an effect to intensity (Oliveira, 2013) .Most important in XRD analysis was the peak, which determined the polymorph form of the co-crystals. From previous studies, two known polymorphs (Form-I and -II) of the CBZ-SAC cocrystal were formed by controlling the experimental kinetic parameters (Abd Rahim, 2012; Lee et al., 2015).

CHAPTER 5

SEEDING PROCESS AND CRYSTAL SIZE DISTRIBUTION

5.1 Introduction

Seeding has been studied over the latest few decades because it can alter the properties of desired final crystal. In seeding process, the supersaturated solution was enhanced by addition of crystalline (seed) to allow the growth of the seed crystals prior to the occurrence of nucleation (Ulrich & Jones, 2012). As co-crystallisation is concerned, an introduction of seeding are mean to provide a co-crystal phase in solution during crystal growth and to prevent inconsistent primary nucleation of another solid phase during crystallisation (Gagniere et al., 2012). By considering the different parameters in seeding process such as size of seed, amount of seed, seeding temperature and cooling profile, seeding is therefore believed can expedite the nucleation process, optimise the crystallisation behaviour and ensure the final particle size (Aamir et al., 2010).

5.2 Metastable Zone Width for Seeding Process

Experiments in Section 3.2, with an initial suspension of 2.0 SAC/CBZ ratio and 17.96 mg/ml CBZ in 200 ml ethanol resulted in crystallisation temperature of 27.84 ^{o}C and a dissolution temperature of 47.55 ^{o}C. MSZW is defined as different between dissolution and crystallisation temperature. In this experiment, the suspension with the CBZ concentration, q_{CBZ} of 19.76 mg /ml and SAC/CBZ mole ratio of 2.0, was chosen due to the range of Tcrys and Tdiss value, which was near to the room temperature and therefore relevant for industrial pharmacy. . This result was further used for seeding experiment, where the point of seeding is based on this MSZW. The calculated seeding point is presented in Table 5.1. Sample calculation of seeding temperature was shown in Appendix J.

Table 5.1   Calculated seeding temperature based on MSZW range of 47.55 to 27.84°C

Seeding temperature (% of MSZW)	Calculated seeding temperature (°C)
95	46.56
85	44.59
75	42.62
65	40.65
55	38.68

5.3   Results of Seeding Experiments

Table 5.2 and Table 5.3 show the results of average crystallisation temperatures for the different seed mass and different seed size respectively. The raw data for both experiments can be seen in Appendix K. In general, the crystallisation temperature increases with seed mass or can be explained as the nucleation occurs earlier as the seed mass increases, as the surface area for nucleation increases. The detailed explanation shown in Section 5.4.

Table 5.2   Average temperature of crystallisation for seed size of 200-150 micron of different seed mass in mg, seed loading (seed wt%) and temperature of seeding, T_{seed}.

Seed mass (mg)	Seed wt%	T_{seed} (°C)	T_{seed} (% of MSZW)	Average T_{crys} (°C)
95.55	1.5	46.56	95	43.02
95.55	1.5	44.59	85	41.78
95.55	1.5	42.62	75	40.02
95.55	1.5	40.65	65	39.51
95.55	1.5	38.68	55	38.22
63.70	1.0	46.56	95	42.34
63.70	1.0	44.59	85	41.95
63.70	1.0	42.62	75	40.23
63.70	1.0	40.65	65	39.17
63.70	1.0	38.68	55	37.33
31.85	0.5	46.56	95	40.08
31.85	0.5	44.59	85	40.33
31.85	0.5	42.62	75	38.57
31.85	0.5	40.65	65	37.83
31.85	0.5	38.68	55	36.45

Table 5.3 shows the results of seeding experiment for different seed sizes of (200-150 µm), (150-125 µm) and (125-100 µm). The experiments were done at different seeding temperature between of 46.56 and 38.68 °C. For all size of CBZ-SAC seed, the crystallisation temperature increases with seeding temperature as the presence of seed particles has significantly narrowed the metastable zone, which will be elaborated in chapter 5.5.

Table 5.3   Average temperature of crystallisation for seed mass of 31.85g ~ Seed wt% = 0.5.

CBZ-SAC co-crystals seed size (µm)	T_{seed} (°C)	T_{seed} (% of MSZW)	average T_{crys} (°C)
(200-150)	46.56	95	37.86
(200-150)	44.59	85	37.04
(200-150)	42.62	75	37.10
(200-150)	40.65	65	33.62
(200-150)	38.68	55	31.82
(150-125)	46.56	95	37.67
(150-125)	44.59	85	36.92
(150-125)	42.62	75	36.26
(150-125)	40.65	65	35.47
(150-125)	38.68	55	36.23
(125-100)	46.56	95	40.77
(125-100)	44.59	85	40.57
(125-100)	42.62	75	38.66
(125-100)	40.65	65	38.53
(125-100)	38.68	55	37.95

5.4   Effect of Seed Loading on Crystallisation of CBZ-SAC Co-Crystal

Figure 5.1 demonstrates that, the crystallisation temperature increased with seed loading. When the seed was added at 55 % of MSZW, which equivalent to 38.68 °C, the crystallisation temperature for 0.5, 1.0 and 1.5 wt% of seed was 36.45, 37.33 and 38.22 °C respectively. The seed provides surface area for nucleation to occur; therefore higher seed loading resulted in higher surface area (Long et al., 2016; Mousaw et al., 2008), which expedites the nucleation process. Therefore, the nucleation occurs faster for seed loading of 1.5 wt %. Similar trends were also can

be seen for seeding temperature of 40.65, 42.62, 44.59 and 46.56 °C. The present finding also supported by Lui et al. (2010), which studied the crystallisation of hen-egg white lysozyme and concluded that a lower seed loading resulted in slow growth of crystals due to the less particle surface area, therefore resulted in higher supersaturation (low crystallisation temperature) (Liu et al., 2010).
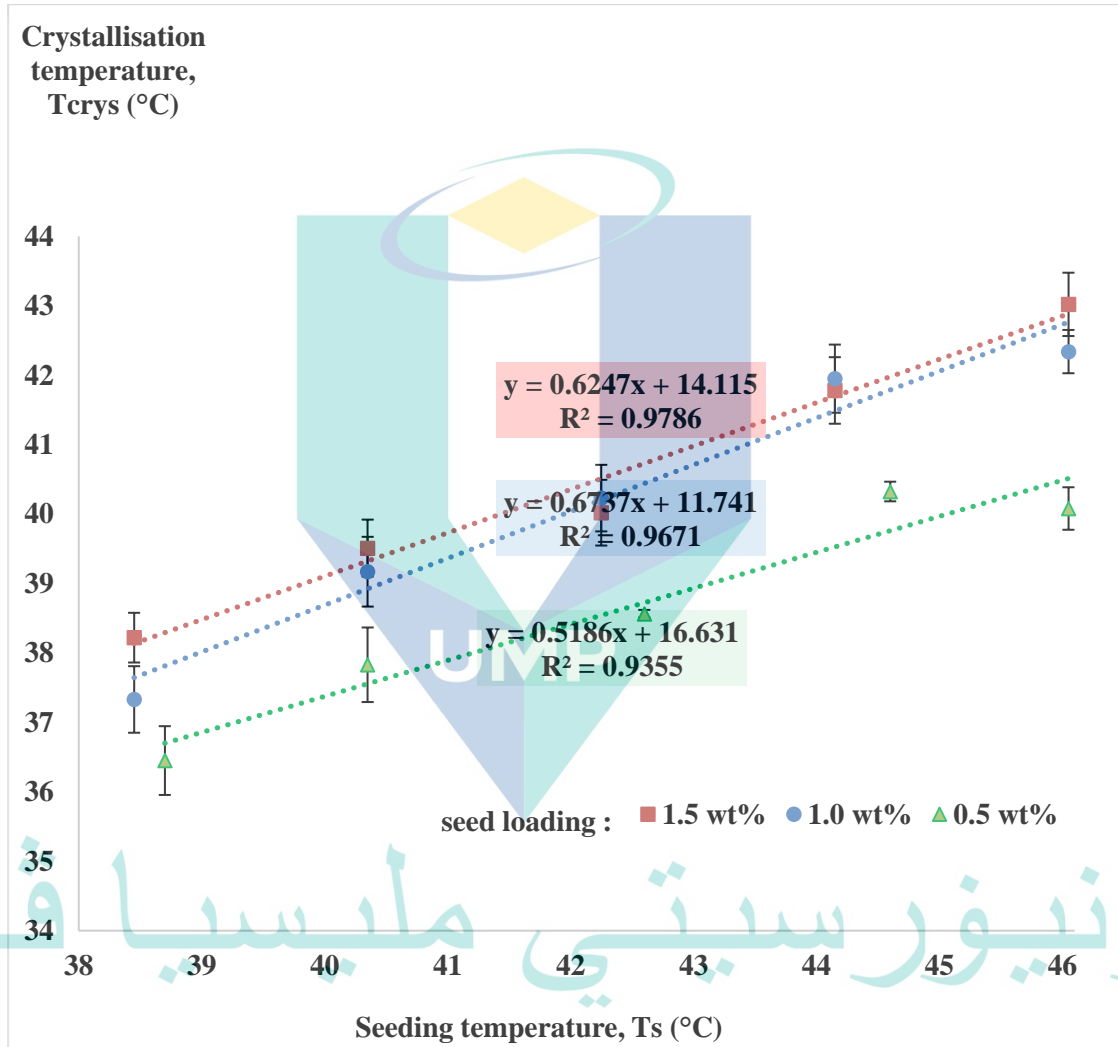
Figure 5.1   Effect of seed loading and seeding temperature on nucleation
.
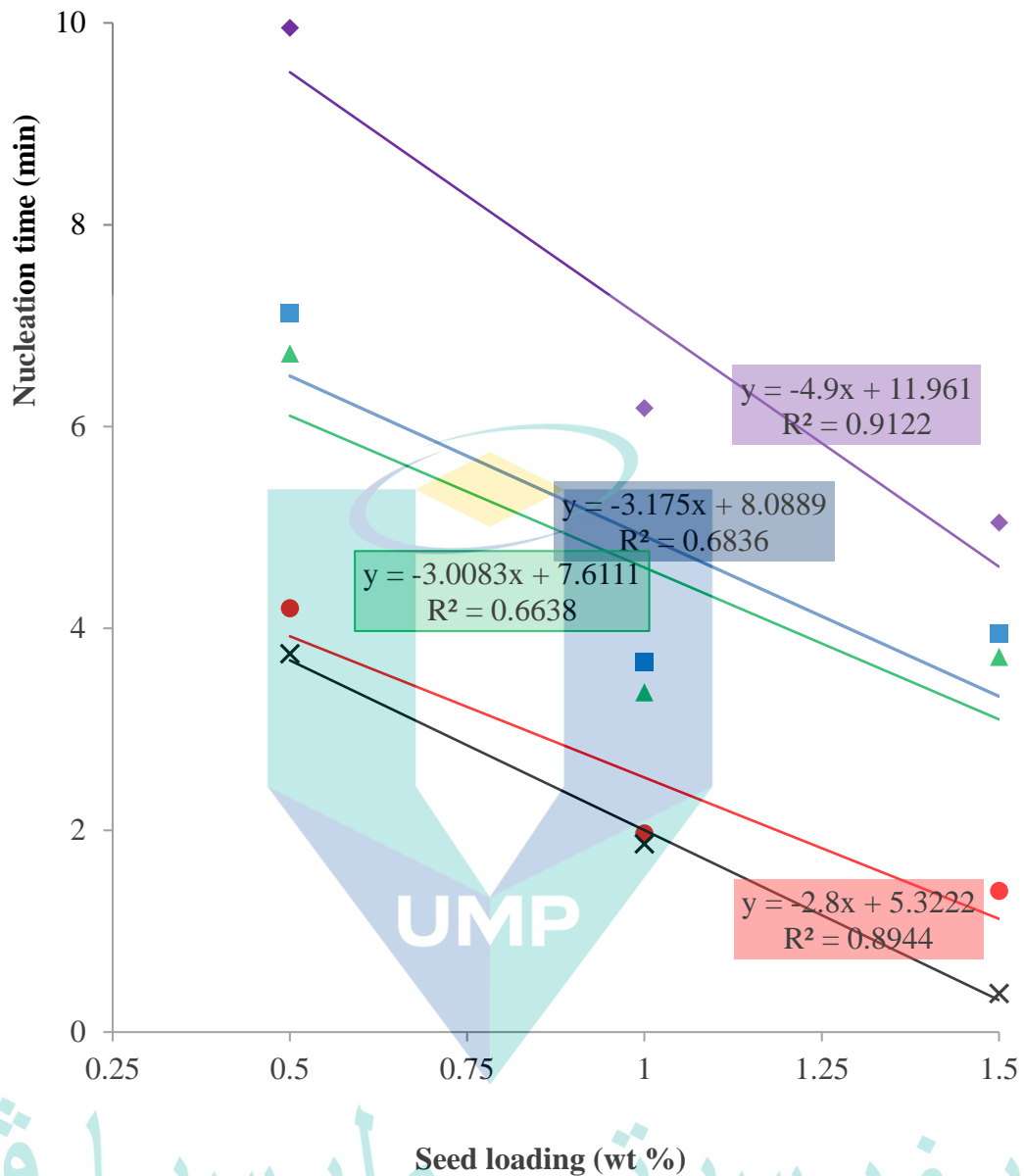
Figure 5.2   Effect of seed loading on nucleation time for different seeding temperatures (°C); ◆46.56, ■44.59, ▲42.62, ●40.65, ✖ 38.68.

5.5   Effect of Seeding Temperature on Crystallisation of CBZ-SAC Co-Crystal

As indicated in Figure 5.1, the crystallisation temperature increased with the seeding temperature. The presence of seed particles has significantly narrowed the metastable zone (Holaň et al., 2015; Liu et al., 2010). During seeding experiment,

the solution temperature was reduced at a constant cooling rate. The earlier introduction of seed (higher seeding temperature) resulted in earlier forming of nucleation. Therefore, the seeding temperature of 1.5 wt % of seed at 95 % of MSZW gave the crystallisation temperature of 43.02 °C, whereas seeding at 55 % of MSZW gave the crystallisation temperature of 38.22 °C. In kinetics view, seeding closed to the solubility curve (46.56 °C), which is at low supersaturation level causing a slow nucleation rate and therefore longer time is required for nucleation to occur (Holaň et al., 2015; O'Sullivan et al., 2012) (see Figure 5.3).
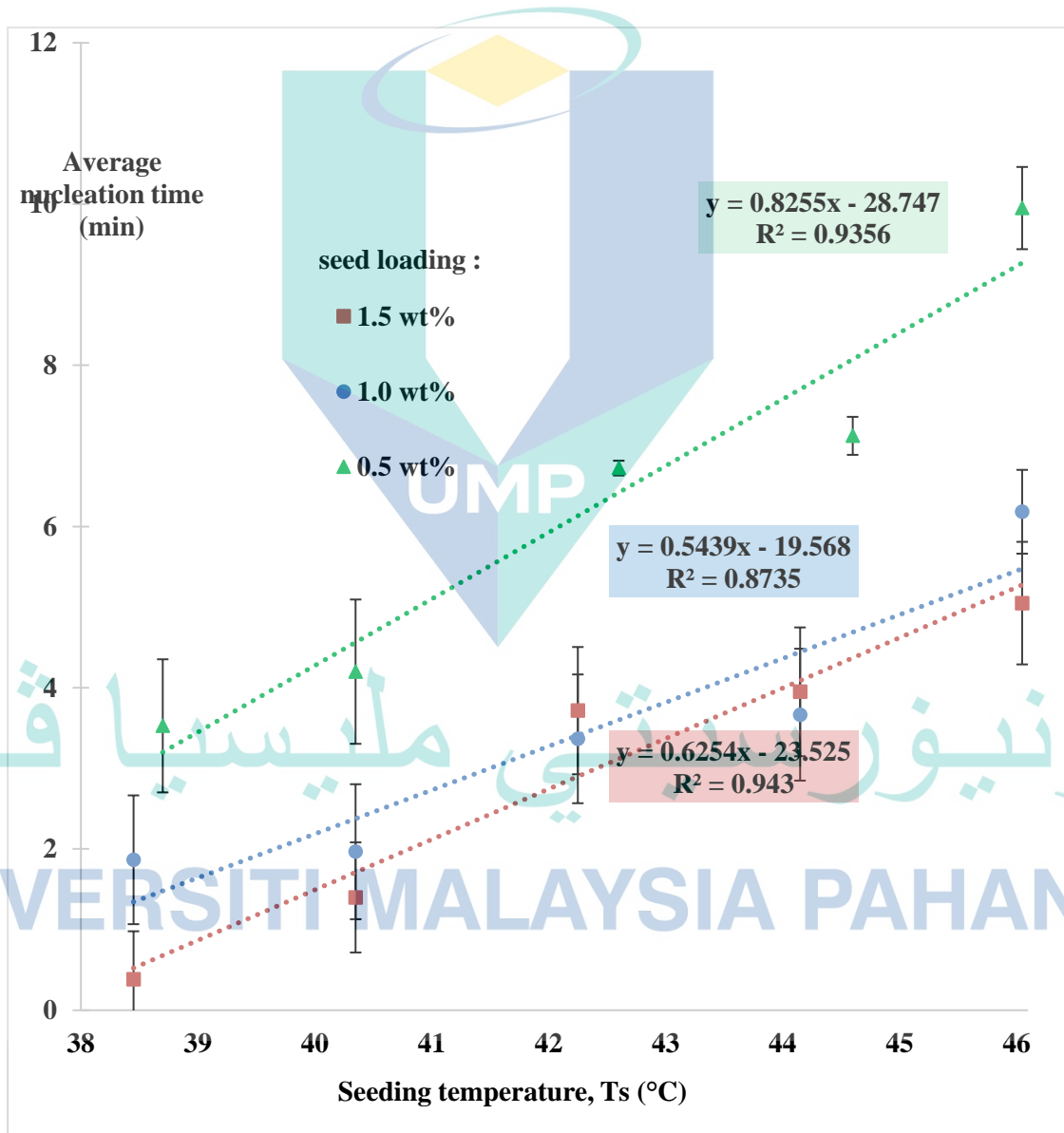
Figure 5.3   Effect of seeding temperature on nucleation time

5.6   Effect of Seed Size on Crystallisation of CBZ-SAC Co-Crystal

Crystallisation kinetics are strongly affected by size and amount of seed added in the system. With constant seed loading, nucleation times for seed sizes of (200-150), (150-125) and (125-100) µm at seeding temperature of 46.56, 44.59, 42.62, 40.65 and 38.68 °C were recorded. Table 5.4 shows the influence of seed size on the nucleation for different seeding temperature of CBZ-SAC co-crystals. Data from Table 5.4 were presented in Figure 5.4 as average seed size for all seeding temperature as a function of average nucleation time. As can been seen from Figure 5.4, the nucleation time is increased with the size of seed for all temperature of seeding. Small seed provides a larger surface area for solute to be deposit, and therefore reduce supersaturation level and expedited the nucleation (Mitchell et al., 2011). According to crystal nucleation theory, seed size must be bigger than critical size , or otherwise it will re-dissolved in the solution (Abbas et al., 2006). Furthermore, small seed crystal tends to dissolve due to Ostwald ripening effect (Chianese & Kramer, 2012b). In this study, the seed size used was between 200 and 100 µm, and the critical size nucleus as calculated in Section 4.3.2 was between 0.Sander et al. explained that, the birth and spread mechanism of growth controlled the nucleation, which is inversely proportional to the crystal size and mass. Bigger size of seed reduced the growth kinetic parameter, g and resulted to the high nucleation time (Sander et al., 2009). An assumption for explaining the effect of seed size to the nucleation is that, the agglomeration, which can lead to the large effectiveness of the seed size is negligible (Tseng & Ward, 2014). If agglomeration among seed crystals occur, selection of large seed crystals are preferable (Narducci et al., 2011).

Table 5.4   Average crystallisation temperature and nucleation time for seed size of 200-150 μm, 150-125 μm and 125-100 μm at different seeding temperature.

Seeding temperature, T_{seed} (°C)	Seed size (μm)	Average nucleation temperature, T_{nucl} (°C)	Average nucleation time,t_{nuc} (min)
46.56	200-150	37.86	13.65
	150-125	38.52	12.55
	125-100	40.77	8.80
44.59	200-150	37.04	11.85
	150-125	39.92	7.05
	125-100	40.57	5.97
42.62	200-150	37.10	8.59
	150-125	38.02	7.05
	125-100	38.66	5.98
40.65	200-150	33.62	11.22
	150-125	35.47	8.13
	125-100	38.53	3.03
38.68	200-150	31.82	11.06
	150-125	36.23	3.70
	125-100	37.95	0.83
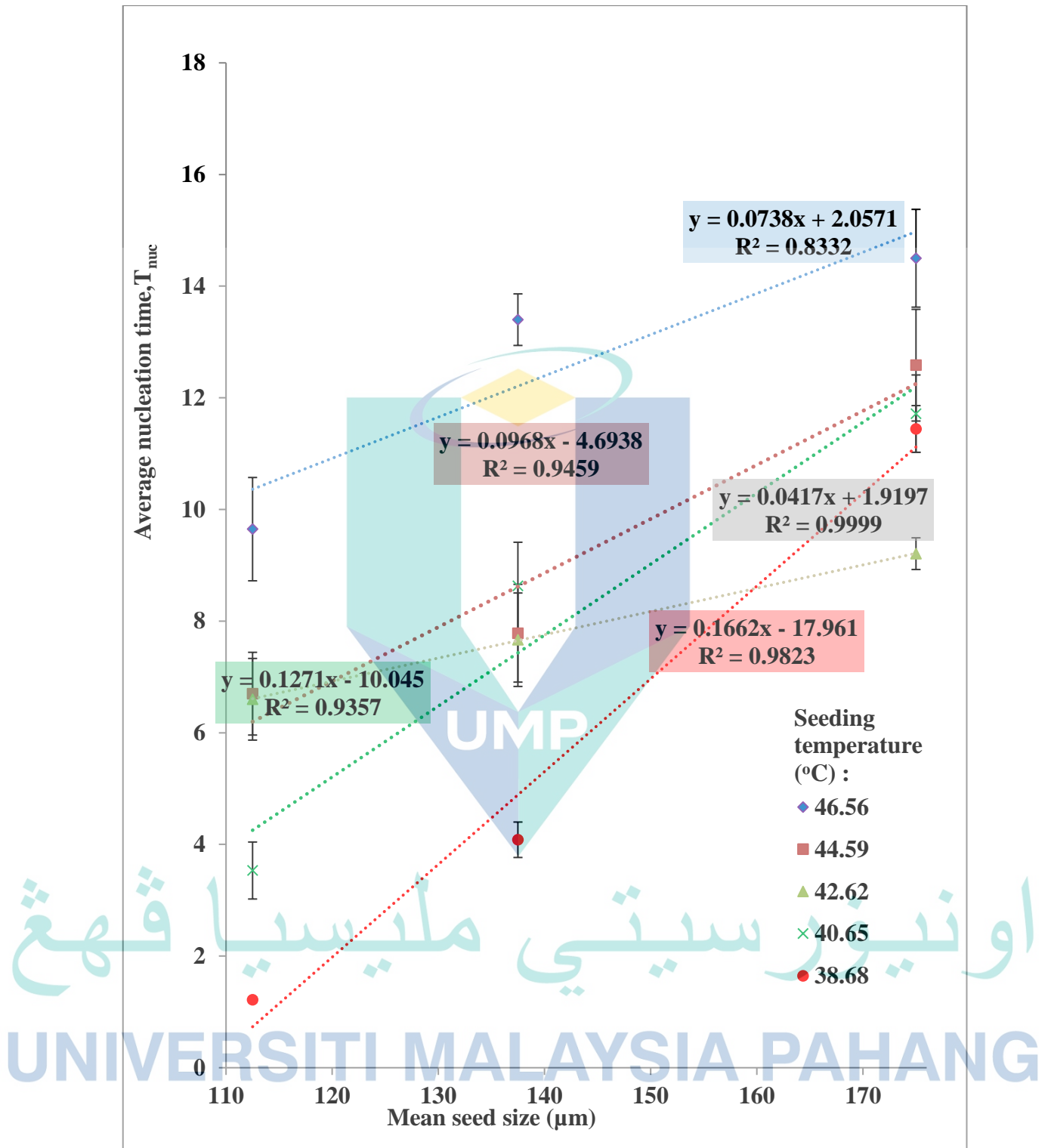
Figure 5.4   Effect of seed size on nucleation time for different seeding temperature

5.7   Crystal Size Distribution of CBZ-SAC Co-Crystal

5.7.1   Effect of Seeding Temperature on Crystal Size Distribution (CSD) of CBZ-SAC Co-Crystal

Figure 5.5 exhibits that, more fine particles formed at seeding temperature of 38.68 ºC (55 % of MSZW) compared to the seeding temperature of 46.56 ºC (95 % of MSZW). The supersaturation is highest at metastable zone limit (0 % of MSZW). Therefore, seeding at high supersaturation leads to the fast nucleation rate which later resulting in more fine particles. On the other hand, slow nucleation occurred when seeding is close to the solubility curve which is at low supersaturation and therefore resulted in least number of fine particles formed. The result is in lines with the work of O'Sullivan et al. (2012) that particle growth is slower if seeding close to the MSZ limit (38.68 ºC), which resulted in the least particle growth. This means, at low seeding temperature, subsequent growth of the nuclei until equilibrium is attained, is limited. Meanwhile, seeding close to the solubility curve (46.56 °C) produces the highest relative growth rate and the greatest number of large particles (O'Sullivan et al., 2012). Similar finding by Holaň et al. (2015), which studied the effect of seeding temperature on agomelatine–citric acid co-crystal found that, when the system seeded early (at higher seeding temperature; i.e. 60 ºC), resulted in larger crystal size. This was due to crystal growth dominated over nucleation because of the concentration was still deep in the MSZ at the time of seeding. Another parameter that can increase the size of crystal produced are fast cooling rate and high initial supersaturation (Zhang et al., 2016).
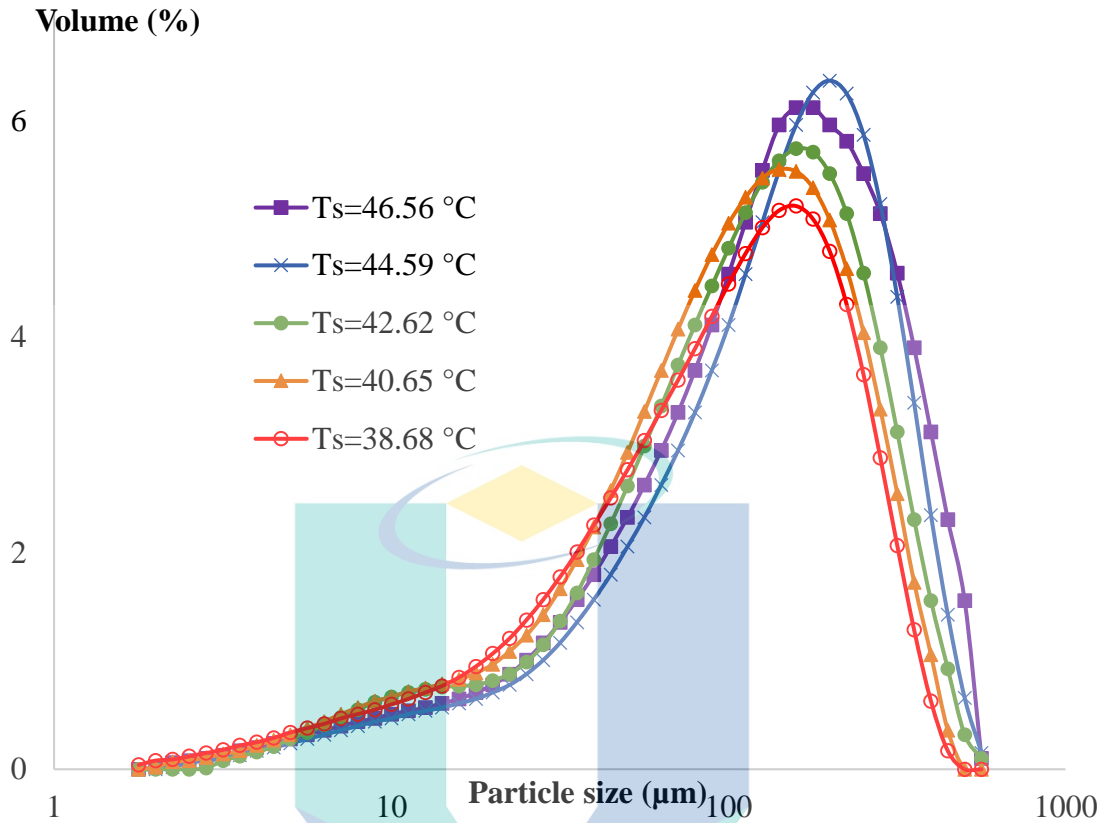
Figure 5.5   Effect of seeding temperature on CSD of CBZ-SAC co-crystal.

5.7.2   Effect of Seed Loading on CSD of CBZ-SAC Co-Crystal

Figure 5.6 presents particle size distributions at three different values of seeding load of CBZ-SAC co-crystals at 38.68°C seeding temperature. It appears that, the product crystal from 0.5 wt% seed experiments are larger in comparison to the 1.0 and 1.5 wt% seed experiment. This suggests that the amount of seed has an effect on the nucleation and growth kinetics of the system, where by at lower seed loading the growth of crystals appears to be favoured (Powell, 2017). The seed mass is proportional to the surface area of seed crystals and their size (Chianese & Kramer, 2012a). Seed load or specifically the seed surface areas critically determines the rate at which supersaturation is consumed by the growing homogeneous seeds (Hayles-Hahn, 2014). Homogenous seed produced by nucleation process when molecular solutes were completely dissolved in a liquid in the absence of any solid interface (LaMer & Dinegar, 1950; Salas et al., 2012; Zadeh, 2014). Industrial seed loading levels range from as low as 0.5 wt.% to as high as 10 wt.% (Aamir

98

et al., 2010). The crystal size distribution is normally unimodal at high seed load , whereas CSD is widespread a low wt% of seed (Hayles-Hahn, 2014; Narducci, 2012).
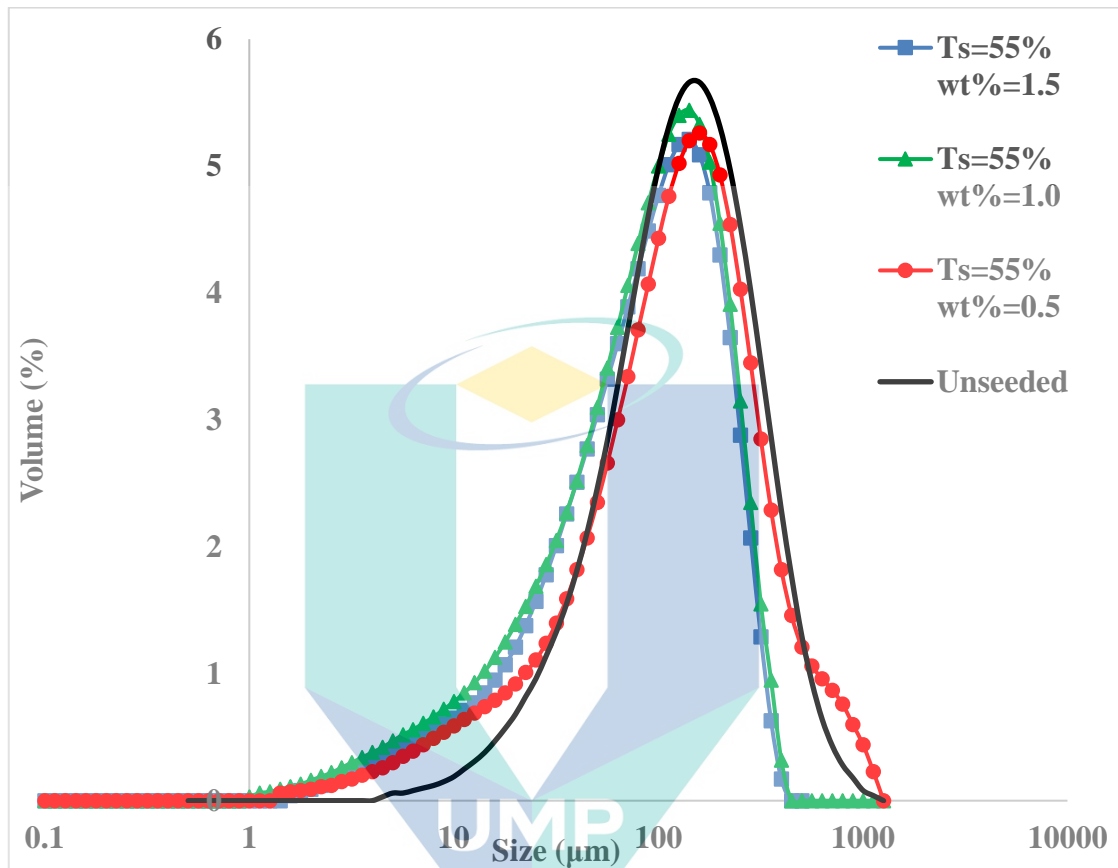
Figure 5.6   Effect of amount of seed on the crystal size distribution of CBZ-SAC co-crystals. Seeding temperature is 38.68 ºC (55% of MSZW range)

5.7.3   Effect of Seed Size on CSD of CBZ-SAC Co-Crystal

A smaller seed size provides a larger specific surface area for the crystal growth process. If crystal growth is dominant, it resulted to the large size of crystal produced. As can be seen in Figure 5.7, the distribution was broadening for seed size of (125-100)μm due to the larger co-crystals produced. This is valid for both seeding temperature of, 42.62 ºC and 38.68 ºC, as shown in the Figure 5.7. As mentioned in section 5.7.1 above, the lower seeding temperature reduced the particle growth and resulted in more fine particles. Therefore, the co-crystal produced from seeding temperature of 38.68 ºC resulted in smaller size as seen in Figure 5.7 compared to co-crystal produced by temperature of seeding of 42.62 ºC.

In industrial application, it is advisable to use smaller seed for controlling final crystal size. Smaller seed accelerates crystal growth, thus large and good quality final crystals can be produced. In contrast, seeds with bigger size can lead to the secondary nucleation , which is due to the attrition occurred during the nucleation process (Lung-Somarriba et al., 2004). But the seed should not be too small to avoid difficult preparation of seed, slow growth and dissolution, and high chance of agglomeration. Ideal seed size in industry is between 0.1% and 3% of total product mass, as suggested by Chianese & Kramer (2012), whilst large seed mass can be uneconomical with respect to process yield and furthermore it can causes an attrition in secondary nucleation.
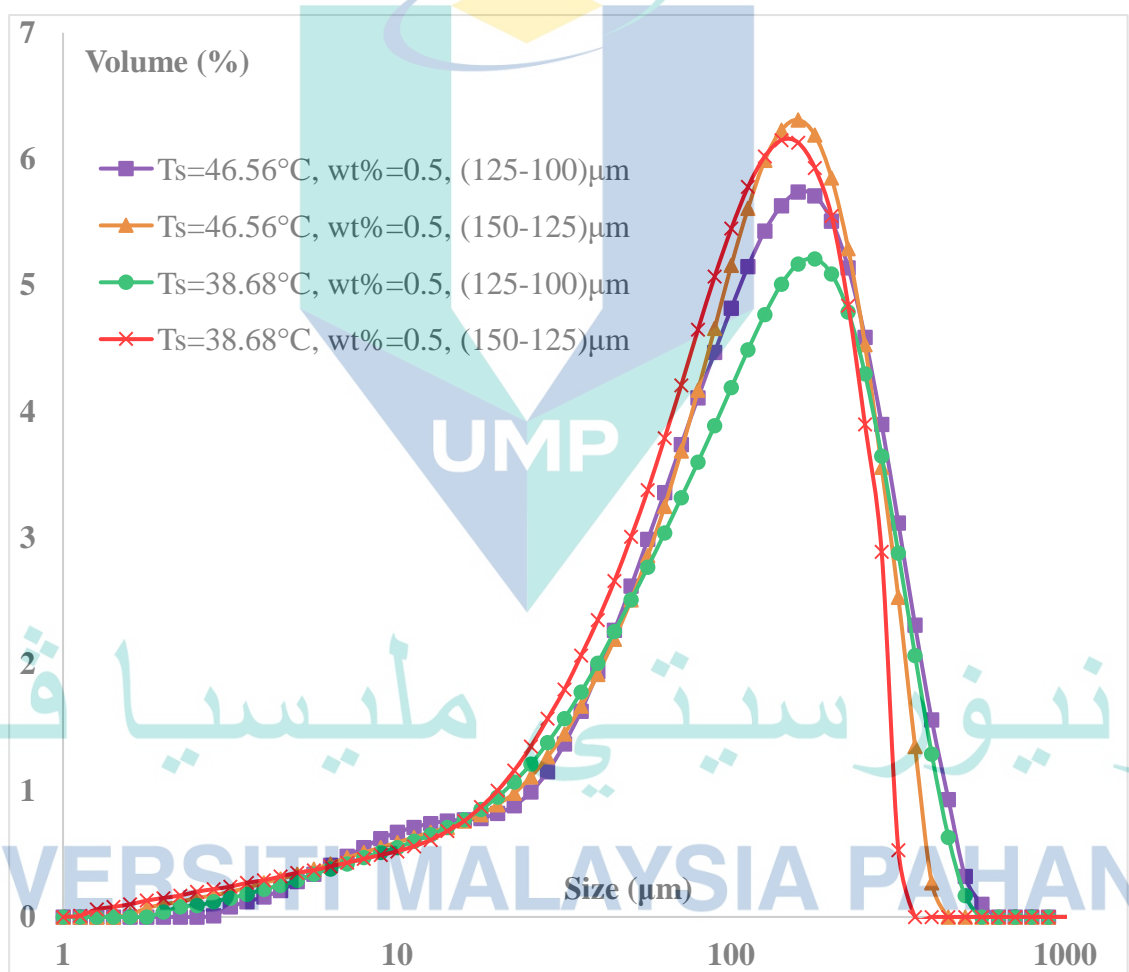
Figure 5.7   Effect of seed size on CSD of CBZ-SAC co-crystals with seeding temperature of 46.56 and 38.68 ºC.

5.8   Summary

The present research was aimed to investigate the effect of seed loading and temperature of seeding on CBZ-SAC co-crystals. These findings suggest that in general the seed loading and the temperature of seeding strongly influences the crystallization kinetics parameters and the produced crystals size distribution. Seed serves as a surface area for initiating the nucleation. By increasing the amount of seed, more surface area exists and therefore the nucleation is likely to occur. Nucleation forms faster in high supersaturated solution. More fine particles can be obtained if seeding in high supersaturated solution. Seeding close to the solubility curve (at $46.05^{\circ}C$) resulted in larger crystal size compared to the seed added close to MSZ limit. The results of this study also indicate that the effect of seeding in co-crystal is similar with that in crystal. Further studies investigating the morphology of seeded and unseeded CBZ-SAC co-crystals, effect of cooling rates and the effect of stirring speed, with different SAC to CBZ molar ratios and various concentration of CBZ, are strongly recommended.
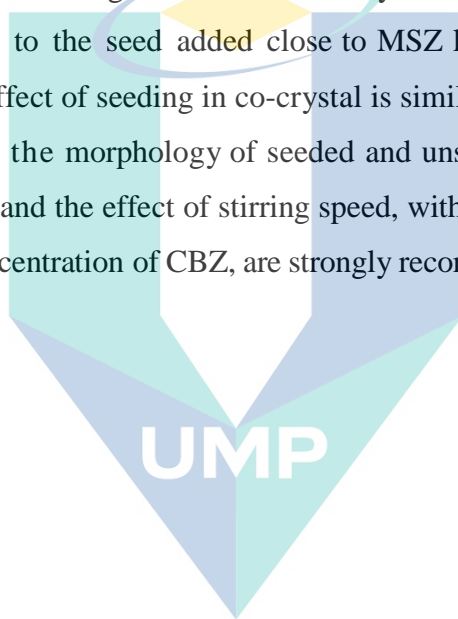
CHAPTER 6

CONCLUSIONS AND RECOMMENDATION FOR FUTURE WORK

6.1   Conclusion

Crystallisation is a process to separate and purify solid or mixture in a solution with an aim to control the properties of desired crystalline products. Co-crystals were introduced in late 1980's to alter the physicochemical properties of active pharmaceutical ingredient (API) through combining API and additional components (i.e. co-formers) in the same crystal structure thereby altering solid-state properties and solution behaviour without modifying chemical structure. The present research focused on the kinetic of carbamazepine (CBZ)-saccharin (SAC) co-crystals, which were to date have been poorly characterised. Slow cooling experiments with a newly improved method for determination of dissolution temperature were conducted at different CBZ concentrations and different SAC to CBZ molar ratios. The crystallisation occurs in a metastable region, which exists in a supersaturated solution. The conclusion of this study was concluded based on following objective and chapters:

6.1.1   Slow Cooling Experiments

In slow cooling experiments, metastable zone width (MSZW) was wide as cooling rate increased from 0.2 to 0.8 °C/min. High degree of cooling rate lead to the delaying of formation of nuclei, due to the changing of molecular structure was slower than the change of temperature. Nucleation theory stated that, at high cooling rate, high relaxation time is required for molecular cluster to reach an equilibrium and form a stable nucleus. Furthermore, MSZW was narrow as CBZ concentrations increased from 15.86 to 19.14 mg/ml. From theory of nucleation, an increased in initial concentration increases the level of supersaturation, thus enhances the nucleation. The earlier the nucleation takes place, the narrower the MSZW. The last variable

observed in this study was molar ratios of SAC to CBZ. The effect of molar ratios to MSZW was similar to the effect of initial CBZ concentration. As molar ratios of SAC to CBZ increased from 1.0 to 3.5, the MSZW was decreased. In conclusion, the mol ratio of SAC to CBZ and the concentration of CBZ gave the tremendous effect on dissolution and crystallization temperature of the CBZ-SAC mixture in ethanol solution. The calculated nucleation order from SAC/CBZ mole ratio of 1.0 in this study showed no correlation with the CBZ concentrations and SAC to CBZ molar ratios, which was in accordance with the previous findings. Nevertheless, the values of nucleation order, m obtained from all experiments were acceptable as it were in the value range of 1.65 to 4.9, which are the normal nucleation order value of the organic compounds. The low value of m indicated that there was strong solute-solvent interaction which induced the formation of stable CBZ-SAC cocrystal (Form I). Furthermore k-value of SAC/CBZ mole ratio of 1.0 increased from 0.14 x 10^{-7} to 7.31 x 10^{-7} as CBZ concentration increase from 15.83 to 19.14 mg/ml. The value of nucleation kinetic constant from SAC/CBZ mole ratio of 2.0 to 3.5 showed rather no correlation with CBZ concentration.

6.1.2 Fast Cooling Experiments

The fast cooling experiments were conducted by selecting one parameter from slow cooling (CBZ concentration of 19.76 mg/ml and SAC to CBZ mole ratio of 2.0), which gave a high MSZW value. The crystallisation and dissolution temperature of selected parameter were between 47.55 and 27.84 °C, which can be easily controlled. Our machine in lab was not capable to handle with the cooling rate of higher than 1.0 °C/min, which can be seen by the inconsistent profiles of targeted and actual temperature, thus the experiments were later on continued with cooling rate of 1.0 °C/min only. As targeted temperature increased from 32 to 44 °C, the supersaturation decreased and lead to a decrease in interfacial energy. Interfacial energy was higher at lower targeting temperature indicated that, the solute can be easily crystallised. Interfacial energy, critical size nucleus and molecular number of critical nucleus were obtained following the equations in Chapter 2, in which the gradient of plotted graph of ln (induction time) against ln (Supersaturation)$^{-2}$ played an important role. As a result, by changing the

isothermal temperature in fast cooling experiment from 32 to 44 $^{\circ}$C, the calculated interfacial energy increased from 1.067 to 1.095 mJm^{-2}. Furthermore, the critical size of nucleus increased with the decreased in supersaturation ratio. High supersaturation ratio led to the lower energy barrier for nucleation and resulted to the formation of small size of nucleus. Therefore, as the supersaturation ratio increased from 1.430 to 1.871, the critical size of nucleus decreased from 1.373 to 0.784 nanometre.

6.1.3 KBHR Method

Nucleation kinetics of CBZ-SAC co-crystals were further analysed using new technique by Kashchiev–Borissova–Hammond–Roberts (KBHR) method. The advantage of this method was that, the experiments can be shorten, as the data from polythermal experiments were ample to calculate the interfacial energy, critical size nucleus and molecular number of critical nucleus of the CBZ-SAC co-crystals. In summary, as the CBZ concentration increased from 15.93 to 19.14 mg/ml, the calculated interfacial energy, critical size nucleus and molecular number of critical nucleus were ranging from 1.69 to 1.62 mJ/m^2, 0.498 to 0.700 nm and 0.541 to 1.501 respectively. As the results from KBHR method were compared with fast cooling experiment, the value of critical size nucleus 2-fold lower and molecular number of critical nucleus 2 to 10 times higher for the fast cooling experiments.

6.1.4 Seeding Experiments

The nucleation process can be expedited by addition of seed, which provide surface area for nucleation to occur. This research focused on the effect of seed loading, seeding temperature and seed size on the crystallisation rate and crystal size distribution (CSD) of the final crystalline products. Likewise, in the fast cooling experiment, the parameter that resulting in high MSZW (CBZ concentration of 19.76 mg/ml and SAC to CBZ mole ratio of 2.0) was chosen, due to that parameter can be easily controlled. As seed loading increased from 0.5 to 1.5 wt%, the crystallisation

rate increased and the crystal size distribution was narrower, which meant that more fine particles were produced. Amount of seed affected the nucleation and growth kinetics of the system, where growth of crystals was favourable with lower amount of seed. Furthermore, when seed was added earlier in the system, 46.56 °C or closed to the solubility curve, the average nucleation time was higher. This meant that, high seeding temperature formed the system is in low supersaturation level. With low degree of supersaturation, longer time needed to form a crystal. As a result, with slow nucleation rate, crystal growth was dominant and larger final crystalline particle produced. On other hand, when seed was added later in the system (38.68 °C), the solution is in high supersaturated, resulted to the faster nucleation rate and more fine particles produced. Lastly, the nucleation time was increased, as seed size increased from 125-100 μm to 200-150 μm. Small seed provides a larger surface area for solute to be deposit, and therefore reduce supersaturation level and expedited the nucleation. The results of this study also indicate that the effect of seeding in co-crystal is similar with that in crystal.

6.1.5   Characterisation

Finally, from characterisation process, it was proven that, for all CBZ-SAC co-crystal in ethanol solution with CBZ concentration of 19.14, 17.96, 17.01 and 15.83 mg/ml and SAC/CBZ molar ratio of 1.0, 2.0, 2.5, 3.0 and 3.5, the CBZ-SAC co-crystals of Form I were formed and no pattern profile from XRD or DSC showed other form instead.

6.2   Recommendation for Future Work

In this study some aspects should be improved to get better and accurate results. Recommendations for future work based on the research results presented in this thesis are mentioned in the following section.

6.2.1 Prerequisite for the Experiments

Design of experiments (DOE) should be done earlier to get the relationship between factor affecting the process of producing CBZ-SAC co-crystal and the output or the properties of co-crystal produced, thus the parameters correctly chosen, thus experiments could be optimised.

Solubility studies should be done for each CBZ concentration and molar ratios of SAC to CBZ. The solubility results are not appropriate to be taken just based on previous research. In any research, there are no exactly same result due to experiment condition internally such as machine, compounds, solvent or external factors such as surrounding, temperature and unavoidable human error.

6.2.2 Experimental Setup

Losing of solvent during crystallisation can be avoided by using vacuum jacketed vessel. Furthermore, the evaporated solvent could be condensed by adding a condenser in the system. Losing the solvent in the next cycle of crystallisation experiments gave huge effect on determining the crystallisation and dissolution temperature of the co-crystals.

pH probe could be added in crystalliser, because pH in solution is one of the important parameters to be considered in crystallisation process. It has been reported that the pH and temperature played an important role in deciding the mean crystal size and shape of crystal produced (Mohod & Gogate, 2018).

6.2.3 Slow Cooling Experiment

Results could be more accurate if the produced co-crystal after the crystallisation process was not reheated, rather the new compound of saccharin, carbamazepine and ethanol should be used for each experiment, but of course this would be very costly.

6.2.4 Fast Cooling Experiments

Improve the machine capability for fast cooling experiments, as machine used in this study can only provide the maximum cooling rate of 1.0 °C/min, which was closed to the maximum cooling rate in slow cooling experiment, 0.8 °C/min.

6.2.5 Characterisation of the Co-Crystal

Malvern Mastersizer for CSD should be calibrated more often or in this study, we might need to get the new one. During the experiments, out of 10 tests, 40% gave an error result, which those results need to be ignored.

Further studies investigating the morphology of seeded and unseeded CBZ-SAC co-crystals, effect of cooling rates and the effect of stirring speed, with different SAC to CBZ molar ratios and various concentration of CBZ, are strongly recommended.

Focused-beam reflectance measurement (FBRM) and particle vision and measurement (PVM) can be introduced, to see "live" change in co-crystals formation and size with time

6.2.6 Modelling and Simulations of CBZ-SAC Co-Crystal

Modelling and simulations of the CBZ-SAC co-crystals are recommended to be done to design and robust control of crystal shape and size. Modelling is an advanced control strategy, which accurately can predict the behaviour of the crystallisation process. Thus, appropriate model structure needs to be chosen, basic experiments need to be performed, data collection and parameter estimation are the vital step in modelling and simulation process.

REFERENCES

Aamir, E., Nagy, Z. K., & Rielly, C. D. (2010). Optimal seed recipe design for crystal size distribution control for batch cooling crystallisation processes. *Chemical Engineering Science*, *65*(11), 3602–3614. https://doi.org/10.1016/j.ces.2010.02.051

Abbas, A., Mostafa Nowee, S., & Romagnoli, J. A. (2006). Model-based optimization for operational policies in seeded cooling crystallization. *Computer Aided Chemical Engineering*, *21*(C), 1347–1352. https://doi.org/10.1016/S1570-7946(06)80234-8

Abd Rahim, S. (2012). *Understanding and predicting the physicochemical properties and crystallisation behaviour of carbamazepine co-crystals* [Doctoral thesis, University of Leeds, UK]. https://ethos.bl.uk/OrderDetails.do?uin=uk.bl.ethos.713468

Abd Rahim, S., & Amanina Mohamad Adaris, N. (2018). Effect of crystallization method on the formation of carbamazepine-saccharin co-crystal. *Materials Today: Proceedings*, *5*(10), 22074–22079. https://doi.org/10.1016/j.matpr.2018.07.071

Abdul Mudalip, S. K. (2016). *Crystallization Process of Mefenamic Acid: Optimization, Molecular Dynamics Simulations and Pat (Process Analytical Technology) Implementation*. (Unpublished doctoral dissertation). International Islamic University Malaysia, Malaysia.

Arunmozhi, G. de, Gomes, E. de M., de M Gomes, E., de, de M Gomes, E., & de M. Gomes, E. (2004). Metastability and crystal growth kinetics on L-arginine phosphate. *Crystal Research and Technology*, *39*(1), 34–39. https://doi.org/10.1002/crat.200310146

Bart, J. C. J. (1968). The crystal and molecular structure of saccharin (o-sulphobenzoic imide). *J. Chem. Soc. B*, *0*, 376–382. https://doi.org/10.1039/J29680000376

Bernardes, C. E. S., & da Piedade, M. E. M. (2010). A fully automatic apparatus for thermal analysis of crystallization from solution and metastable zone width determinations. *Journal of Thermal Analysis and Calorimetry*, *100*(2), 493–500. https://doi.org/10.1007/s10973-009-0652-9

Bernardo, A., & Giulietti, M. (2010). Modeling of crystal growth and nucleation rates for pentaerythritol batch crystallization. *Chemical Engineering Research and Design*, *88*(10), 1356–1364. https://doi.org/10.1016/j.cherd.2009.07.019

Berthoud, A. (1912). Théorie de la formation des faces d'un cristal. *Journal de Chimie Physique*, *10*, 624–635.

Bonnin-Paris, J., Bostyn, S., Havet, J.-L., & Fauduet, H. (2011). Determination of the Metastable Zone Width of Glycine Aqueous Solutions for Batch Crystallizations. *Chemical Engineering Communications*, *198*(8), 1004–1017. https://doi.org/10.1080/00986445.2011.545301

Borissova, A., Khan, S., Mahmud, T., Roberts, K. J., Andrews, J., Dallin, P., Chen, Z.-P., & Morris, J. (2009). In Situ Measurement of Solution Concentration during the Batch Cooling Crystallization of L-Glutamic Acid using ATR-FTIR Spectroscopy Coupled with Chemometrics. *Crystal Growth & Design*, *9*(2), 692–706. https://doi.org/10.1021/cg7010265

Braga, D., Maini, L., & Grepioni, F. (2013). Mechanochemical preparation of co-crystals. *Chemical Society Reviews*, *42*(18), 7638–7648. https://doi.org/10.1039/c3cs60014a

Byrn, S. R., Zografi, G., & Chen, X. S. (2017). Solid State Properties of Pharmaceutical Materials. In *Solid State Properties of Pharmaceutical Materials*. John Wiley &amp; Sons, Inc. https://doi.org/10.1002/9781119264408

Camacho Corzo, D. M., Borissova, A., Hammond, R. B., Kashchiev, D., Roberts, K. J., Lewtas, K., & More, I. (2014). Nucleation mechanism and kinetics from the analysis of polythermal crystallisation data: methyl stearate from kerosene solutions. *CrystEngComm*, *16*(6), 974–991. https://doi.org/10.1039/C3CE41098F

Çelikbilek, M., Ersundu, A. E., & Aydın, S. (2012). Crystallization kinetics of amorphous materials. In Y. Mastai (Ed.), *Advances in Crystallization Processes*. IntechOpen. http://www.intechopen.com/books/advances-in-crystallization-processes/crystallization-kinetics-ofamorphous-%0Amaterials

Chen, A.-Z., Chen, L.-Q., Wang, S., Wang, Y.-Q., & Zha, J.-Z. (2015). Study of magnetic silk fibroin nanoparticles for massage-like transdermal drug delivery. *International Journal of Nanomedicine*, *10*, 4639. https://doi.org/10.2147/IJN.S85999

Chianese, A., & Kramer, H. J. (2012a). *Industrial Crystallization Process Monitoring and Control*. https://doi.org/10.1002/9783527645206

Chianese, A., & Kramer, H. J. (2012b). *Industrial Crystallization Process Monitoring and Control Fine Chemicals Crystal Growth Processes Based on Capillarity Crystal Growth Technology*.

Childs, S. L., & Zaworotko, M. J. (2009). The Reemergence of Cocrystals: The Crystal Clear Writing Is on the WallIntroduction to Virtual Special Issue on Pharmaceutical Cocrystals. *Crystal Growth & Design*, *9*(10), 4208–4211. https://doi.org/10.1021/cg901002y

Cuadra, I. A., Cabañas, A., Cheda, J. A. R., & Pando, C. (2018). Polymorphism in the co-crystallization of the anticonvulsant drug carbamazepine and saccharin using supercritical CO2 as an anti-solvent. *Journal of Supercritical Fluids*, *136*(December 2017), 60–69. https://doi.org/10.1016/j.supflu.2018.02.004

Cysewski, P., & Przybyłek, M. (2017). Selection of effective cocrystals former for dissolution rate improvement of active pharmaceutical ingredients based on lipoaffinity index. *European Journal of Pharmaceutical Sciences*, *107*(April), 87–96. https://doi.org/10.1016/j.ejps.2017.07.004

Dasgupta, S., Rettig, F., & Ay, P. (2016). Nucleation Kinetics during Melt Crystallization of Plant Based High Oleic and Linoleic Polyunsaturated Fatty Acid Mixtures. *Crystal Growth and Design*, *16*(2), 861–866. https://doi.org/10.1021/acs.cgd.5b01432

Davey, R. J., & Garside, J. (2000). *From Molecules to Crystallizers An Introduction to Crystallization*. Oxford University Press.

Doki, N. (2002). Determination of Critical Seed Loading Ratio for the Production of Crystals of Uni-Modal Size Distribution in Batch Cooling Crystallization of Potassium Alum. *Journal of Chemical Engineering of Japan*, *35*(7), 670–676.

Du, G., Sun, Z., Xian, Y., Jing, H., Chen, H., & Yin, D. (2016). The nucleation kinetics of ammonium metavanadate precipitated by ammonium chloride. *Journal of Crystal Growth*, *441*, 117–123. https://doi.org/10.1016/j.jcrysgro.2016.02.016

Dunitz, J. D. (2003). Crystal and co-crystal: a second opinion. *CrystEngComm*, *5*(91), 506. https://doi.org/10.1039/b315687g

Eder, R. J. P., Radl, S., Schmitt, E., Innerhofer, S., Maier, M., Gruber-Woelfler, H., & Khinast, J. G. (2010). Continuously seeded, continuously operated tubular crystallizer for the production of active pharmaceutical ingredients. *Crystal Growth and Design*, *10*(5), 2247–2257. https://doi.org/10.1021/cg9015788

Erdemir, D., Lee, A. Y., & Myerson, A. S. (2009). Nucleation of crystals from solution: Classical and two-step models. *Accounts of Chemical Research*, *42*(5), 621–629. https://doi.org/10.1021/ar800217x

Friščić, T., & Jones, W. (2010). Benefits of cocrystallisation in pharmaceutical materials science: An update. *Journal of Pharmacy and Pharmacology*, *62*(11), 1547–1559. https://doi.org/10.1111/j.2042-7158.2010.01133.x

Gadade, D. D., & Pekamwar, S. S. (2016). Pharmaceutical Cocrystals: Regulatory and Strategic Aspects, Design and Development. *Advanced Pharmaceutical Bulletin*, *6*(4), 479–494. https://doi.org/10.15171/apb.2016.062

Gadamasetti, K. (2007). Process Chemistry in the Pharmaceutical Industry. In *Process Chemistry in the Pharmaceutical Industry, Volume 2* (pp. 1–11). CRC Press. https://doi.org/10.1201/9781420008357.ch1

Gagniere, E., Mangin, D., Veesler, s, & Puel, f. (2012). Chapter 9 Co-crystallization in Solution and Scale-up Issues. In *Pharmaceutical Salts and Co-crystals* (pp. 188–211). The Royal Society of Chemistry. https://doi.org/10.1039/9781849733502-00188

Ghadi, R., Ghuge, A., Ghumre, S., Waghmare, N., & Kadam, V. J. (2014). Co-Crystals: Emerging Approach in Pharmaceutical Design. *Indo American Journal of Pharmaceutical Research*, *4*(7), 3881–3893. https://doi.org/10.1044/1980-iajpr.14727

Gherras, N., & Fevotte, G. (2012). Comparison between approaches for the experimental determination of metastable zone width: A case study of the batch cooling crystallization of ammonium oxalate in water. *Journal of Crystal Growth*, *342*(1), 88–98. https://doi.org/10.1016/j.jcrysgro.2011.06.058

Gillespie, C. (2018). Substances That Won ' t Dissolve in Water. *Sciencing*. https://sciencing.com/substances-wont-dissolve-water-12013209.html

Grzesiak, A. L., Lang, M., Kim, K., & Matzger, A. J. (2003). Comparison of the Four Anhydrous Polymorphs of Carbamazepine and the Crystal Structure of Form I. *Journal of Pharmaceutical Sciences*, *92*(11), 2260–2271. https://doi.org/10.1002/jps.10455

Hammond, R. B., Hussain, Q., More, I., & Roberts, K. J. (2016). *Optimising Cold-Flow Behaviour of Biodiesel Fuels : Nucleation Kinetics Analysis*. https://www.researchgate.net/profile/KJ_Roberts/publication/267708153_OPTIMI SING_COLD-FLOW_BEHAVIOUR_OF_BIODIESEL_FUELS_NUCLEATION_KINETICS_ANALYSIS/links/552652ff0cf295bf160ed361/OPTIMISING-COLD-FLOW-BEHAVIOUR-OF-BIODIESEL-FUELS-NUCLEATION-KINETICS-ANALY

Hattori, Y., Sato, M., & Otsuka, M. (2015). Initial dissolution kinetics of cocrystal of carbamazepine with nicotinamide. *Journal of Pharmacy and Pharmacology*, *67*(11), 1512–1518. https://doi.org/10.1111/jphp.12461

Hayles-Hahn, C. (2014). *Nanoseeds for pharmaceutical batch crystallisation* [Doctoral Thesis, Imperial College London, South Kensington, London]. http://hdl.handle.net/10044/1/24428

He, G., Jacob, C., Guo, L., Chow, P. S., & Tan, R. B. H. (2008). Screening for Cocrystallization Tendency: The Role of Intermolecular Interactions. *The Journal of Physical Chemistry B*, *112*(32), 9890–9895. https://doi.org/10.1021/jp803019m

Herrera, M. L., Rodríguez-Batiller, M. J., Rincón-Cardona, J. A., Agudelo-Laverde, L. M., Martini, S., & Candal, R. J. (2015). Effect of Cooling Rate and Temperature Cycles on Polymorphic Behavior of Sunflower Oil Stearins for Applications as Trans-fat Alternatives in Foods. *Food and Bioprocess Technology*, *8*(8), 1779–1790. https://doi.org/10.1007/s11947-015-1535-7

Holaň, J., Ridvan, L., Billot, P., & Štěpánek, F. (2015). Design of co-crystallization processes with regard to particle size distribution. *Chemical Engineering Science*, *128*, 36–43. https://doi.org/10.1016/j.ces.2015.01.045

Howard, K. (2011). *Institutional Repository Process analytical technology investigation of the crystallization of pharmaceutical polymorphs , salts and hydrates* (Issue July) [Doctoral thesis, Loughborough University]. https://dspace.lboro.ac.uk/2134/8464

Jayasankar, A., Good, D. J., & Rodríguez-Hornedo, N. (2007). Mechanisms by which moisture generates cocrystals. *Molecular Pharmaceutics*, *4*(3), 360–372.

https://doi.org/10.1021/mp0700099

Jiang, M., Wong, M. H., Zhu, Z., Zhang, J., Zhou, L., Wang, K., Ford Versypt, A. N., Si, T., Hasenberg, L. M., Li, Y. E., & Braatz, R. D. (2012). Towards achieving a flattop crystal size distribution by continuous seeding and controlled growth. *Chemical Engineering Science*, *77*, 2–9. https://doi.org/10.1016/j.ces.2011.12.033

Jie Lu. (2012). Crystallization and transformation of pharmaceutical solid forms. *African Journal of Pharmacy and Pharmacology*, *6*(9), 581–591. https://doi.org/10.5897/AJPP12.044

Jones, A. G. (2002). *Crystallization Process Systems*. Butterworth-Heinemann.

Kadam, S. S. (2012). *Monitoring and Characterization of Crystal Nucleation and Growth during Batch Crystallization* [Doctoral thesis, Technische Universiteit Delft, Netherlands]. http://resolver.tudelft.nl/uuid:7bb6b44b-4382-4018-9cd2-da6e4a3582cb

Kannan, V., & Brahadeeswaran, S. (2013). Investigations on influence of coloration on growth of high quality hydrazonium l-tartrate single crystal. *Journal of Crystal Growth*, *374*, 71–78. https://doi.org/10.1016/j.jcrysgro.2013.03.039

Kobari, M., Kubota, N., & Hirasawa, I. (2011). Computer simulation of metastable zone width for unseeded potassium sulfate aqueous solution. *Journal of Crystal Growth*, *317*(1), 64–69. https://doi.org/10.1016/j.jcrysgro.2010.12.069

Kubota, N. (2008). A new interpretation of metastable zone widths measured for unseeded solutions. *Journal of Crystal Growth*, *310*(3), 629–634. https://doi.org/10.1016/j.jcrysgro.2007.11.123

Kubota, N., Kobari, M., & Hirasawa, I. (2014). Effects of detector sensitivity and resolution on induction time reading. *CrystEngComm*, *16*(6), 1103–1112. https://doi.org/10.1039/C3CE42019A

LaMer, V. K., & Dinegar, R. H. (1950). Theory, Production and Mechanism of Formation of Monodispersed Hydrosols. *Journal of the American Chemical Society*, *72*(11), 4847–4854. https://doi.org/10.1021/ja01167a001

Lee, M. J., Wang, I. C., Kim, M. J., Kim, P., Song, K. H., Chun, N. H., Park, H. G., & Choi, G. J. (2015). Controlling the polymorphism of carbamazepine-saccharin cocrystals formed during antisolvent cocrystallization using kinetic parameters. *Korean Journal of Chemical Engineering*, *32*(9), 1910–1917. https://doi.org/10.1007/s11814-014-0384-9

Lenka, M., & Sarkar, D. (2014). Determination of metastable zone width, induction period and primary nucleation kinetics for cooling crystallization of L-asparaginenohydrate. *Journal of Crystal Growth*, *408*, 85–90. https://doi.org/10.1016/j.jcrysgro.2014.09.027

Lewis, A. E., & Olsen, C. (2007). *BIWIC 2007 14th International Workshop on Industrial Crystallization*. IOS Press. https://books.google.com.my/books?id=lwnvAgAAQBAJ

Li, J., Sun, Q., Jin, C., & Li, J. (2015). Comprehensive studies of the hydrothermal growth of ZnO nanocrystals on the surface of bamboo. *Ceramics International*, *41*(1), 921–929. https://doi.org/10.1016/j.ceramint.2014.09.010

Lipert, M. P., & Rodríguez-Hornedo, N. (2015). Cocrystal Transition Points: Role of Cocrystal Solubility, Drug Solubility, and Solubilizing Agents. *Molecular Pharmaceutics*, *12*(10), 3535–3546. https://doi.org/10.1021/acs.molpharmaceut.5b00111

Liu, J. J., Ma, C. Y., Hu, Y. D., & Wang, X. Z. (2010). Effect of seed loading and cooling rate on crystal size and shape distributions in protein crystallization-A study using morphological population balance simulation. *Computers and Chemical Engineering*, *34*(12), 1945–1952. https://doi.org/10.1016/j.compchemeng.2010.06.020

Long, B., Yang, H., & Ding, Y. (2016). Impact of seed loading ratio on the growth kinetics of mono-ammonium phosphate under isothermal batch crystallization. *Korean Journal of Chemical Engineering*, *33*(2), 623–628. https://doi.org/10.1007/s11814-015-0173-0

Lu, E., Rodríguez-Hornedo, N., & Suryanarayanan, R. (2008). A rapid thermal method for cocrystal screening. *CrystEngComm*, *10*(6), 665. https://doi.org/10.1039/b801713c

Lung-Somarriba, B. L. M., Moscosa-Santillan, M., Porte, C., & Delacroix, A. (2004). Effect of seeded surface area on crystal size distribution in glycine batch cooling crystallization: A seeding methodology. *Journal of Crystal Growth*, *270*(3–4), 624–632. https://doi.org/10.1016/j.jcrysgro.2004.07.015

Ma, K., Zhang, Y., Kan, H., Cheng, L., Luo, L., Su, Q., Gao, J., Gao, Y., & Zhang, J. (2014). Thermodynamic and kinetic investigation on the crucial factors affecting adefovir dipivoxil-saccharin cocrystallization. *Pharmaceutical Research*, *31*(7), 1766–1778. https://doi.org/10.1007/s11095-013-1281-3

Malvern Instruments. (2007). *Mastersizer 2000 User Manual*.

Mao, S., Zhang, Y., Rohani, S., & Ray, A. K. (2010). Kinetics of (R,S)- and (R)-mandelic acid in an unseeded cooling batch crystallizer. *Journal of Crystal Growth*, *312*(22), 3340–3348. https://doi.org/10.1016/j.jcrysgro.2010.08.027

Martini, S., Herrera, M. L., & Hartel, R. W. (2001). Effect of cooling rate on nucleation behavior of milk fat--sunflower oil blends. *Journal of Agricultural and Food Chemistry*, *49*(7), 3223–3229. https://doi.org/10.1021/jf001101j

Md Azmi, N. S., Anuar, N., Abu Bakar, N. F., & Zakaria, M. A. (2015). Induction Time

of L-Isoleucine Crystallization with the Presence of Electric Field. In M. Hashim (Ed.), *ICGSCE 2014*. Springer Singapore. https://doi.org/10.1007/978-981-287-505-1_17

Miers, H. A., & Isaac, F. (1906). XLVII.—The refractive indices of crystallising solutions, with especial reference to the passage from the metastable to the labile condition. *J. Chem. Soc., Trans.*, *89*(0), 413–454. https://doi.org/10.1039/CT9068900413

Mitchell, N. A., Frawley, P. J., & Ó'Ciardhá, C. T. (2011). Nucleation kinetics of paracetamolethanol solutions from induction time experiments using Lasentec FBRM?? *Journal of Crystal Growth*, *321*(1), 91–99. https://doi.org/10.1016/j.jcrysgro.2011.02.027

Mohod, A. V., & Gogate, P. R. (2018). Improved crystallization of ammonium sulphate using ultrasound assisted approach with comparison with the conventional approach. *Ultrasonics Sonochemistry*, *41*(May 2017), 310–318. https://doi.org/10.1016/j.ultsonch.2017.09.047

Mota, F. L., Teychéne, S., & Biscans, B. (2014). Measurement of the Nucleation and Growth Kinetics of Some Middle Distillate Fuels and Their Blends with a Model Biodiesel Fuel. *Industrial & Engineering Chemistry Research*, *53*(7), 2811–2819. https://doi.org/10.1021/ie402984p

Mousaw, P., Saranteas, K., & Prytko, B. (2008). Crystallization improvements of a diastereomeric kinetic resolution through understanding of secondary nucleation. *Organic Process Research and Development*, *12*(2), 243–248. https://doi.org/10.1021/op700276w

Mullin, J. W. (2001). *Crystallization* (Fourth). Butterworth Heinemann.

Myerson, A. S. (Ed.). (2001). *Handbook of Industrial Crystallization* (2nd ed.). Oxford: Butterworth Heinemann.

Myerson, A. S. (2015). Concluding remarks. *Faraday Discuss.*, *179*, 543–547. https://doi.org/10.1039/C5FD00042D

Nagy, Z. K., Gillon, A. L., Steele, G., Makwana, N., & Rielly, C. D. (2007). Using Process Analytical Technology for In Situ Monitoring of The Polymorphic Transformation of Organic Compounds. *IFAC Proceedings Volumes*, *40*(5), 131–136. https://doi.org/10.3182/20070606-3-MX-2915.00140

Narducci, O. (2012). *Particle Engineering via Sonocrystallization: the aqueous adipic acid system* (Issue October). University of College London.

Narducci, O., Jones, A. G., & Kougoulos, E. (2011). Crystal product engineering in the seeded cooling crystallization of adipic acid from aqueous solution. *Organic Process Research and Development*, *15*(5), 974–980. https://doi.org/10.1021/op200029h

Nemdili, L., Koutchoukali, O., Bouhelassa, M., Seidel, J., Mameri, F., & Ulrich, J. (2016). Crystallization kinetics of citric acid anhydrate. *Journal of Crystal Growth*, *451*, 88–94. https://doi.org/10.1016/j.jcrysgro.2016.07.008

Nernst, W., & von Lerch, F. (1904). Über die Verwendung des elektrolytischen Detektors in der Brückenkombination. *Annalen Der Physik*, *320*(14), 836–841. https://doi.org/10.1002/andp.19043201409

Nguyen, T. N. P., & Kim, K. J. (2008). Kinetic study on hemipenta hydrate risedronate monosodium in batch crystallization by cooling mode. *International Journal of Pharmaceutics*, *364*(1), 1–8. https://doi.org/10.1016/j.ijpharm.2008.05.037

Nguyen, T. T. H. (2013). *Influence of crystallisation environment on the nucleation and growth of single crystals of (RS)-Ibuprofen* [Doctoral thesis, University of Leeds, UK]. http://ethos.bl.uk/OrderDetails.do?uin=uk.bl.ethos.666569

Novartis Pharmaceuticals Corporation. (2018). *Tegretol (carbamazepine) chewable tablets, tablets, and suspension and Tegretol XR (carbamazepine) extended-release tablets prescribing information. East Hanover, NJ; 2018 Mar.* https://www.pharma.us.novartis.com/sites/www.pharma.us.novartis.com/files/tegretol.pdf

Noyes, A. A., & Whitney, W. R. (1897). The rate of solution of solid substances in their own solutions. *Journal of the American Chemical Society*, *19*(12), 930–934. https://doi.org/10.1021/ja02086a003

Nývlt, J. (1968). Kinetics of nucleation in solutions. *Journal of Crystal Growth*, *3–4*, 377–383. https://doi.org/10.1016/0022-0248(68)90179-6

O'Mahony, M. A., Maher, A., Croker, D. M., Rasmuson, Å. C., & Hodnett, B. K. (2012). Examining Solution and Solid State Composition for the Solution-Mediated Polymorphic Transformation of Carbamazepine and Piracetam. *Crystal Growth & Design*, *12*(4), 1925–1932. https://doi.org/10.1021/cg201665z

O'Mullane, M., Fields, B., & Stanley, G. (2014). Food Additives: Sweeteners. In Y. B. T.-E. of F. S. Motarjemi (Ed.), *Encyclopedia of Food Safety* (pp. 477–484). Elsevier. https://doi.org/10.1016/B978-0-12-378612-8.00231-6

O'Sullivan, B., Smith, B., & Baramidze, G. (2012). Recent Advances for Seeding a Crystallization Process. *Columbia, USA: Mettler Toledo Auto-Chem.* https://www.mt.com/ch/en/home/library/white-papers/automated-reactors/Seeding-A-Crystallization-Process.html

Oliveira, F. (2013). *How to explain the differences of XRD peak intensities the same material?*

Pagire, S. K., Jadav, N., Vangala, V. R., Whiteside, B., & Paradkar, A. (2017). Thermodynamic Investigation of Carbamazepine-Saccharin Co-Crystal Polymorphs. *Journal of Pharmaceutical Sciences*, *106*(8), 2009–2014.

https://doi.org/10.1016/j.xphs.2017.04.017

Pagire, S. K., Korde, S. A., Whiteside, B. R., Kendrick, J., & Paradkar, A. (2013). Spherical Crystallization of Carbamazepine/Saccharin Co-Crystals: Selective Agglomeration and Purification through Surface Interactions. *Crystal Growth & Design*, *13*(10), 4162–4167. https://doi.org/10.1021/cg400804x

Pando, C., Cabañas, A., & Cuadra, I. A. (2016). Preparation of pharmaceutical co-crystals through sustainable processes using supercritical carbon dioxide: a review. *RSC Advances*, *6*(75), 71134–71150. https://doi.org/10.1039/C6RA10917A

Park, M. W., & Yeo, S. Do. (2012). Antisolvent crystallization of carbamazepine from organic solutions. *Chemical Engineering Research and Design*, *90*(12), 2202–2208. https://doi.org/10.1016/j.cherd.2012.05.001

Parsons, A. R., Black, S., & Colling, R. (2003). Automated Measurement of Metastable Zones for Pharmaceutical Compounds. *Trans IChemE*, *81*, 700–704.

Pinto, M. A. L., Ambrozini, B., Ferreira, A. P. G., & Cavalheiro, É. T. G. (2014). Thermoanalytical studies of carbamazepine: Hydration/dehydration, thermal decomposition, and solid phase transitions. *Brazilian Journal of Pharmaceutical Sciences*, *50*(4), 877–884. https://doi.org/10.1590/S1984-82502014000400023

Porter III, W. W., Elie, S. C., & Matzger, A. J. (2008). Polymorphism in Carbamazepine Cocrystals. *Crystal Growth & Design*, *8*(1), 14–16. https://doi.org/10.1021/cg701022e

Powell, K. A. (2017). *Improving continuous crystallisation using process analytical technologies : design of a novel periodic flow process* [Doctoral thesis, Loughborough University, United Kingdom]. http://ethos.bl.uk/OrderDetails.do?did=1&uin=uk.bl.ethos.706226

Qian, Y., Lu, G., Sun, Y., Song, X., & Yu, J. (2014). Metastable zone width of SrCl 2 ?6H 2 O during cooling crystallization. *Crystal Research and Technology*, *49*(1), 78–83. https://doi.org/10.1002/crat.201300303

Qiu, S. (2015). *Effects of Polymers on Carbamazepine cocrystals phase transformation and release profiles* [Doctoral thesis, De Montfort University, Leicester]. https://ethos.bl.uk/OrderDetails.do?uin=uk.bl.ethos.676019

Rahim, S. A., Hammond, R. B., Sheikh, A. Y., & Roberts, K. J. (2013). A comparative assessment of the influence of different crystallization screening methodologies on the solid forms of carbamazepine co-crystals. *CrystEngComm*, *15*(19), 3862–3873. https://doi.org/10.1039/c3ce26878k

Rajoub, N. (2014). *Monitoring of Crystallization and Kinetics in Batch Crystalliser by FBRM and PIV* [Doctorial thesis, Heriot-Watt University, Edinburgh, United Kingdom]. http://hdl.handle.net/10399/2836

Ramisetty, K. A., Pandit, A. B., & Gogate, P. R. (2013). Ultrasound-assisted antisolvent crystallization of benzoic acid: Effect of process variables supported by theoretical simulations. *Industrial and Engineering Chemistry Research*, *52*(49), 17573–17582. https://doi.org/10.1021/ie402203k

Randall, D. G. G., Nathoo, J., Genceli-Güner, F. E. E., Kramer, H. J. M. J. M., Witkamp, G. J. J., & Lewis, A. E. E. (2012). Determination of the metastable ice zone for a sodium sulphate system. *Chemical Engineering Science*, *77*, 184–188. https://doi.org/10.1016/j.ces.2011.12.022

Randolph, A., & Larson, M. A. (1988). *Theory of Particulate Processes*. Academic Press.

Rodr guez-Spong, B., Price, C. P., Jayasankar, A., Matzger, A. J., & Rodr guez-Hornedo, N. r. (2004). General principles of pharmaceutical solid polymorphism: a supramolecular perspective. *Advanced Drug Delivery Reviews*, *56*, 241–274.

Salas, G., Costo, R., & Morales, M. del P. (2012). Synthesis of Inorganic Nanoparticles. In J. M. de la Fuente & V. B. T.-F. of N. Grazu (Eds.), *Nanobiotechnology* (Vol. 4, pp. 35–79). Elsevier. https://doi.org/10.1016/B978-0-12-415769-9.00002-9

Sander, A., Kalšan, M., & Kardum, J. P. (2009). Kinetics of the seeded batch cooling crystallization. *Chemical Engineering Transactions*, *17*(January 2009), 753–758. https://doi.org/10.3303/CET0917126

Sangwal, K. (2009). A novel self-consistent Nývlt-like equation for metastable zone width determined by the polythermal method. *Crystal Research and Technology*, *44*(3), 231–247. https://doi.org/10.1002/crat.200800501

Shan, N., Toda, F., & Jones, W. (2002). Mechanochemistry and co-crystal formation: effect of solvent on reaction kineticsElectronic supplementary information (ESI) available for PXRD profiles showing the grinding results for CTA + Bipy with and without solvent as well as CTA + 2fPh with differe. *Chemical Communications*, *20*, 2372–2373. https://doi.org/10.1039/b207369m

Shiau, L. D. (2016). Comparison of the interfacial energy and pre-exponential factor calculated from the induction time and metastable zone width data based on classical nucleation theory. *Journal of Crystal Growth*, *450*, 50–55. https://doi.org/10.1016/j.jcrysgro.2016.06.023

Smith, L. A., Roberts, K. J., Machin, D., & McLeod, G. (2001). An examination of the solution phase and nucleation properties of sodium, potassium and rubidium dodecyl sulphates. *Journal of Crystal Growth*, *226*(1), 158–167. https://doi.org/10.1016/S0022-0248(01)01368-9

Stahly, G. P. (2007). Diversity in single- and multiple-component crystals. the search for and prevalence of polymorphs and cocrystals. *Crystal Growth and Design*, *7*(6), 1007–1026. https://doi.org/10.1021/cg060838j

Sun, C. C., & Hou, H. (2008). Improving Mechanical Properties of Caffeine and Methyl Gallate Crystals by Cocrystallization. *Crystal Growth & Design*, *8*(5), 1575–1579. https://doi.org/10.1021/cg700843s

Sun, H., Wang, J., & Gong, J. (2010). Determination of nucleation kinetics of lovastatin in acetone solution. *Crystal Research and Technology*, *45*(7), 707–711. https://doi.org/10.1002/crat.201000060

Sun, X., Sun, Y., & Yu, J. (2015). Cooling crystallization of aluminum sulfate in pure water modulated by sodium dodecylbenzenesulfonate. *Crystal Research and Technology*, *50*(8), 682–687. https://doi.org/10.1002/crat.201500116

Surov, A. O., Volkova, T. V., Churakov, A. V., Proshin, A. N., Terekhova, I. V., & Perlovich, G. L. (2017). Cocrystal formation, crystal structure, solubility and permeability studies for novel 1,2,4-thiadiazole derivative as a potent neuroprotector. *European Journal of Pharmaceutical Sciences*, *109*(June), 31–39. https://doi.org/10.1016/j.ejps.2017.07.025

Tahti, T., Louhi-Kultanen, M., & Palosaari, S. (1999). *14th International Symposium on Industrial Crystallization*. Institution of Chemical Engineers Rugby, UK.

Toroz, D., Rosbottom, I., Turner, T. D., Corzo, D. M. C., Hammond, R. B., Lai, X., & Roberts, K. J. (2015). Towards an understanding of the nucleation of alpha-para amino benzoic acid from ethanolic solutions: a multi-scale approach. *Faraday Discuss*, *179*, 79–114. https://doi.org/10.1039/c4fd00275j

Trask, A. V., Motherwell, W. D. S., & Jones, W. (2004). Solvent-drop grinding: green polymorph control of cocrystallisation. *Chemical Communications*, *7*, 890. https://doi.org/10.1039/b400978a

Tseng, Y.-T. T., & Ward, J. D. (2014). Critical seed loading from nucleation kinetics. *AIChE Journal*, *60*(5), 1645–1653. https://doi.org/10.1002/aic.14366

Turner, T. D., Corzo, D. M. C., Toroz, D., Curtis, A., Dos Santos, M. M., Hammond, R. B., Lai, X., & Roberts, K. J. (2016). The influence of solution environment on the nucleation kinetics and crystallisability of para-aminobenzoic acid. *Phys. Chem. Chem. Phys.*, *18*(39), 27507–27520. https://doi.org/10.1039/C6CP04320H

Turner, Thomas Daniel. (2015). *Molecular Self-Assembly , Nucleation Kinetics and Cluster Formation Associated with Solution Crystallisation* [Doctoral thesis, University of Leeds, UK]. http://etheses.whiterose.ac.uk/id/eprint/11929

U. S. Food and Drug Administration. (2018). *Guidance for Industry: Regulatory Classification of Pharmaceutical Cocrystals*. https://www.fda.gov/media/81824/download

Ulrich, J., & Jones, M. J. (2012). Seeding Technique in Batch Crystallization. In A. Chianese & H. J. M. Kramer (Eds.), *Industrial Crystallization Process Monitoring and Control* (pp. 127–138). Wiley-VCH Verlag & Co. KGaA.

Ulrich, J., & Strege, C. (2002). Some aspects of the importance of metastable zone width and nucleation in industrial crystallizers. *Journal of Crystal Growth*, *237–239*(1-4 III), 2130–2135. https://doi.org/10.1016/S0022-0248(01)02284-9

Vasenko, L., & Qu, H. (2017). Effect of NH4-N/P and Ca/P molar ratios on the reactive crystallization of calcium phosphates for phosphorus recovery from wastewater. *Journal of Crystal Growth*, *459*(November 2016), 61–66. https://doi.org/10.1016/j.jcrysgro.2016.11.076

Veesler, S., & Puel, F. (2014). Crystallization of Pharmaceutical Crystals. In T. Nishinaga (Ed.), *Handbook of Crystal Growth* (2nd ed.). Elsevier.

Volmer, M. (1939). *Kinetics of Phase Formation (Kinetik der Phasenbildung)*. FOREIGN TECHNOLOGY DIV WRIGHT-PATTERSONAFB OH.

Wang, I. C., Lee, M. J., Sim, S. J., Kim, W. S., Chun, N. H., & Choi, G. J. (2013). Anti-solvent co-crystallization of carbamazepine and saccharin. *International Journal of Pharmaceutics*, *450*(1–2), 311–322. https://doi.org/10.1016/j.ijpharm.2013.04.012

Wang, L.-Y., Zhu, L., Yang, L. Bin, Wang, Y. F., Sha, Z. L., & Zhao, X. Y. (2016). Thermodynamic equilibrium, metastable zone widths, and nucleation behavior in the cooling crystallization of gestodene-ethanol systems. *Journal of Crystal Growth*, *437*, 32–41. https://doi.org/10.1016/j.jcrysgro.2015.12.020

Wang, L., Feng, H., Dong, Y., Peng, J., & Li, W. (2016). Solubility and metastable zone width of aqueous sodium dichromate dihydrate solutions in the presence of sodium chromate additive. *Journal of Crystal Growth*, *454*, 105–110. https://doi.org/10.1016/j.jcrysgro.2016.09.011

Wang, L., Feng, H., Peng, J., Dong, N., Li, W., & Dong, Y. (2015). Solubility, Metastable Zone Width, and Nucleation Kinetics of Sodium Dichromate Dihydrate. *Journal of Chemical & Engineering Data*, *60*(1), 185–191. https://doi.org/10.1021/je5009069

Wohlgemuth, K. (2012). *Induced Nucleation Processes during Batch Cooling Crystallization* [Doctoral thesis, Technischen Universität Dortmund, Germany]. http://www.apt.bci.tu-dortmund.de/cms/Medienpool/Dissertationen/Kerstin_Wohlgemuth_2012_-_Induced_Nucleation_Processes_during_Bath.pdf

Zadeh, F. M. N. (2014). *Synthesis and Investigation of the Properties of Water Soluble Quantum Dots for Bioapplications*. The University of New South Wales Thesis/.

Zhang, F., Liu, T., Huo, Y., Guan, R., & Wang, X. Z. (2016). Investigation of the operating conditions to morphology evolution of β-l-glutamic acid during seeded cooling crystallization. *Journal of Crystal Growth*, *469*, 136–143. https://doi.org/10.1016/j.jcrysgro.2016.09.041

Zhang, Y., You, S., & Zhang, Y. (2015). Nucleation of ammonium aluminum sulfate dodecahydrate from unseeded aqueous solution. *Journal of Crystal Growth*, *411*,

24–29. https://doi.org/10.1016/j.jcrysgro.2014.11.006

Zhou, L., Wang, Z., Zhang, M., Guo, M., Xu, S., & Yin, Q. (2016). Determination of metastable zone and induction time of analgin for cooling crystallization. *Chinese Journal of Chemical Engineering*, 5–10. https://doi.org/10.1016/j.cjche.2016.05.046
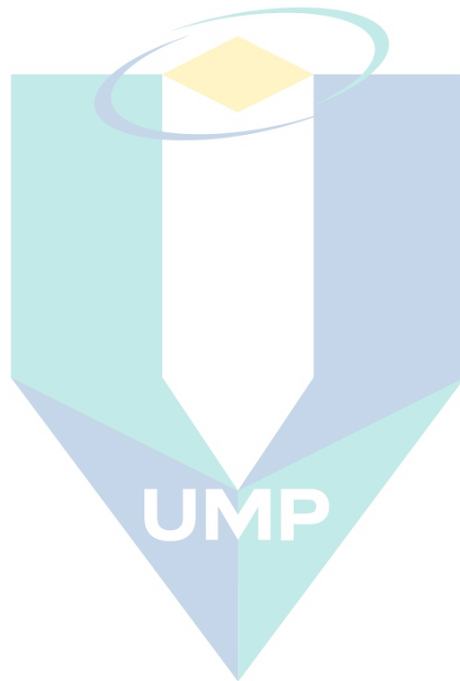
APPENDICES
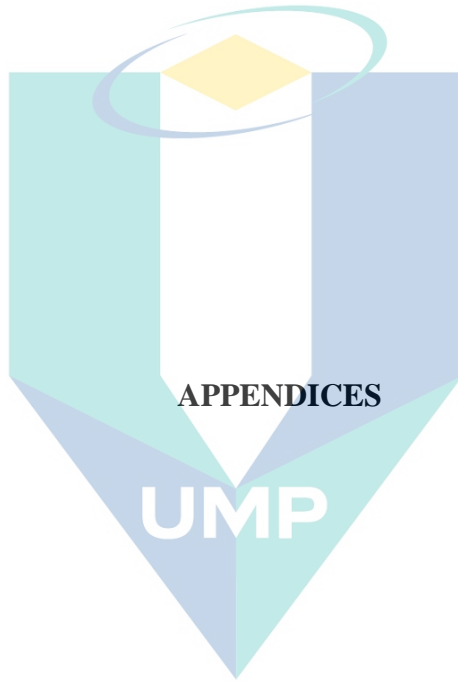
Appendix A: Sample calculation for amount of CBZ and SAC in the experiment

mol mass of CBZ = 236.27 , mol mass of SAC =183.18

Pre-dicided
total amount of solution need = 200ml (g) , due to size of vessel is 250ml
Parameter;
SAC/CBZ ratio : 3.5, 3.0, 2.5, 2.0, 1.5, 1.0 (pre decided based on previous work)
no of mol of CBZ =0.8 (pre decided)

Calculation
no of mol SAC = no of mol CBZ * SAC/CBZ ratio
CBZ concentration = mol mass of CBZ * no of mol CBZ
SAC concentration = mol mass of SAC * no of mol SAC
for 200ml solution, amount of CBZ = CBZ concentration * 0.2
for 200ml solution, amount of SAC = SAC concentration * 0.2

SAC/CBZ RATIO	MOL MASS		no of mol		conc		weight in 200ml (g)	
	CBZ	SAC	CBZ	SAC	CBZ	SAC	CBZ	SAC
3.50	236.27	183.18	0.08	0.28	19.14	51.93	3.83	10.39
3.00	236.27	183.18	0.08	0.24	19.14	44.51	3.83	8.90
2.50	236.27	183.18	0.08	0.20	19.14	37.09	3.83	7.42
2.00	236.27	183.18	0.08	0.16	19.14	29.68	3.83	5.94
1.50	236.27	183.18	0.08	0.12	19.14	22.26	3.83	4.45
1.00	236.27	183.18	0.08	0.08	19.14	14.84	3.83	2.97

Appendix B: Raw data for slow cooling experiments

CBZ concentration: 19.14 mg/ml

SAC/CBZ mol ratio	Cooling Rate (°C/min)	Tcrys1 (°C)	Tcrys2 (°C)	Tcrys3 (°C)	Average Tcrys (°C)	Tdiss1 (°C)	Tdiss2 (°C)	Tdiss3 (°C)	Average Tdiss (°C)
3.5	0.20	33.56	34.06	33.06	33.56	53.09	54.29	51.89	53.09
3.5	0.40	30.01	31.11	28.90	30.01	53.98	54.99	52.97	53.98
3.5	0.60	29.00	30.00	28.00	29.00	54.09	53.09	55.09	54.09
3.5	0.80	24.87	23.87	25.87	24.87	54.65	55.70	53.60	54.65
3	0.20	33.24	32.62	32.93	32.93	51.00	53.45	53.45	52.63
3	0.40	30.77	28.52	29.65	29.65	51.47	53.93	53.93	53.11
3	0.60	29.98	28.40	29.19	29.19	51.51	54.49	54.49	53.50
3	0.80	25.54	23.96	24.75	24.75	52.43	54.38	54.38	53.73
2.5	0.20	31.92	30.17	31.05	31.05	51.20	51.3	51.1	51.20
2.5	0.40	27.19	27.28	27.10	27.19	51.74	51.98	51.5	51.74
2.5	0.60	24.75	24.83	24.67	24.75	51.44	51.66	51.22	51.44
2.5	0.80	23.18	23.36	23.00	23.18	51.85	51.7	52	51.85
2	0.20	25.46	25.03	25.88	25.46	49.01	48	50.02	49.01
2	0.40	22.59	22.80	22.38	22.59	49.35	48.35	50.35	49.35
2	0.60	19.00	19.22	18.78	19.00	50.01	52.02	48	50.01
2	0.80	18.43	19.43	17.43	18.43	49.94	48.98	50.9	49.94
1	0.20	15.11	15.00	15.22	15.11	40.29	42.29	38.29	40.29
1	0.40	10.07	10.00	10.14	10.07	40.17	40.30	40.04	40.17
1	0.60	7.50	7.65	7.35	7.50	40.41	40.31	40.51	40.41
1	0.80	5.94	6.00	5.88	5.94	40.18	40.20	40.16	40.18

CBZ concentration: 17.96 mg/ml

SAC/CBZ mol ratio	Cooling Rate (°C/min)	Tcrys1 (°C)	Tcrys2 (°C)	Tcrys3 (°C)	Average Tcrys (°C)	Tdiss1 (°C)	Tdiss2 (°C)	Tdiss3 (°C)	Average Tdiss (°C)
3.5	0.20	32.26	31.22	33.06	32.18	52.70	52.50	52.90	52.70
3.5	0.40	31.22	32.25	30.35	31.27	54.00	52.72	53.00	53.24
3.5	0.60	28.50	27.94	26.42	27.62	54.00	53.25	52.65	53.30
3.5	0.80	26.46	25.84	27.45	26.58	54.55	53.60	53.50	53.88
3	0.20	31.12	33.40	32.26	32.26	51.80	51.70	51.90	51.80
3	0.40	29.63	29.50	29.76	29.63	51.99	51.90	52.08	51.99
3	0.60	28.27	28.13	28.41	28.27	52.28	52.20	52.36	52.28
3	0.80	27.37	27.30	27.44	27.37	52.61	52.50	52.72	52.61
2.5	0.20	30.68	30.80	30.56	30.68	50.65	50.70	50.60	50.65
2.5	0.40	26.63	26.74	26.52	26.63	50.76	50.86	50.66	50.76
2.5	0.60	23.20	23.53	22.87	23.20	51.63	51.76	51.50	51.63
2.5	0.80	22.82	23.20	22.42	22.81	52.30	52.44	52.16	52.30
2	0.20	25.10	25.20	25.00	25.10	47.68	47.88	47.48	47.68
2	0.40	21.64	21.44	21.84	21.64	47.85	47.45	48.25	47.85
2	0.60	19.30	19.35	19.25	19.30	47.95	47.9	48	47.95
2	0.80	16.17	16.00	16.34	16.17	48.11	48	48.22	48.11
1	0.20	10.96	10.06	11.86	10.96	37.00	36.85	37.15	37.00
1	0.40	7.95	7.70	8.10	7.92	38.34	38.42	38.26	38.34
1	0.60	4.26	4.16	4.36	4.26	37.39	37.23	37.55	37.39
1	0.80	2.17	2.10	2.24	2.17	37.93	38.06	37.80	37.93

CBZ concentration: 17.01 mg/ml

SAC/CBZ mol ratio	Cooling Rate (°C/min)	Tcrys1 (°C)	Tcrys2 (°C)	Tcrys3 (°C)	Average Tcrys (°C)	Tdiss1 (°C)	Tdiss2 (°C)	Tdiss3 (°C)	Average Tdiss (°C)
3.5	0.20	31.11	31.22	31.33	31.22	52.80	51.68	52.40	52.29
3.5	0.40	28.39	29.41	28.36	28.72	53.00	53.15	52.75	52.97
3.5	0.60	25.79	25.52	25.60	25.64	53.50	52.76	52.96	53.07
3.5	0.80	25.46	25.40	25.52	25.46	54.30	53.05	54.05	53.80
3	0.20	27.36	31.58	29.47	29.47	47.75	49.6	48.68	48.68
3	0.40	24.90	28.21	26.56	26.56	47.86	50.24	49.05	49.05
3	0.60	22.77	24.44	24.62	23.94	48.60	50.71	49.66	49.66
3	0.80	23.02	26.16	24.98	24.72	48.60	51.20	49.90	49.90
2.5	0.20	30.48	30.45	20.70	27.21	48.47	48.54	48.4	48.47
2.5	0.40	26.29	26.03	18.46	23.59	48.64	48.72	48.56	48.64
2.5	0.60	25.80	25.12	14.13	21.68	49.09	49.18	49.00	49.09
2.5	0.80	22.50	22.79	12.48	19.26	49.60	49.40	49.80	49.60
2	0.20	21.78	21.90	21.66	21.78	45.31	45	45.62	45.31
2	0.40	17.08	17.00	17.16	17.08	45.7	45.5	45.9	45.70
2	0.60	15.98	16.28	15.68	15.98	46.82	46.7	46.94	46.82
2	0.80	12.68	12.66	12.70	12.68	46.96	46.92	47	46.96
1	0.20	9.88	10.00	9.76	9.88	36.87	36.8	36.94	36.87
1	0.40	7.08	6.98	7.18	7.08	37.03	36.83	37.23	37.03
1	0.60	3.32	3.30	3.34	3.32	37.24	37.16	37.32	37.24
1	0.80	1.19	1.15	1.23	1.19	37.34	37.20	37.48	37.34

CBZ concentration: 15.83 mg/ml

SAC/CBZ mol ratio	Cooling Rate (°C/min)	Tcrys1 (°C)	Tcrys2 (°C)	Tcrys3 (°C)	Average Tcrys (°C)	Tdiss1 (°C)	Tdiss2 (°C)	Tdiss3 (°C)	Average Tdiss (°C)
3.5	0.20	31.11	31.00	31.22	31.11	52.10	52.00	52.20	52.10
3.5	0.40	28.39	28.48	28.30	28.39	52.95	53.00	52.90	52.95
3.5	0.60	25.80	25.75	25.78	25.78	52.86	52.80	52.92	52.86
3.5	0.80	22.50	22.52	22.51	22.51	53.55	53.00	54.10	53.55
3	0.20	27.36	31.58	29.47	29.47	48.97	49.04	48.90	48.97
3	0.40	24.90	28.21	26.56	26.56	49.13	49.00	49.26	49.13
3	0.60	22.77	24.44	24.62	23.94	49.57	49.47	49.67	49.57
3	0.80	23.02	26.16	24.98	24.72	49.79	49.60	49.98	49.79
2.5	0.20	26.06	23.00	24.53	24.53	47.45	47.60	47.30	47.45
2.5	0.40	22.28	22.39	22.17	22.28	47.45	47.58	43.33	46.12
2.5	0.60	18.95	21.00	19.98	19.98	48.33	48.44	48.22	48.33
2.5	0.80	19.07	18.99	19.15	19.07	48.32	48.20	48.44	48.32
2	0.20	18.21	18.00	18.42	18.21	43.55	43.44	43.66	43.55
2	0.40	15.71	15.61	15.81	15.71	43.71	44.33	44.25	44.10
2	0.60	8.68	9.68	7.68	8.68	44.26	44.06	44.46	44.26
2	0.80	9.59	7.65	7.43	8.22	44.33	44.38	44.29	44.33
1	0.20	4.38	4.28	4.48	4.38	34.96	34.86	35.06	34.96
1	0.40	0.32	0.20	0.44	0.32	35.26	35.32	35.20	35.26
1	0.60	0.06	0.00	0.12	0.06	35.85	36.00	35.70	35.85
1	0.80	-4.53	-4.73	-4.33	-4.53	35.17	36.16	34.18	35.17

Appendix C: Graph of crystallisation and dissolution temperature of CBZ-SAC co-crystals for different molar ratio of SAC/CBZ
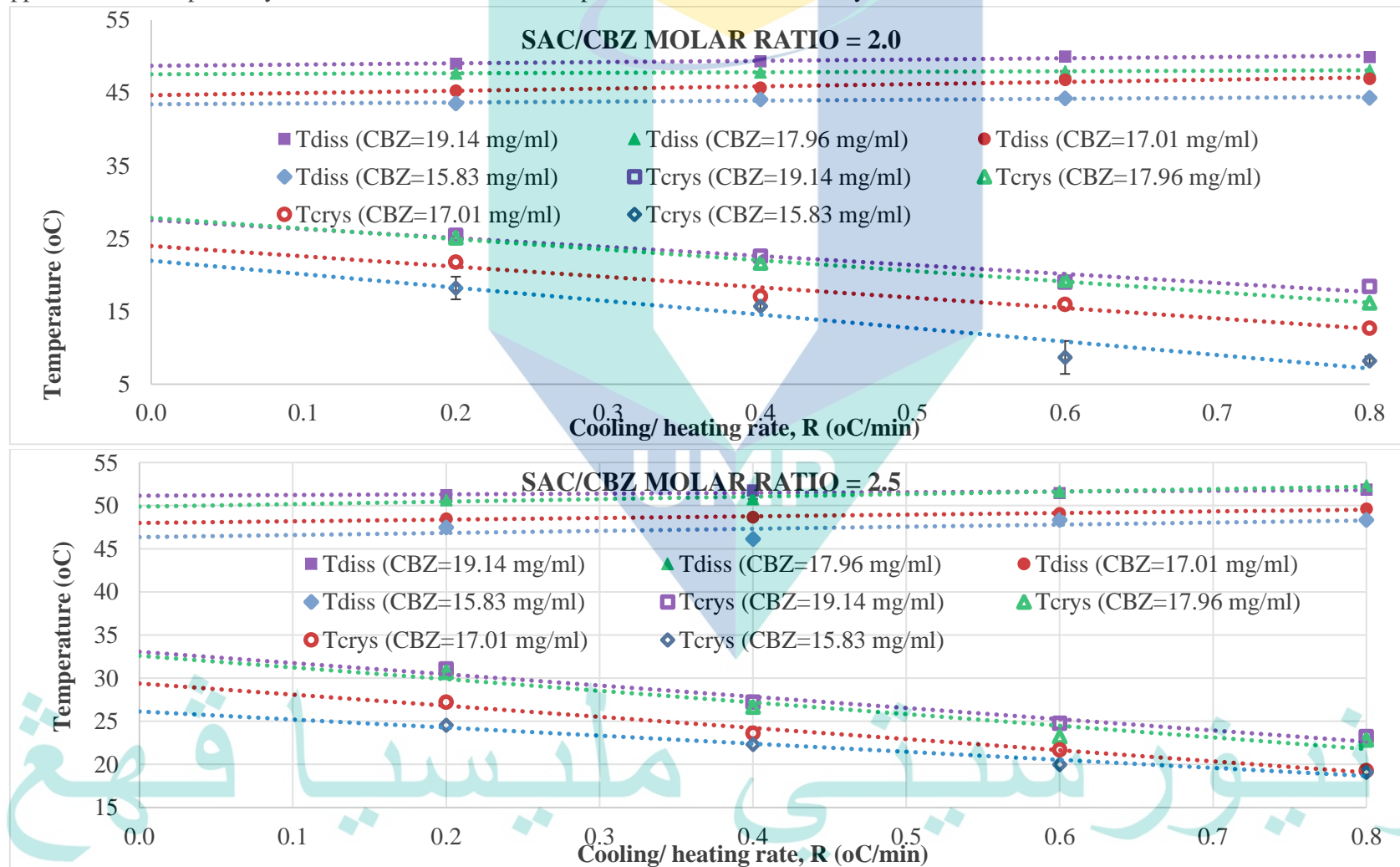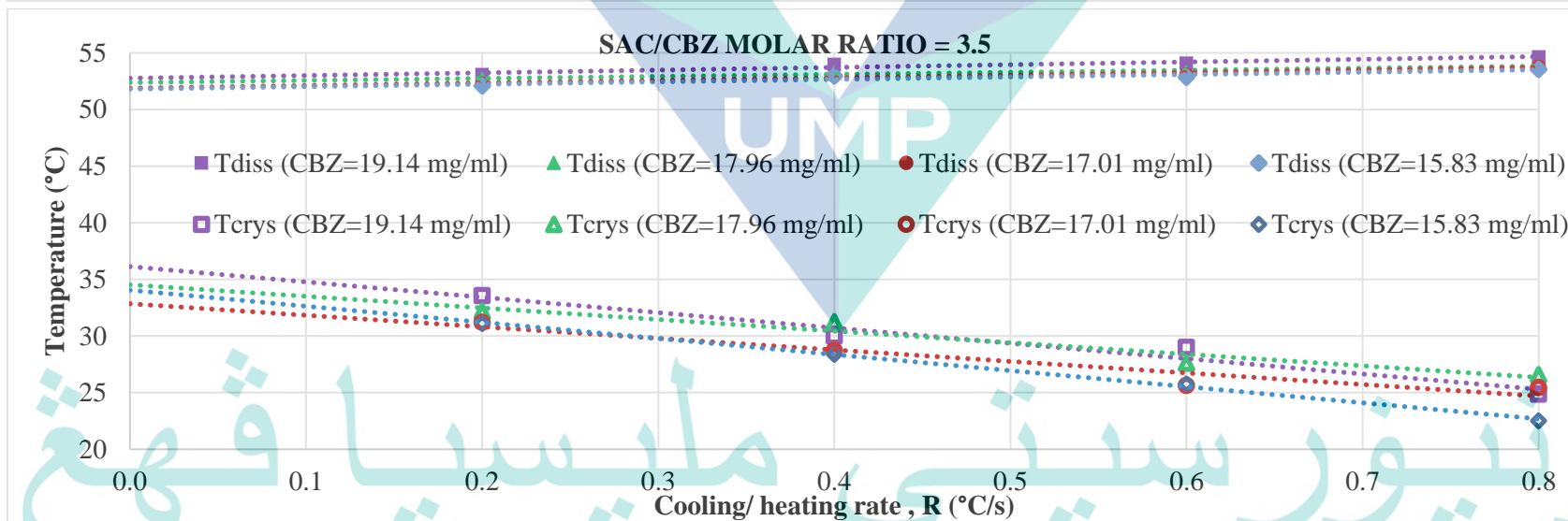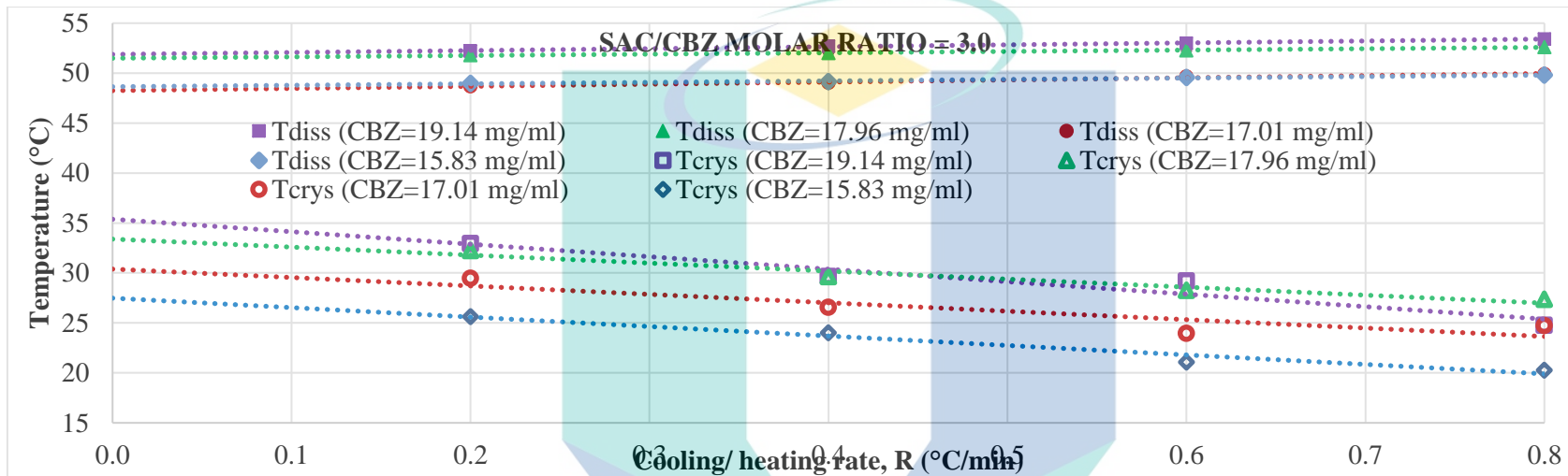
Appendix D:MSZW of CBZ-SAC co-crystals at different CBZ concentrations and SAC/CBZ molar ratio of 2.0, 2.5, 3.0 and 3.5.
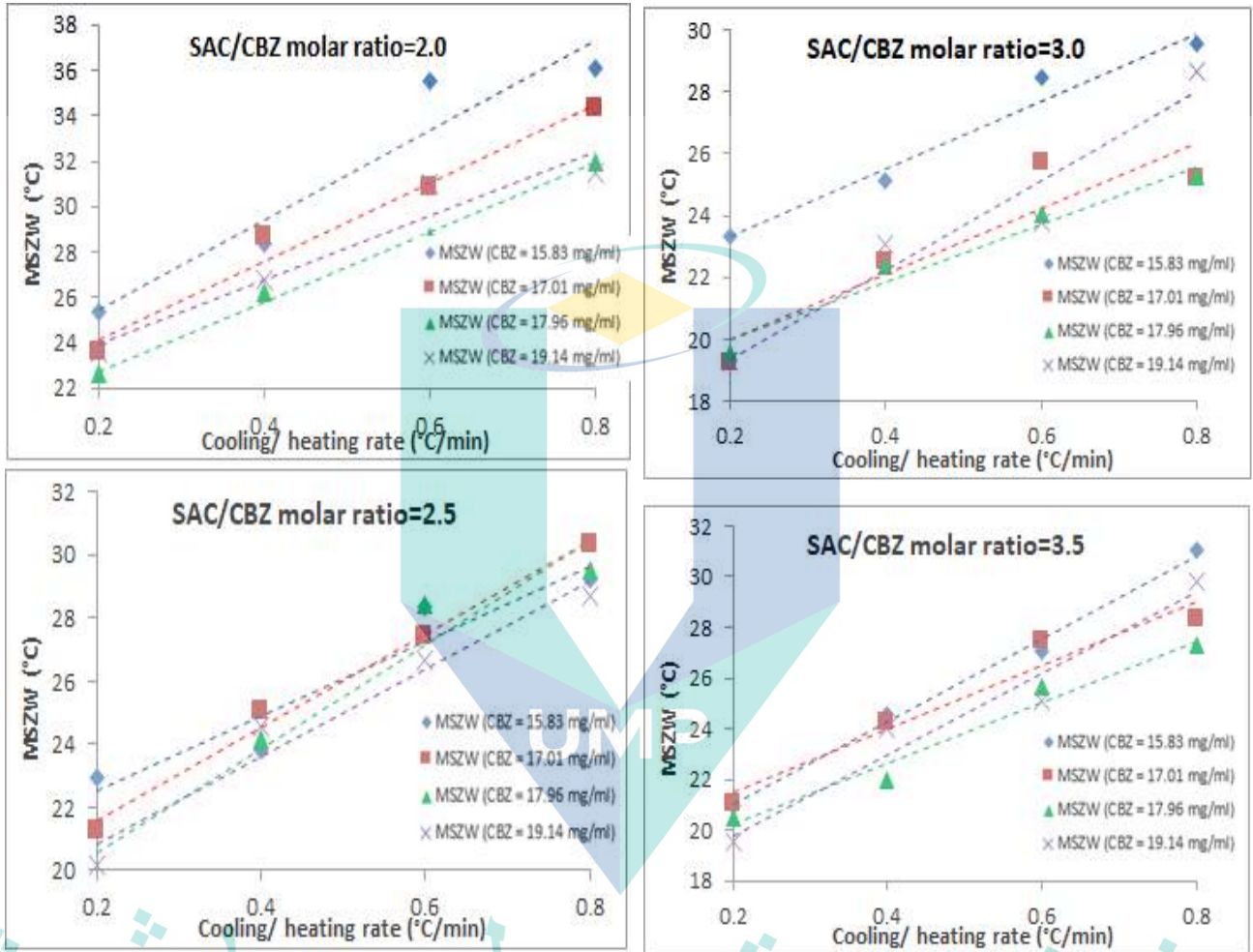
Appendix E: Graphs MSZW vs CBZ concentration for all molar ratios
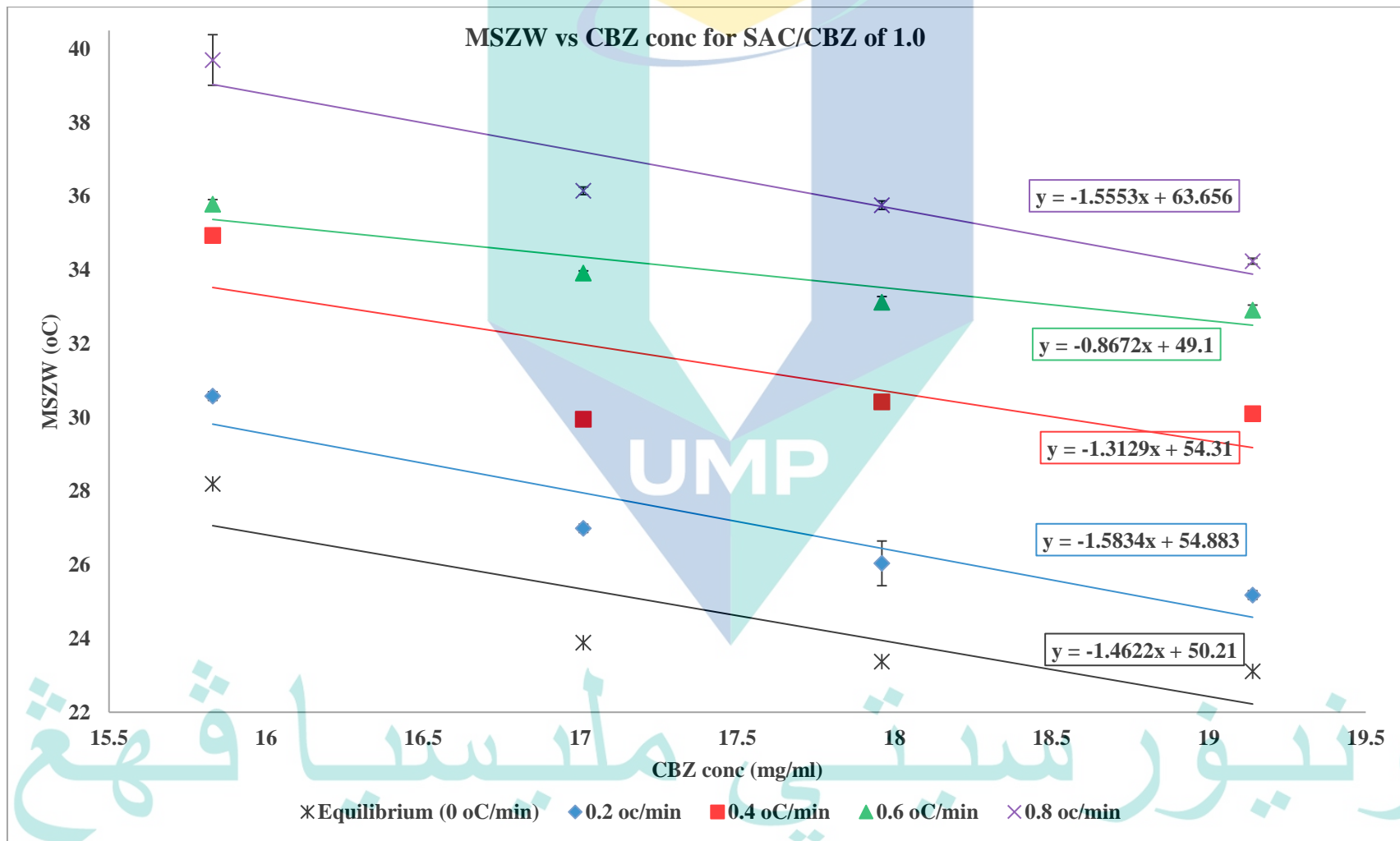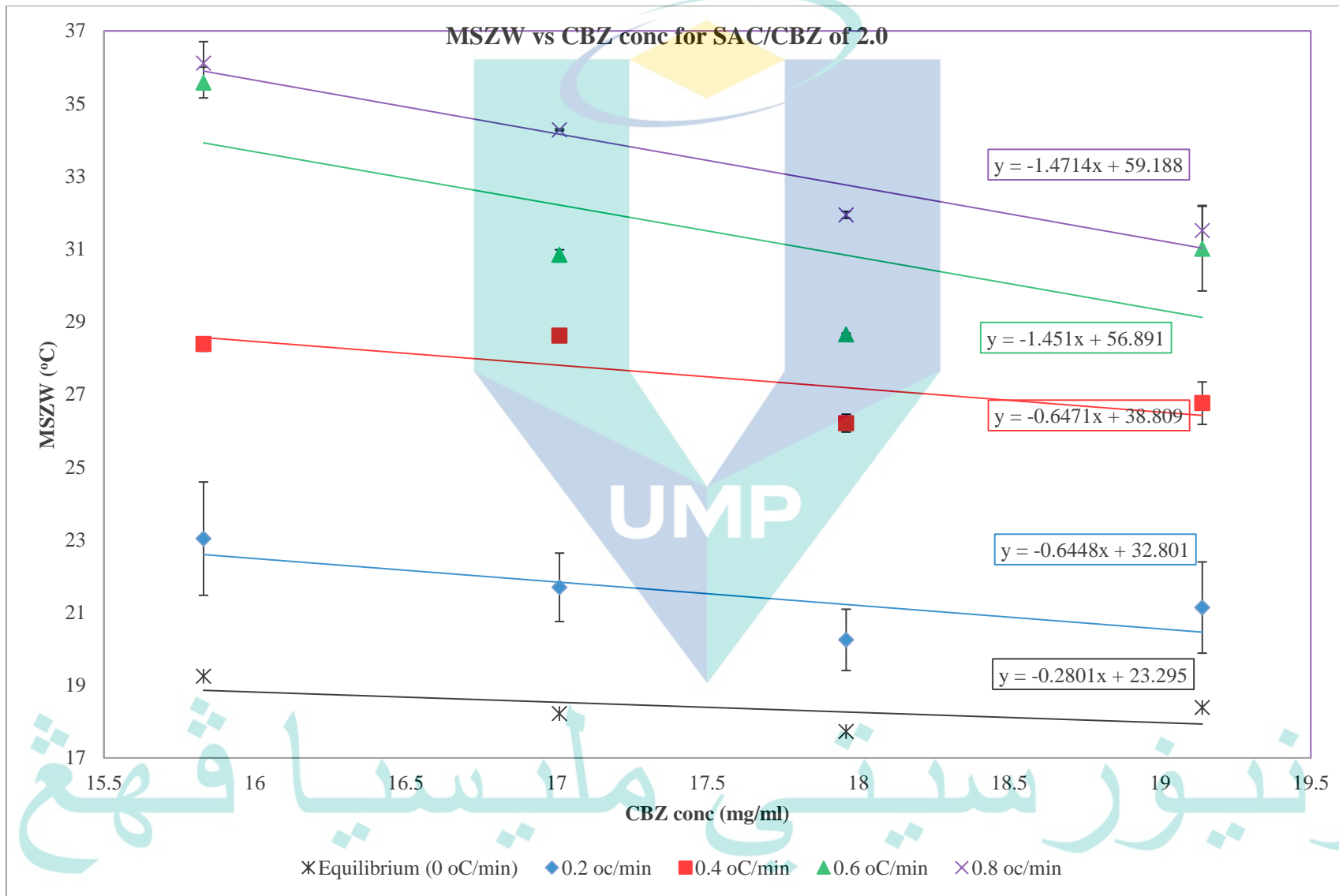
MSZW vs CBZ conc for SAC/CBZ of 2.0

$y = -1.4714x + 59.188$

$y = -1.451x + 56.891$

$y = -0.6471x + 38.809$

$y = -0.6448x + 32.801$

$y = -0.2801x + 23.295$

MSZW (ºC)

CBZ conc (mg/ml)

✳Equilibrium (0 oC/min)   ◆0.2 oc/min   ■0.4 oC/min   ▲0.6 oC/min   ✕0.8 oc/min

Effect of cooling rate on MSZW for different CBZ Conc and (SAC/CBZ) ratio of 2.5

Legend:
- 0.8 K/s
- 0.6 K/s
- 0.4 K/s
- 0.2 K/s
- Saturation

Y-axis: MSZW (oC)

X-axis: CBZ conc,C (mg/ml)

Effect of cooling rate on MSZW for different CBZ Conc and (SAC/CBZ) ratio of 3.0

Legend:
- 0.8 K/s
- 0.6 K/s
- 0.4 K/s
- 0.2 K/s
- Saturation

Y-axis: MSZW (oC)

X-axis: CBZ conc,C (mg/ml)
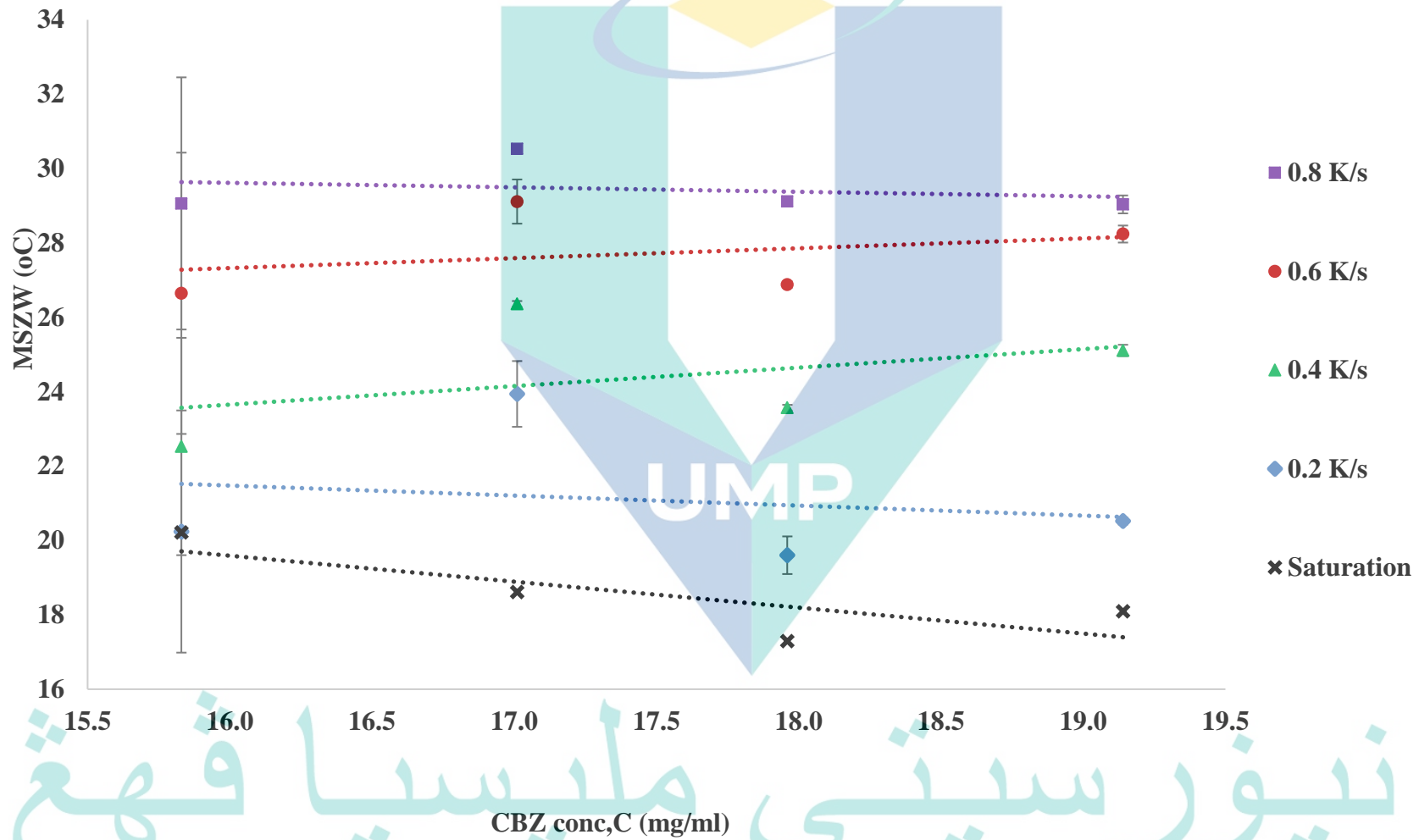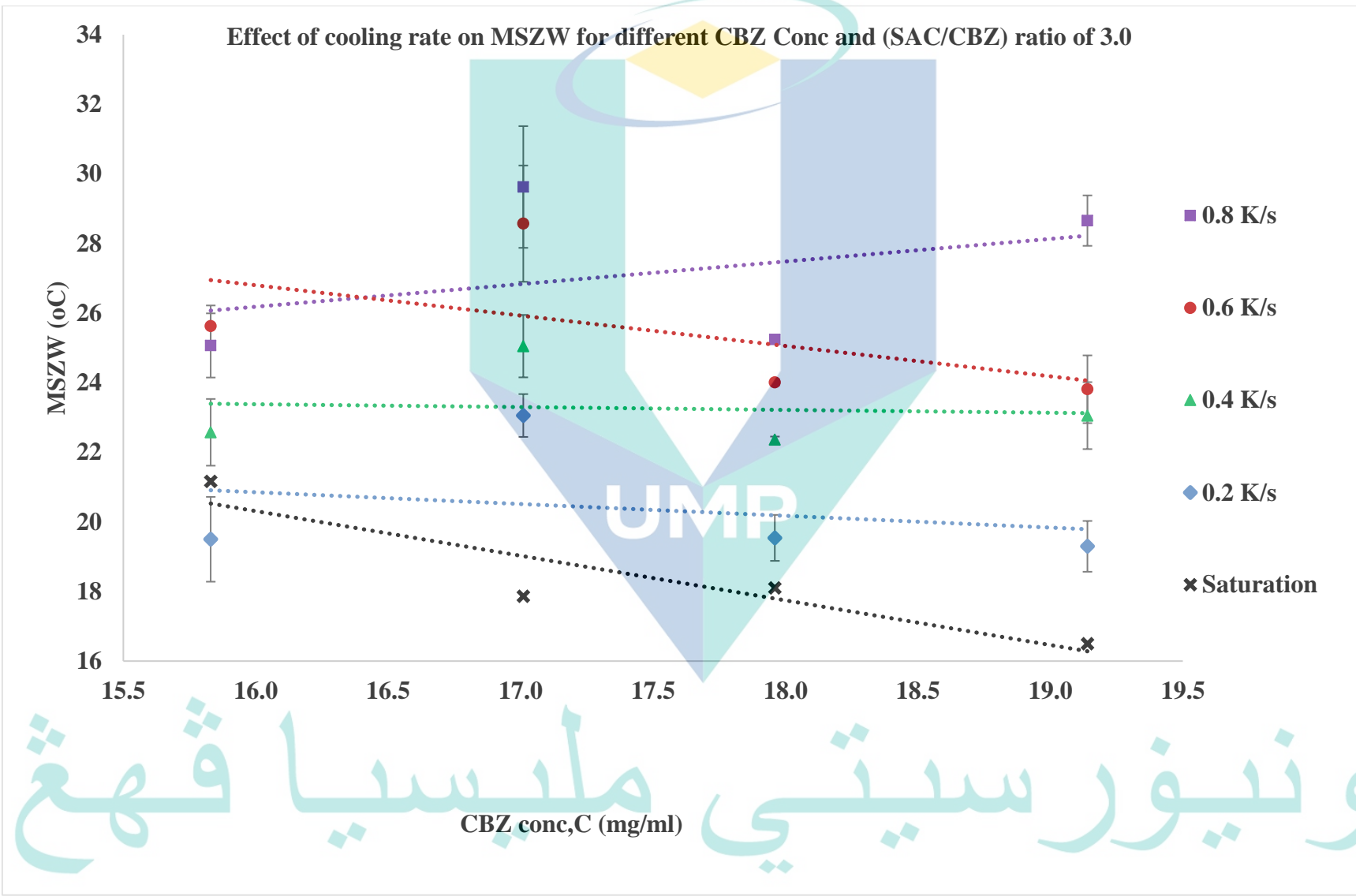
Appendix F:Graphs LOG (R) vs LOG (MSZW) for all SAC/CBZ mol ratios
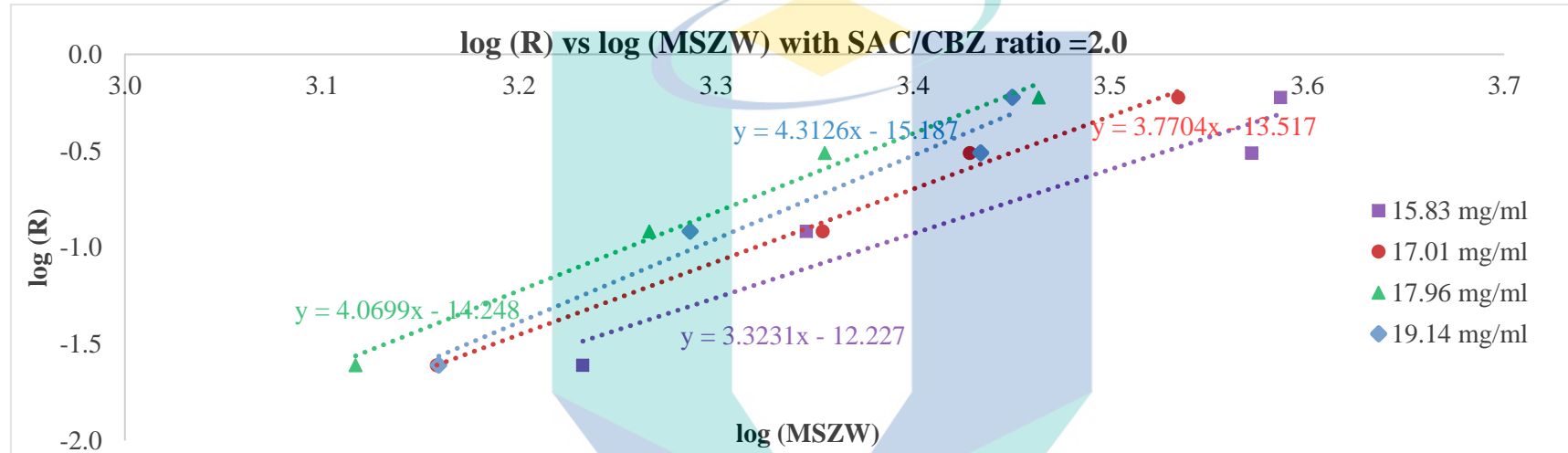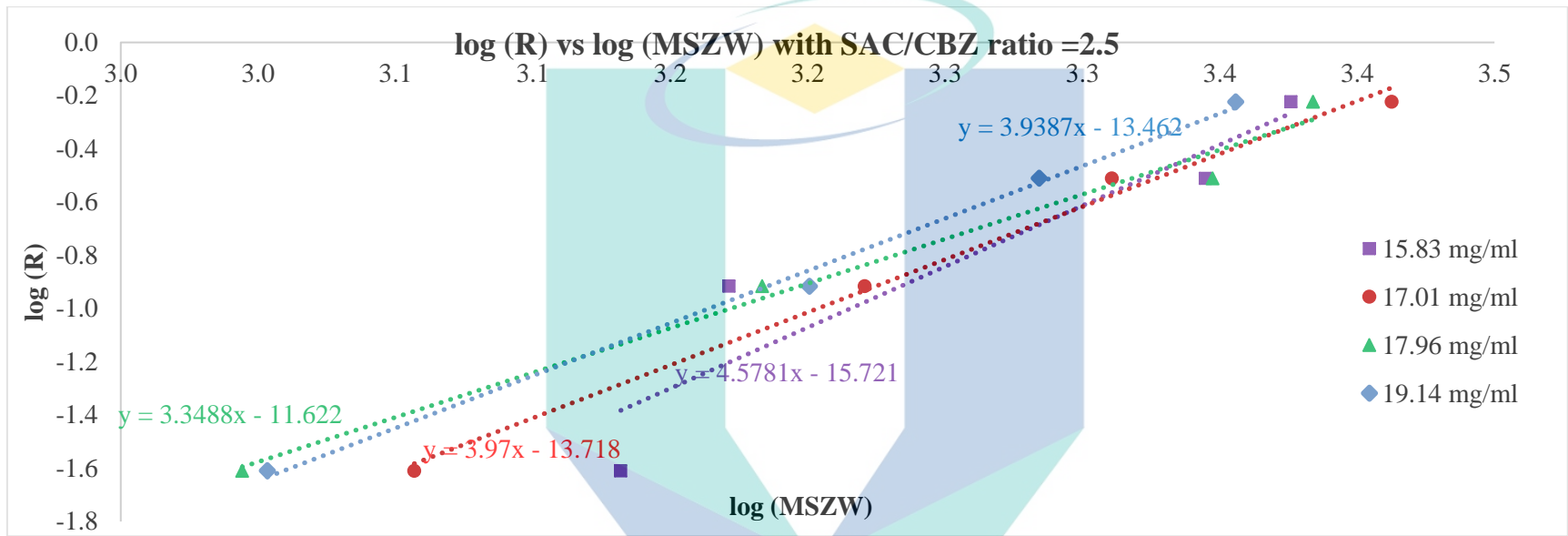
log (R) vs log (MSZW) with SAC/CBZ ratio =2.0

y = 4.3126x - 15.187

y = 3.7704x - 13.517

y = 4.0699x - 14.248

y = 3.3231x - 12.227

log (R)

log (MSZW)

- ■ 15.83 mg/ml
- ● 17.01 mg/ml
- ▲ 17.96 mg/ml
- ◆ 19.14 mg/ml

log (R) vs log (MSZW) with SAC/CBZ ratio =2.5

$y = 3.9387x - 13.462$

$y = 4.5781x - 15.721$

$y = 3.3488x - 11.622$

$y = 3.97x - 13.718$

log (R)

log (MSZW)

■ 15.83 mg/ml
● 17.01 mg/ml
▲ 17.96 mg/ml
◆ 19.14 mg/ml

log (R) vs log (MSZW) with SAC/CBZ ratio =3.5

$y = 3.3779x - 11.595$

$y = 3.5999x - 12.496$

$y = 4.3476x - 14.579$

$y = 4.4337x - 15.105$

- ■ 15.83 mg/ml
- ● 17.01 mg/ml
- ▲ 17.96 mg/ml
- ◆ 19.14 mg/ml

log (R)

log (MSZW)

log (R) vs log (MSZW) with SAC/CBZ ratio =3.0

$y = 3.5554x - 12.035$

$y = 4.3448x - 14.438$

$y = 5.4041x - 17.685$

$y = 5.3762x - 18.434$

- ■ 15.83 mg/ml
- ● 17.01 mg/ml
- ▲ 17.96 mg/ml
- ◆ 19.14 mg/ml

log (R)

log (MSZW)
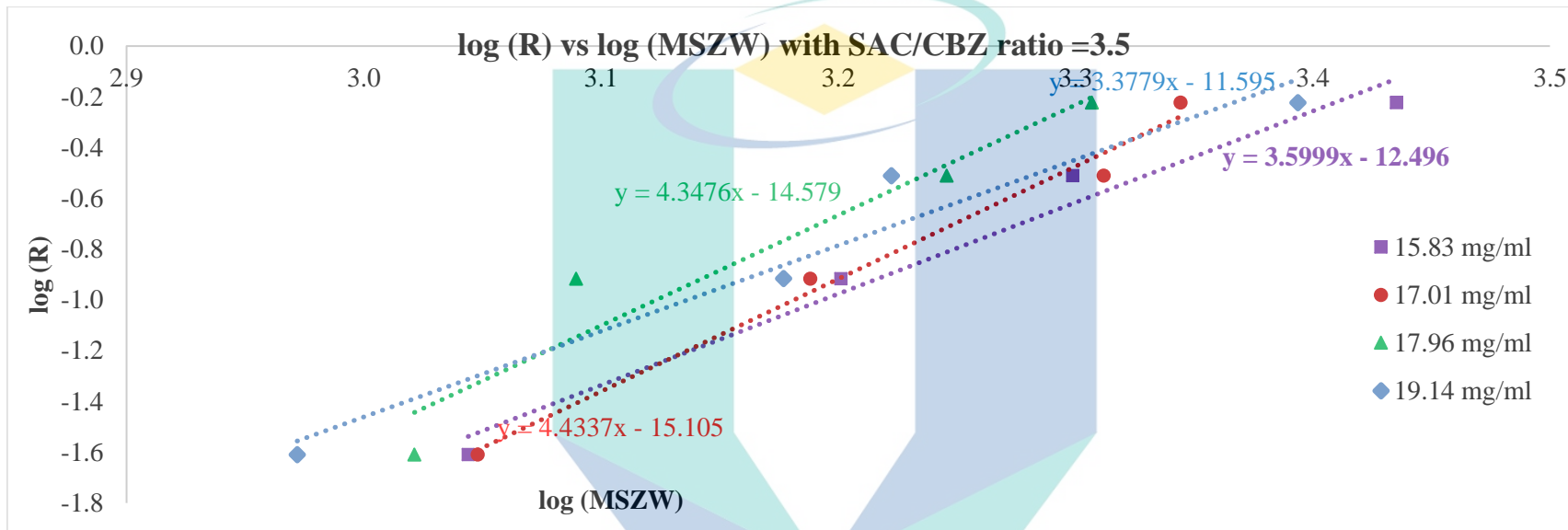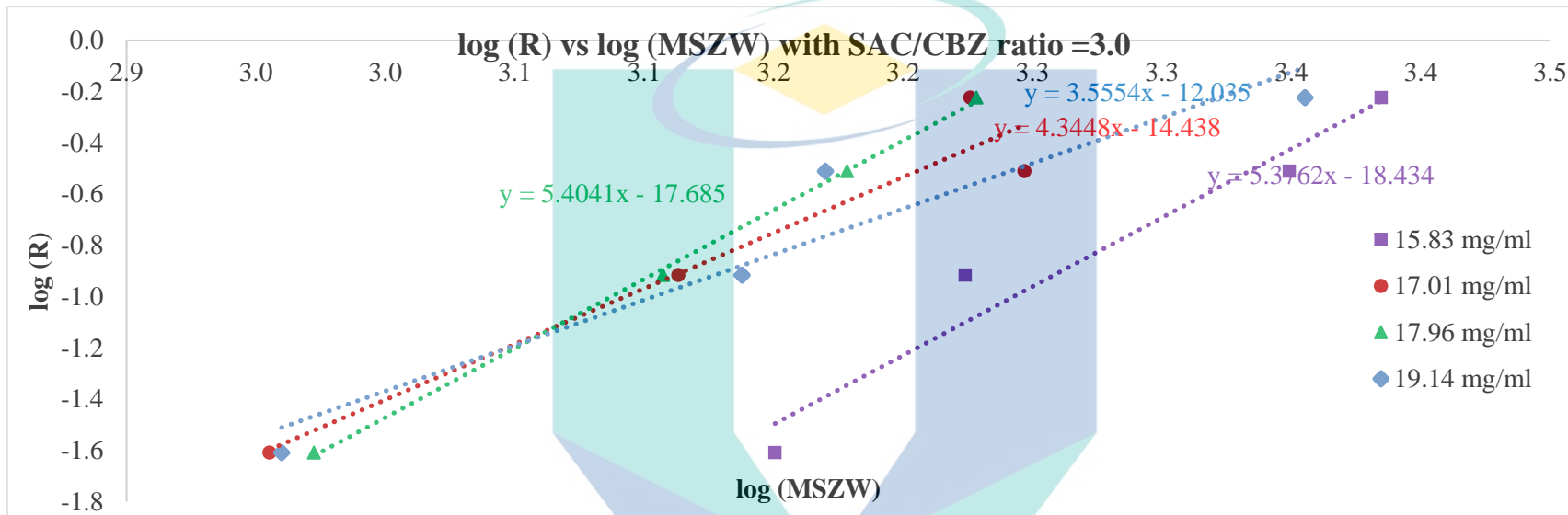
Appendix G: Raw data for fast cooling experiments

cooling rate (°C/min)	target supercooling Temp (°C)														
	28.00			30.00			32.00			34.00			36.00		
	tind(min)	tind(s)	ln(t)	tind(min)	tind(s)	ln(t)	tind(min)	tind(s)	ln(t)	tind(min)	tind(s)	ln(t)	tind(min)	tind(s)	ln(t)
1.00	40.10	2406.0	7.79	47.50	2850.00	7.96	84.45	5067.0	8.53	110.20	6612.0	8.80	142.50	8550.0	9.05
1.00	38.25	2295.0	7.74	46.50	2790.00	7.93	90.00	5400.0	8.59	102.74	6164.4	8.73	151.00	9060.0	9.11
1.00	42.25	2535.0	7.84	48.00	2880.00	7.97	87.20	5232.0	8.56	118.35	7101.0	8.87	133.00	7980.0	8.98
1 (mean)	40.20	2412.00	7.79	47.33	2840.00	7.95	87.22	5233.00	8.56	110.43	6625.80	8.80	142.17	8530.00	9.05
1 (Std Dev)	2.00	120.1	0.05	0.76	45.83	0.02	2.78	166.5	0.03	7.81	468.5	0.07	9.00	540.3	0.06
1 (Std Err)	1.16	69.3	0.03	0.44	26.46	0.01	1.60	96.1	0.02	4.51	270.5	0.04	5.20	311.9	0.04

cooling rate (°C/min)	target supercooling Temp (°C)														
	28			30			32			34			36		
	tind(min)	tind(s)	ln(t)	tind(min)	tind(s)	ln(t)	tind(min)	tind(s)	ln(t)	tind(min)	tind(s)	ln(t)	tind(min)	tind(s)	ln(t)
1.2	50.10	3006.0	8.01	70.63	4237.8	8.35	83.45	5007.0	8.52	87.67	5260.2	8.57	165.34	9920.4	9.20
1.2	54.00	3240.0	8.08	55.20	3312.0	8.11	77.40	4644.0	8.44	101.00	6060.0	8.71	176.21	10572.6	9.27
1.2	41.00	2460.0	7.81	53.54	3212.4	8.07	70.00	4200.0	8.34	99.20	5952.0	8.69	171.63	10297.8	9.24
1.2 (mean)	48.37	2902.0	7.97	59.79	3587.40	8.18	76.95	4617.0	8.43	95.96	5757.4	8.66	171.06	10263.6	9.24
1.2 (Std Dev)	6.67	400.3	0.14	9.42	565.46	0.15	6.74	404.2	0.09	7.23	434.0	0.08	5.46	327.4	0.03
1.2 (Std Err)	3.85	231.1	0.08	5.44	326.47	0.09	3.89	233.4	0.05	4.18	250.5	0.04	3.15	189.0	0.02

Appendix H: Flowchart of KBHR method

Calculate critical undercooling, ΔT_c

calculate relative critical undercooling, u_c

Plot graph of ln u_c vs ln (R)

Apply (RULE OF THREE)

Slope

< 3 → Instantaneous Nucleation

> 3

Progressive Nucleation

Follow step in Camacho Corzo et al. (2014)

Follow inequalities $u_c < 0.1$ and $au_c < 1$

Plot ln R vs u_c → Obtain kinetic parameter
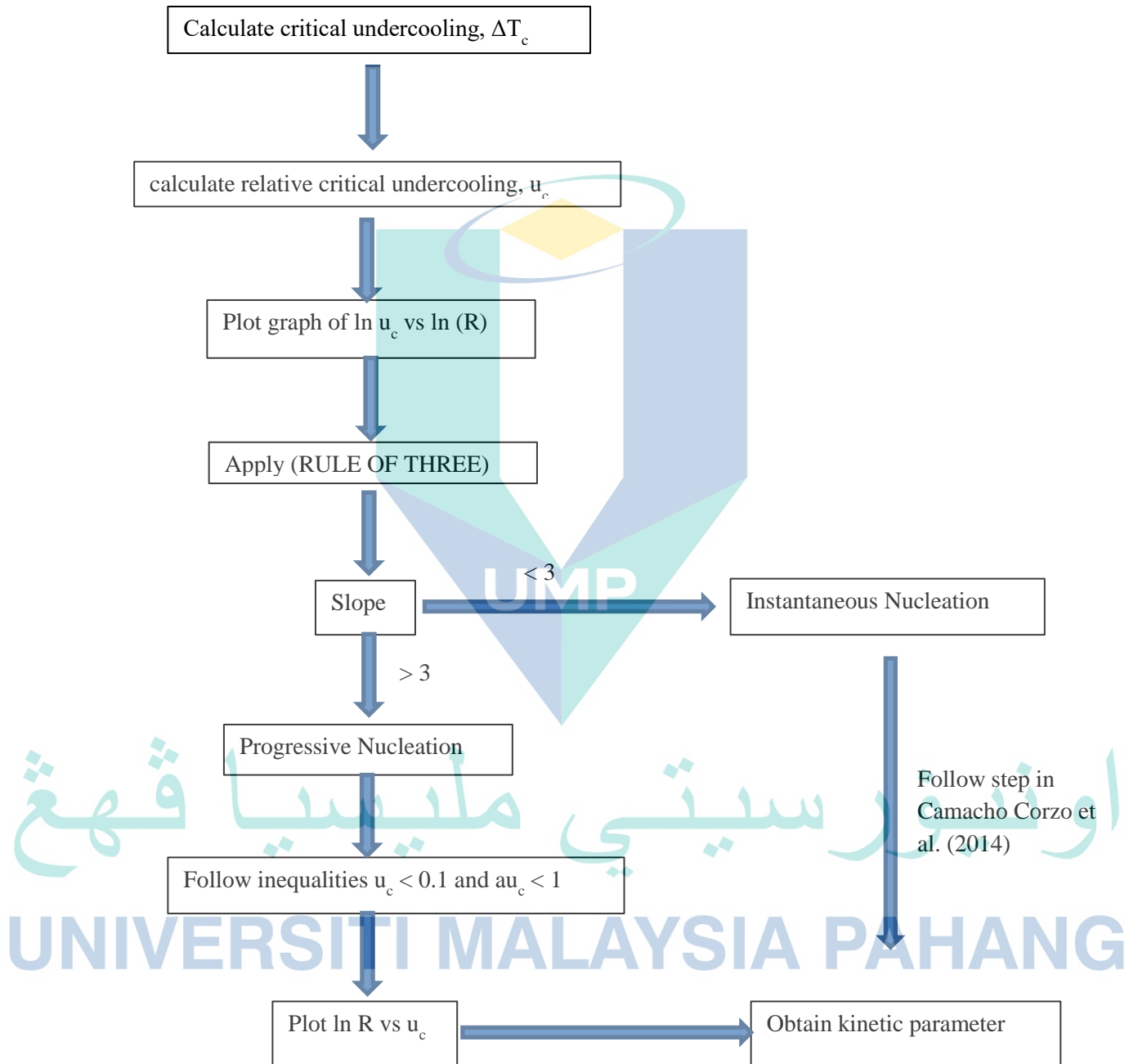
Appendix I:Raw data T_{crys}, T_{diss}, T_e, ΔT_c and u_c for SAC/CBZ mole ratio of 1.0, 2.5, 3.0 and 3.5

Table A6.1 T_{crys}, T_{diss}, T_e, ΔT_c and u_c for SAC/CBZ mole ratio of 1.0.

ρ_{CBZ} /mgmL^{-1}	Cooling rate, R /^{o}C min^{-1}	T_{crys} /^{o}C	T_{diss} /^{o}C	T_e /^{o}C	ΔT_c /^{o}C	u_c /K
15.83	0.2	4.38	34.96	35.01	30.63	0.099
	0.4	0.32	35.26		34.68	0.113
	0.6	0.06	35.85		34.95	0.113
	0.8	-4.53	35.17		39.54	0.128
17.01	0.2	9.88	36.87	36.72	26.84	0.087
	0.4	7.08	37.03		29.64	0.096
	0.6	3.32	37.24		33.40	0.108
	0.8	1.19	37.34		35.53	0.115
17.96	0.2	10.96	37.00	37.21	26.25	0.085
	0.4	7.92	38.34		29.29	0.094
	0.6	4.26	37.39		32.95	0.106
	0.8	2.17	37.93		35.04	0.113
19.14	0.2	15.11	40.29	40.29	25.18	0.080
	0.4	10.07	40.17		30.22	0.096
	0.6	7.50	40.41		32.79	0.105
	0.8	5.94	40.18		34.35	0.110

Table A6.2 T_{crys}, T_{diss}, T_e, ΔT_c and u_c for SAC/CBZ mole ratio of 2.5.

ρ_{CBZ} /mgmL^{-1}	Cooling rate, R /^{o}C min^{-1}	T_{crys} /^{o}C	T_{diss} /^{o}C	T_e /^{o}C	ΔT_c /^{o}C	u_c /K
15.83	0.2	24.53	47.45	46.35	21.82	0.068
	0.4	22.28	46.12		24.07	0.075
	0.6	19.98	48.33		26.37	0.083
	0.8	19.07	48.32		27.28	0.085
17.01	0.2	27.21	48.47	47.99	20.78	0.065
	0.4	23.59	48.64		24.40	0.076
	0.6	21.68	49.09		26.31	0.082
	0.8	19.26	49.60		28.73	0.089
17.96	0.2	30.68	50.65	49.88	19.20	0.059
	0.4	26.63	50.76		23.25	0.072
	0.6	23.20	51.63		26.68	0.083
	0.8	22.81	52.30		27.07	0.084
19.14	0.2	31.05	51.20	51.15	20.10	0.062
	0.4	27.19	51.74		23.96	0.074
	0.6	24.75	51.44		26.40	0.081
	0.8	23.18	51.85		27.97	0.086

Table A6.3 T_{crys}, T_{diss}, T_e, ΔT_c and u_c for SAC/CBZ mole ratio of 3.0.

ρ_{CBZ} /mgmL^{-1}	Cooling rate, R /^{o}C min^{-1}	T_{crys} /^{o}C	T_{diss} /^{o}C	T_e /^{o}C	ΔT_c /^{o}C	u_c /K
15.83	0.2	25.62	48.97		23.02	0.072
	0.4	24.00	49.13	48.64	24.64	0.077
	0.6	21.09	49.57		27.55	0.086
	0.8	20.28	49.79		28.36	0.088
17.01	0.2	29.47	48.68		18.78	0.058
	0.4	26.56	49.05	48.25	21.70	0.068
	0.6	23.94	49.66		24.31	0.076
	0.8	24.72	49.90		23.53	0.073
17.96	0.2	32.26	51.80		19.23	0.059
	0.4	29.63	51.99	51.49	21.86	0.067
	0.6	28.27	52.28		23.22	0.072
	0.8	27.37	52.61		24.12	0.074
19.14	0.2	32.93	52.23		18.94	0.058
	0.4	29.65	52.70	51.87	22.23	0.068
	0.6	29.19	53.00		22.68	0.070
	0.8	24.75	53.41		27.12	0.083

Table A6.4 T_{crys}, T_{diss}, T_e, ΔT_c and u_c for SAC/CBZ mole ratio of 3.5.

ρ_{CBZ} /mgmL^{-1}	Cooling rate, R /^{o}C min^{-1}	T_{crys} /^{o}C	T_{diss} /^{o}C	T_e /^{o}C	ΔT_c /^{o}C	u_c /K
15.83	0.2	31.11	52.10		20.69	0.064
	0.4	28.39	52.95	51.80	23.41	0.072
	0.6	25.78	52.86		26.02	0.080
	0.8	22.51	53.55		29.29	0.090
17.01	0.2	31.22	52.29		20.66	0.064
	0.4	28.72	52.97	51.88	23.16	0.071
	0.6	25.64	53.07		26.24	0.081
	0.8	25.46	53.80		26.42	0.081
17.96	0.2	32.18	52.70		20.20	0.062
	0.4	31.27	53.24	52.38	21.11	0.065
	0.6	27.62	53.30		24.76	0.076
	0.8	26.58	53.88		25.80	0.079
19.14	0.2	33.56	53.09		19.20	0.059
	0.4	30.01	53.98	52.76	22.75	0.070
	0.6	29.00	54.09		23.76	0.073
	0.8	24.87	54.65		27.89	0.086

Appendix J:Calculation of seeding temperature

Sample calculation as follows:

MSZW was between 47.55 °C as 100 % MSZW and 27.84 °C as 0% MSZW.

Seed was added within MSZW (47.55 °C to 27.84 °C).

Seeding temperature for 95% of MSZW

= Temperature at 0%MSZW + 95% * (Temperature at 100%MSZW - temperature at 0%MSZW)

= 27.84 °C + 95% * (47.55 °C - 27.84 °C)

= 46.56 °C

Seeding temperature for 55% of MSZW

= Temperature at 0%MSZW + 55% * (Temperature at 100%MSZW - temperature at 0%MSZW)

= 27.84 °C + 55% * (47.55 °C - 27.84 °C)

= 38.68 °C

Seeding temperature (% of MSZW)	Calculated seeding temperature (°C)
95	46.56
85	44.59
75	42.62
65	40.65
55	38.68

Appendix K: Raw data: results from seeding experiments

Crystallisation temperature for seed size of 200-150 micron of different seed mass in mg, seed loading (seed wt%) and temperature of seeding, T_{seed}.

Seed mass (mg)	Seed wt%	Tseed (°C)	Tseed (% of MSZW)	Crystallisation temperature, Tcrys (°C)			
				test1	test2	test3	average
95.55	1.5	46.56	95	43.02	43.81	42.23	43.02
95.55	1.5	44.59	85	41.78	42.61	40.95	41.78
95.55	1.5	42.62	75	40.02	40.84	39.20	40.02
95.55	1.5	40.65	65	39.51	40.22	38.80	39.51
95.55	1.5	38.68	55	38.22	38.84	37.60	38.22
63.70	1.0	46.56	95	42.34	42.88	41.80	42.34
63.70	1.0	44.59	85	41.95	42.80	41.10	41.95
63.70	1.0	42.62	75	40.23	41.06	39.40	40.23
63.70	1.0	40.65	65	39.17	40.04	38.30	39.17
63.70	1.0	38.68	55	37.33	38.16	36.50	37.33
31.85	0.5	46.56	95	39.55	40.61	40.08	40.08
31.85	0.5	44.59	85	40.57	40.08	40.33	40.33
31.85	0.5	42.62	75	38.66	38.47	38.57	38.57
31.85	0.5	40.65	65	37.83	38.76	36.90	37.83
31.85	0.5	38.68	55	37.50	35.80	36.45	36.45

Nucleation/ crystallisation temperature for seed mass of 31.85g ~ Seed wt% = 0.5.

Seed size (µm)	Mean seed size (µm)	Seeding temperature, Tseed (°C)	Tseed (%)	Nucleation temperature, Tcrys (°C)			Average nucleation temperature, Tnucl (°C)
200-150	175	46.56	95.00	37.86	38.77	36.95	37.86
150-125	137.5	46.56	95.00	38.52	38.04	39.00	38.52
125-100	112.5	46.56	95.00	40.77	41.73	39.81	40.77
200-150	175	44.59	85.00	37.04	38.08	36.00	37.04
150-125	137.5	44.59	85.00	39.92	40.83	39.01	39.92
125-100	112.5	44.59	85.00	40.57	41.34	39.80	40.57
200-150	175	42.62	75.00	36.80	37.39	37.10	37.10
150-125	137.5	42.62	75.00	37.34	39.00	37.72	38.02
125-100	112.5	42.62	75.00	38.66	39.42	37.90	38.66
200-150	175	40.65	65.00	33.62	34.34	32.90	33.62
150-125	137.5	40.65	65.00	36.28	34.66	35.47	35.47
125-100	112.5	40.65	65.00	38.53	39.06	38.00	38.53
200-150	175	38.68	55.00	31.38	32.25	31.82	31.82
150-125	137.5	38.68	55.00	36.23	36.56	35.90	36.23
125-100	112.5	38.68	55.00	37.95	37.90	38.00	37.95

Appendix L: List of Publications

Journals

- Mohammad, K. A. A., Rahim, S. A., Bakar, M. R. A. R. A., & Zainudin, E. N. H. E. (2017). Effect of Seed Loading and Temperature of Seeding on Carbamazepine-Saccharin Co-Crystal. *Indian Journal of Science and Technology*, *10*(6), 1–5. https://doi.org/10.17485/ijst/2017/v10i6/111137
- Mohammad, K. A., Abd Rahim, S., & Abu Bakar, M. R. (2015). Nucleation Kinetics of Carbamazepine-Saccharin (CBZ-SAC) Co-crystal. In A. M. Hashim (Ed.), *ICGSCE 2014* (pp. 263–270). Singapore: Springer Singapore. https://doi.org/10.1007/978-981-287-505-1_31
- Mohammad, K. A., Abd Rahim, S., & Abu Bakar, M. R. (2017). Kinetics and nucleation mechanism of carbamazepine–saccharin co-crystals in ethanol solution. *Journal of Thermal Analysis and Calorimetry*, *130*(3), 1663–1669. https://doi.org/10.1007/s10973-017-6483-1

Presented Papers at Conferences / Symposiums / Seminars

- Khairool Azizul Mohammad, Syarifah Abd Rahim, Mohd Rushdi Abu Bakar (2014). Nucleation Kinetics of Carbamazepine-Saccharin (CBZ-SAC) Co-crystal, International Conference on Global Sustainability and Chemical Engineering ICGSCE 2014, Kuala Lumpur, Malaysia , 20-23 August 2014.
- Khairool Azizul Mohammad, Syarifah Abd Rahim, Mohd Rushdi Abu Bakar (2017). Effect of Seed Loading and Temperature of Seeding on Carbamazepine-Saccharin Co-Crystal, International Conference on Fluids and Chemical Engineering FluidsChE 2017, Kota Kinabalu, Sabah, Malaysia, 4-6 April 2017.